PACIFIC EARTHQUAKE ENGINEERING RESEARCH CENTER

Capturing Directivity Effects in the Mean and Aleatory Variability of the NGA-West2 Ground-Motion Prediction Equations

Jennie A. Watson-Lamprey

Slate Geotechnical Consultants
Berkeley, California

PEER Report No. 2018/04
Pacific Earthquake Engineering Research Center
Headquarters at the University of California, Berkeley

November 2018

PEER 2018/04
November 2018

Capturing Directivity Effects in the Mean and Aleatory Variability of the NGA-West2 Ground-Motion Prediction Equations

Jennie A. Watson-Lamprey
Slate Geotechnical Consultants
Berkeley, California

PEER Report 2018/04
Pacific Earthquake Engineering Research Center
Headquarters at the University of California, Berkeley

November 2018

ABSTRACT

We expect there to be locations around a rupture that experience both positive and negative directivity effects more than others. The concept was to develop a simple model of additional mean and standard deviation to add to existing published ground motion prediction equations to account for this. The directivity effect predicted by Chiou and Youngs [2014] using the directivity parameter DPP [Spudich et al. 2013] was selected as the basis for the model. A suite of rupture geometries for strike-slip and reverse ruptures was generated and the mean and standard deviation of the change in the 5% damped pseudo-spectral acceleration at sites out to rupture distances of 70 km was calculated. Models are presented for the change in mean and standard deviation for both strike-slip and reverse ruptures that use only simple parameters as inputs.

ACKNOWLEDGMENTS

This study was sponsored by the Pacific Earthquake Engineering Research Center (PEER) and funded by the Pacific Gas & Electric Company and Arizona Public Service. Any opinions, findings, and conclusions or recommendations expressed in this material are those of the authors and do not necessarily reflect those of the sponsoring organizations, PEER, or the Regents of the University of California.

CONTENTS

LIST OF TABLES

LIST OF FIGURES

1 Study Overview

1.1 INTRODUCTION

To incorporate the effect of directivity on earthquake ground motion, engineers have relied on models developed as a correction to the median. These models were developed by fitting residuals from ground motion prediction equations (GMPEs) to functional forms that use additional parameters beyond what is included in the GMPE. These models include: Sommerville et al. [1997], Abrahamson [2000], Spudich and Chiou [2008], and Rowshandel [2010]. The most widely used of these is the Sommerville et al. (1997) model with the Abrahamson [2000] update.

There are a number of problems associated with the most widely used directivity models. The major concerns include: (1) The parameters are normalized and lump moderate magnitude data with large magnitude data, which leads to very large directivity effects for large faults contrary to seismological principles; (2) the average directivity effect of the dataset is assumed to be the median ground motion regardless of the sampling; and (3) the directivity effect in the most widely used model has been shown to overestimate directivity effects when compared with the updated ground-motion dataset of the NGA West project [Watson-Lamprey 2007].

To address these problems, the NGA-West2 project included a Directivity Working Group that produced directivity parameters to be considered by the NGA-West2 developers for inclusion in their GMPEs. Of the five NGA-West2 GMPEs produced, only one included a directivity parameter in their GMPE. The other four NGA-West2 developer teams did not include directivity explicitly in their models.

The single GMPE that explicitly includes directivity is Chiou and Youngs [2014]. It is expected that additional work on the directivity parameters will take place and that in the near future additional GMPEs will be produced that include directivity explicitly. In the meantime, there is a lack of sufficient models to include the effects of directivity.

This study aims to take advantage of the work done by the Directivity Working Group to produce a model of the effect of directivity as an additional term in the median and standard deviation. This does not solve all of the problems inherent with the existing directivity models, but provides a simple model that can be used as a stop-gap for projects that take place in the interim.

1.2 INCOPORATING THE EFFECT OF DIRECTIVITY IN ALEATORY VARIABILITY

We know that for any given site and earthquake rupture pair in the NGA-West2 ground-motion dataset there is a change in the median ground motion that could be predicted by including a directivity term. For any given site then, there is an unknown average change in the median given all sources and ruptures. This unknown average change in the median ground motion is a site-specific bias that is not being modeled. The variability of this bias from site to site—and the average variability over all sites of the bias at a given site—is included in the aleatory variability of the GMPE. We can write the equation for the aleatory variability from a GMPE as:

$$\sigma_{GMPE}^2 = \sigma_{WithoutDirectivity}^2\left(T, M_j, Site_i\right) + \sigma_{S2S|RandomHypocenters}^2 + \overline{\sigma_{Site|RandomHypocenters}^2} \tag{1.1}$$

where the first term in the equation is the aleatory variability that is not due to directivity, the second term is the variability from site to site of the average change in the median at each site due to directivity over all sources and hypocenters, and the last term is the average over the dataset of the variability of the change in the median due to directivity at a given site from all sources and hypocenters. The majority of the median GMPEs published by the NGA-West2 do not explicitly include a directivity term. Thus the median ground motion predicted by most of the NGA-West2 GMPEs is biased at some sites, and there are some sites where the aleatory variability predicted by most of the NGA-West2 GMPEs is biased as well.

To create a model of site-specific aleatory variability that explicitly includes the effect of directivity one would first take the published aleatory variability from a GMPE, reduce this aleatory variability by the average variability due to directivity described above, and then add on a site-specific variability due to the local sources, hypocenter distributions and rupture geometries. The equation for this would look like:

$$\sigma_i^2 = \sigma_{GMPE}^2 - \left(\sigma_{S2S|RandomHypocenters}^2 + \overline{\sigma_{Site|RandomHypocenters}^2}\right) + \sigma_{i|RandomHypocenters}^2 \tag{1.2}$$

where σ_i is the aleatory variability at site i, σ_{GMPE} is the aleatory variability from a published GMPE, $\sigma_{S2S|RandomHypocenters}^2 + \overline{\sigma_{Site|RandomHypocenters}^2}$ is the average change in aleatory variability due to the effect of directivity, and $\sigma_{i,RandomHypocenters}$ is the aleatory variability of the change in the median at a given site due to directivity from all sources and hypocenters.

The average change in aleatory variability due to the effect of directivity can be calculated by taking a GMPE and performing one regression with a directivity term, a second regression without a directivity term, and then taking the difference of the two aleatory variabilities. That is, it is the savings in aleatory variability due to the inclusion of an additional term in the regression. Equation (1.2) can then be rewritten as:

$$\sigma_i^2 = \sigma_{GMPE}^2 - \sigma_{Reduction}^2 + \sigma_{i|RandomHypocenters}^2 \tag{1.3}$$

This equation can then be used as the basis for a model to be added to existing GMPEs to give a site-specific aleatory variability.

1.3 MODEL DEVELOPMENT PROCEDURE FOR THE CHANGE IN THE MEDIAN GROUND MOTION

To develop a model of the change in the median ground motion due to the effect of directivity, one must calculate the difference between the change in the median at a given site and across all sites for the same rupture and rupture distance due to the effect of directivity. The equation for this is given by:

$$\Delta \ln Sa_i = \sum_{j=1,N_{hypo}} P_j\left(\ln Sa_i\left(Rupture, Rrup, Directivity_j\right) - \overline{\ln Sa_j}\left(Rupture, Rrup\right)\right) \tag{1.4}$$

where $\ln Sa_i$ is the 5% damped pseudo-spectral acceleration for a given rupture geometry, rupture distance, and directivity parameter for hypocenter location j; $\overline{\ln Sa_j}$ is the average 5% damped pseudo-spectral acceleration over all sites that have the rupture distance *Rrup* for a given rupture geometry and hypocenter location j; P_j is the probability of hypocenter j; and N_{hypo} is the number of hypocenter locations. In order to calculate ln*Sa*, one must have a GMPE that includes a directivity term in the mean equation.

The Chiou and Youngs [2014] model includes GMPEs for median ground motion both with and without the directivity parameter ΔDPP [Spudich et al. 2013]. Thus, a significant amount of the work necessary to develop a model of the change in mean and aleatory variability of 5% damped pseudo-spectral acceleration due to directivity effects was completed for the directivity parameter ΔDDP. While it would be preferable to develop models for a larger number of GMPEs and directivity parameters, in the interest of time the decision was made to move forward using only the Chiou and Youngs [2014] GMPE and ΔDPP directivity parameter.

The change in the median due to directivity is calculated for a range of magnitudes and distances by creating a suite of rupture geometries (see Table 1.1) and a suite of sites defined at a spacing of 0.5 km at rupture distances of 1, 5, 10, 20, 30, 40, 50 and 70 km. The adjustment to the median is then calculated using the following steps:

1. Hypocenters are distributed in the rupture at a spacing of 1 km down-dip and 1 km along-strike.
2. For each hypocenter j and site i, $DPP_{i,j}$ is calculated.
3. At each rupture distance, $\Delta DPP_{i,j}$ is calculated by taking the difference between $DPP_{i,j}$ and the average value of $DPP_{i,j}$ for that rupture distance.
4. For each hypocenter j and site i, 5% damped pseudo-spectral acceleration $\ln Sa_i\left(Rupture, Rrup, \Delta DPP_{ij}\right)$ is calculated for the periods: 0.5, 0.75, 1, 1.5, 2, 3, 5, 7.5, and 10 sec.
5. The mean change in the 5% damped pseudo-spectral acceleration at each site $\Delta \ln Sa_i$ is calculated using Equation (1.4), where the probability of the hypocenter location is defined using a hypocenter distribution model from Chiou and Youngs [2008].

The model of the change in the mean 5% damped pseudo-spectral acceleration is based on the results from the final step of the procedure described above. The results are modeled as a function of rupture geometry and magnitude. This model can be added to the published mean from a GMPE to estimate the mean at a site explicitly including the effect of directivity.

Table 1.1 Rupture geometries for randomization of hypocenters.

Rupture geometry	Magnitude	Sense of slip	Width (km)	Length (km)
1	6	Strike-slip	10	10
2	6.5	Strike-slip	15	21
3	7	Strike-slip	15	67
4	7.5	Strike-slip	15	211
5	8	Strike-slip	15	667
6	6	Reverse	10	10
7	6.5	Reverse	18	18
8	7	Reverse	21	47
9	7.5	Reverse	21	149

1.4 MODEL DEVELOPMENT PROCEDURE FOR THE CHANGE IN THE ALEATORY VARIABILITY

To develop a model of the change in the aleatory variability of ground motion due to the effect of directivity, one must reduce the published aleatory variability by $\sigma_{Reduction}$ and then increase it by $\sigma_{i|RandomHypocenters}$ as described in the previous section. The aleatory variability reduction has been estimated for the Chiou and Youngs [2014] ground motion prediction model by Bob Youngs (Personal communication, 2015]. The Chiou and Youngs [2014] directivity model was designed such that the mean change in the ground motion predicted by the directivity model across all sites equidistant from a given rupture is zero. Thus, there should be little to no impact on the inter-event residuals of the GMPE if the data for each earthquake are spatially evenly distributed. This is not the case for all earthquakes in the NGA-West2 dataset, but for simplicity Bob Youngs assumed it was. This allowed him to use only the intra-event residuals, and the change in the intra-event aleatory variability (ϕ_2) to estimate the aleatory variability reduction.

To compute the reduction in the aleatory variability, first the standard deviation of the intra-event residuals of the Chiou and Youngs [2014] model for earthquakes with magnitude greater than or equal to 6.5 (ϕ_2) was calculated. The directivity term predicted by the Chiou and Youngs [2014] directivity model was then removed from the intra-event residuals, and the standard deviation of those residuals recalculated. The difference in the square of the two estimates of ϕ_2 is then $\sigma_{Reduction}$. The estimates of ϕ_2 are shown in Figure 1.1, and the difference between the two shown in Figure 1.2. The figures show that at periods greater than 2 sec, the ϕ_2 reduction increases from 0 to a maximum value of 0.25 at 10 sec.

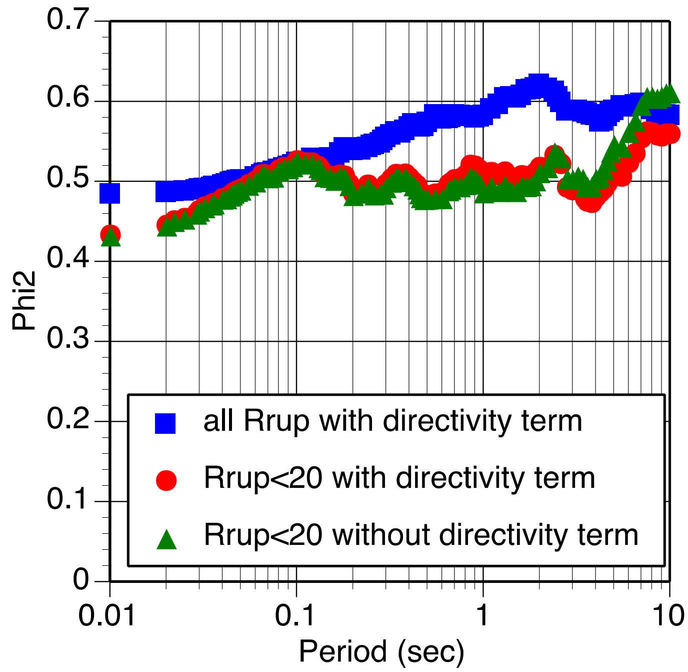

Figure 1.1 **Estimates of the intra-event aleatory variability (ϕ_2) of 5% damped pseudo-spectral acceleration for Chiou and Youngs [2014] GMPE for moment-magnitude 6.5 or greater data with rupture distances of 20 km both including and excluding DPP from the equation for the mean.**

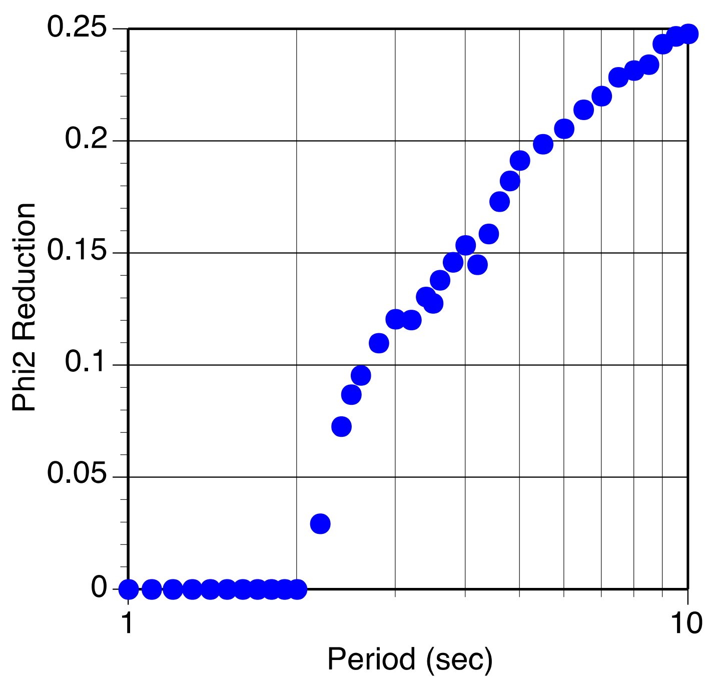

Figure 1.2 **Change in intra-event aleatory variability (ϕ_2) of 5% damped pseudo-spectral acceleration for Chiou and Youngs [2014] GMPE for moment-magnitude 6.5 or greater data with rupture distances of 20 km or less from excluding DPP from the equation for the mean.**

To estimate the site-specific aleatory variability of the change in the median ground motion due to directivity from all sources and hypocenters ($\sigma_{i|RandomHypocenters}$), one must calculate the variability of the difference between the change in the median at a given site and across all sites for the same rupture and rupture distance due to the effect of directivity. The equation for this is given by:

$$\sigma^2_{i,RandomHypocenters} = \sum_{j=1,N_{hypo}} P_j \left(\ln Sa_i \left(Rupture, Rrup, DPP_j \right) - \left(\overline{\ln Sa}_j \left(Rupture, Rrup \right) + \Delta \ln Sa_i \right) \right)^2 \tag{1.5}$$

where $\ln Sa_i$ is the 5% damped pseudo-spectral acceleration for a given rupture geometry, rupture distance, and directivity parameter for hypocenter location *j*; $\overline{\ln Sa_j}$ is the average 5% damped pseudo-spectral acceleration over all sites that have the rupture distance *Rrup* for a given rupture geometry and hypocenter location *j*; $\Delta \ln Sa_i$ is from Equation (1.4); P_j is the probability of hypocenter *j*, and N_{hypo} is the number of hypocenter locations. The directivity effect is modeled using the effect modeled in Chiou and Youngs [2014] and the directivity parameter DPP described in Spudich et al. [2013].

The Chiou and Youngs [2014] model does not predict an inter-event change in the mean ground motion values; thus the change in aleatory variability is confined to the intra-event standard deviation for large magnitudes (ϕ_2). For this reason, the variability due to hypocenter randomization in this case can be labeled as $\phi_{i|RandomHypocenters}$. The equation for calculating site-specific aleatory variability that explicitly includes the effect of directivity [Equation (1.3)] would then be:

$$\phi_i^2 = \phi^2_{GMPE} - \phi^2_{Reduction} + \phi^2_{i|RandomHypocenters} \tag{1.6}$$

The suite of ruptures from Table 1.1 and the results of the procedure outlined in the previous section are used to estimate $\phi_{i|RandomHypocenters}$ following the procedure outlined above. The total change in aleatory variability that would be added to that predicted by a GMPE would then be:

$$\Delta \phi_i = \begin{Bmatrix} 0 \quad for \quad \phi_{i|RandomHypocenters} < \phi_{Reduction} \\ \sqrt{\phi^2_{i|RandomHypocenters} - \phi^2_{Reduction}} \quad else \end{Bmatrix} \tag{1.7}$$

The results of Equation (1.7) are then modeled as a function of rupture geometry and magnitude. The final model of the change in aleatory variability of 5% damped pseudo-spectral acceleration can be added to published GMPE aleatory variabilities to estimate the aleatory variability at a site explicitly including the effect of directivity.

2 Change in Mean and Standard Deviation of Ground Motion Due to Randomization of Hypocenters

2.1 INTRODUCTION

The change in mean and aleatory variability of the 5% damped pseudo-spectral acceleration experienced at a site due to the effect of directivity by randomizing over hypocenters is calculated for a suite of sites out to a rupture distance of 70 km. The change in pseudo-spectral acceleration is calculated using the Chiou and Youngs [2014] model. The rupture scenarios are given in Table 1.1, and the changes in mean and aleatory variability of 5% damped pseudo-spectral acceleration are calculated for the periods: 0.5, 0.75, 1, 1.5, 2, 3, 5, 7.5, and 10 sec. Figures of all of the 1, 3 and 5 sec results are shown in electronic Appendix A. Selected results are shown in the following sections.

2.2 STRIKE–SLIP RUPTURES

2.2.1 Directivity Parameter DPP

The change in the mean and aleatory variability of the ground motion is based on the directivity model from Chiou and Youngs [2014]. In order to understand the results of the hypocenter randomization, we first examine the directivity parameter DDP. The directivity parameter DPP is a function of three parameters: the length *E*, the parameter $\hat{c}'$, and $\overline{FS}$ [Spudich et al. 2013]. The length *E* is the length of fault from the hypocenter to the direct point. The parameter $\hat{c}'$ is the isochrone velocity ratio, the ratio between the length *E* and the difference in arrival time of shear waves from the hypocenter and shear waves from the end of length *E*, normalized by the local shear-wave velocity [Spudich et al. 2004]. The parameter $\overline{FS}$ is an average shear-wave radiation pattern along the length *E*.

The three parameters that are used to calculate DPP as well as DPP itself are presented in Figures 2.1—2.4 for two moment-magnitude 7 strike–slip ruptures. The first rupture has a hypocenter located in the middle of the rupture; the second has a hypocenter located 1 km from the left-hand edge of the rupture and 14 km down-dip, as shown in the figures.

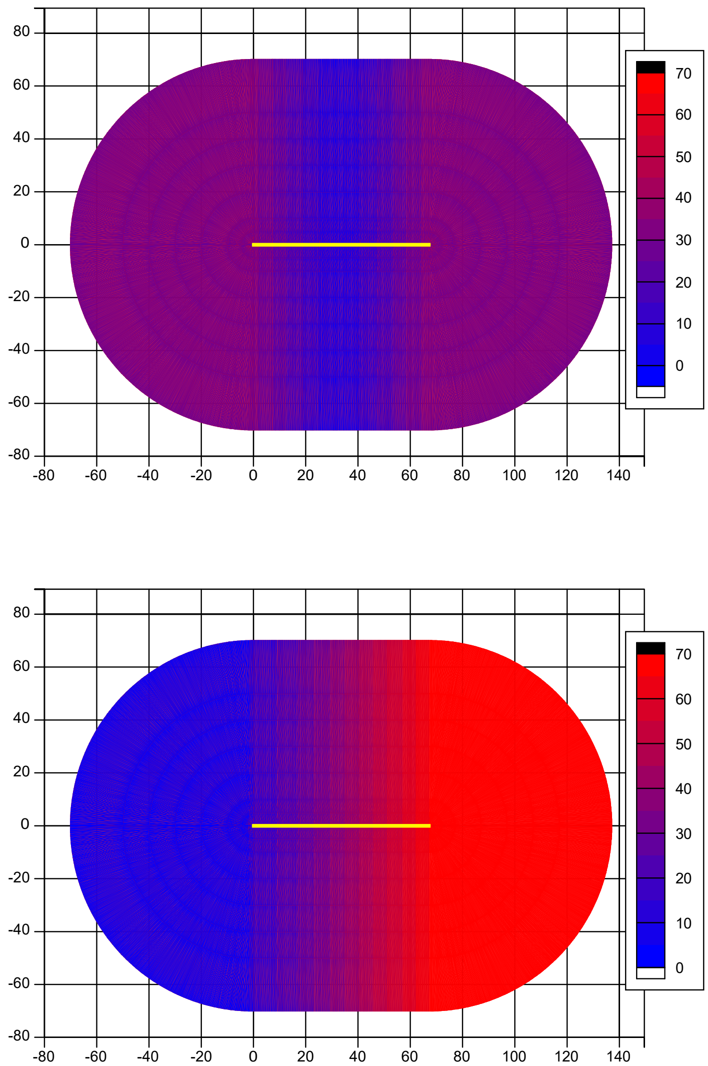

Figure 2.1 **The length of the fault from the hypocenter to the direct point (*E*) in kilometers for two moment-magnitude 7, strike–slip ruptures where the hypocenter of the upper figure is located at the center of the rupture and that of the lower is located 1 km from the left edge of the rupture length and 14 km down-dip.**

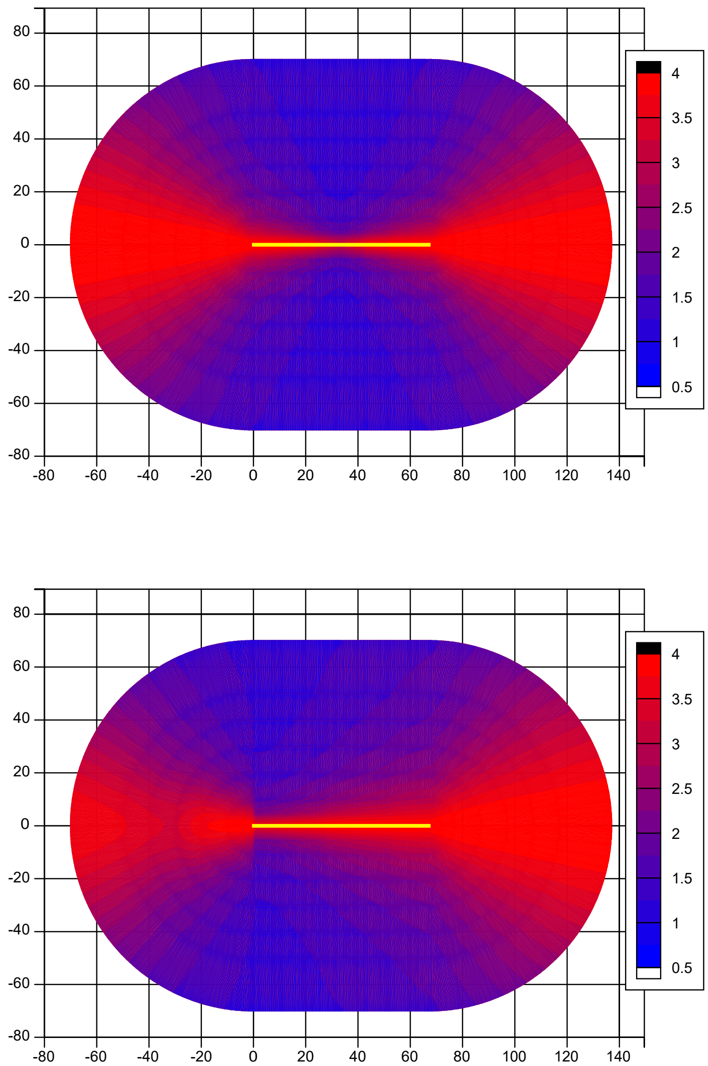

Figure 2.2 **The isochrone velocity ratio ($\hat{c}'$) along the length of the fault from the hypocenter to the direct point for two moment-magnitude 7, strike–slip ruptures where the hypocenter of the upper figure is located at the center of the rupture and that of the lower is located 1 km from the left edge of the rupture length and 14 km down-dip.**

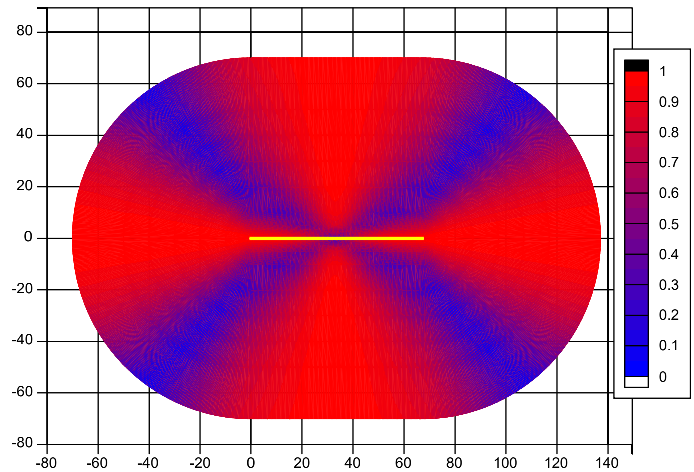

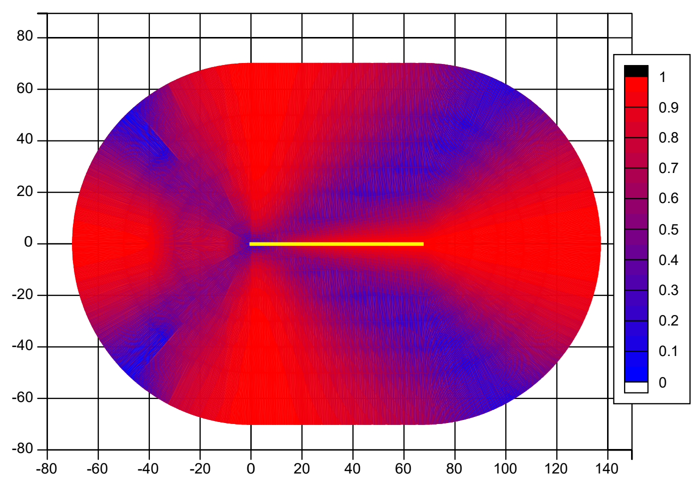

Figure 2.3 **The average shear-wave radiation pattern ($\overline{FS}$) along the length of the fault from the hypocenter to the direct point for two moment-magnitude 7, strike–slip ruptures where the hypocenter of the upper figure is located at the center of the rupture and that of the lower is located 1 km from the left edge of the rupture length and 14 km down-dip.**

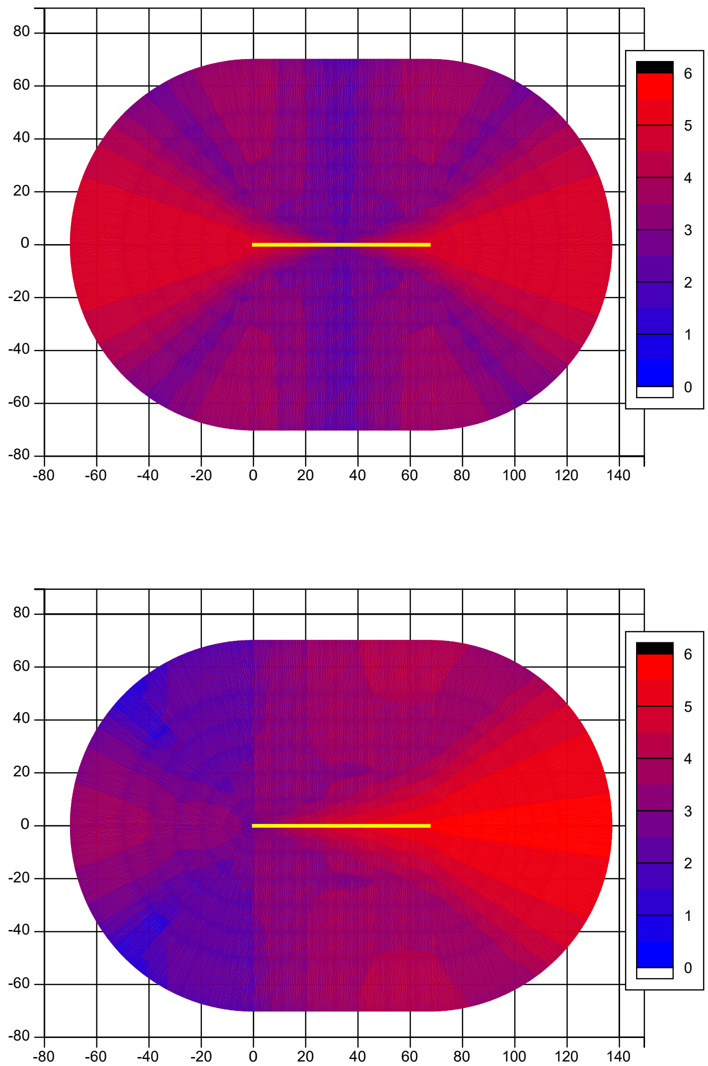

Figure 2.4 **The direct point parameter (DPP) for two moment-magnitude 7, strike–slip ruptures where the hypocenter of the upper figure is located at the center of the rupture and that of the lower is located 1 km from the left edge of the rupture length and 14 kilometers down-dip.**

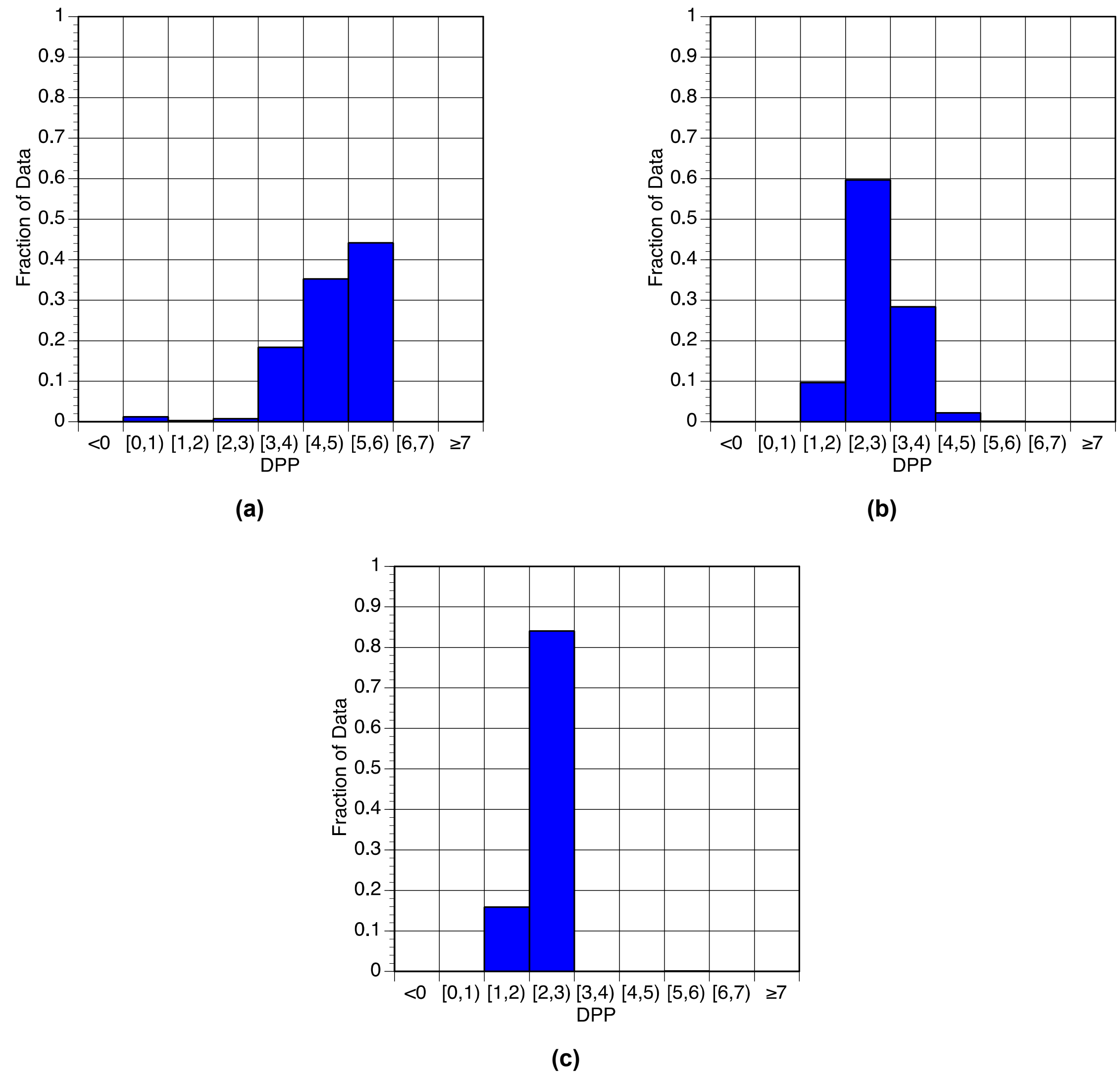

Figure 2.5 **Histogram of direct point parameter (DPP) for three sites 20 km from moment-magnitude 7, strike–slip ruptures where the hypocenters have been randomly distributed using hypocenter distribution models from Chiou and Youngs [2008]. The location of the sites are shown in Figure 2.4 where site a is located 20 km to the left of the edge of the top of the rupture and sites b and c are located counterclockwise from site a.**

These two example hypocenters show us the center and the extremes of the DPP distributions. If we look at three sites around the rupture, notice how the parameters $\hat{c}'$, $\overline{FS}$, and E affect DPP and its distribution. At sites off the very ends of the rupture, $\hat{c}'$ and $\overline{FS}$ remain very similar and high for the two hypocenters, but E varies from 0 to 70 km; this change in E causes the DPP value to vary from moderate to high values. If we look at a histogram of DPP values as shown in Figure 2.5(a), most of the DPP values are high, but there is a small tail down to very low DPP values corresponding to those hypocenters where E is 0. At sites roughly 45° from the end of the rupture, the greatest variability of DPP values are seen as at these sites $\overline{FS}$

$\overline{FS}$ and E are positively correlated; thus very small DPP values are calculated for near hypocenters, and very large DPP values are calculated for distant hypocenters. This is shown in Figure 2.5(b). Lastly, at sites off the sides of the rupture $\overline{FS}$ and E are inversely correlated, resulting in moderate DPP values with little variability as shown in Figure 2.5(c).

2.2.2 Mean Change

The change in the mean is calculated using Equation (1.4), where the change in pseudo-spectral acceleration is calculated using the Chiou and Youngs [2014] model, for the five strike–slip rupture scenarios detailed in Table 1.1. The change in the mean for 5% damped pseudo-spectral acceleration at 3 sec is shown for moment magnitudes of 6–8 in Figures 2.6–2.10. The results of these calculations are consistent with the DPP values presented in the previous section. There is an increase in the mean off the ends of the rupture and a slight decrease off the sides for the larger magnitudes. The smaller magnitude ruptures do not have as much variability, thus their change looks more like a DPP map from a rupture with a hypocenter in the center of the rupture with a large increase in the mean off the ends of the rupture, no change off the sides, and a reduction in the mean for sites 45°-angle off strike.

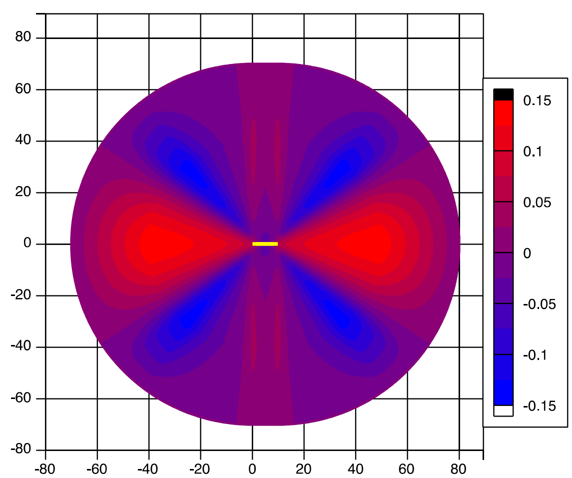

Figure 2.6 **Change in the mean of the natural log of the 5% damped pseudo-spectral acceleration at 3 sec due to the randomization of hypocenters using hypocenter distribution models from Chiou and Youngs [2008] for a moment-magnitude 6, strike–slip rupture.**

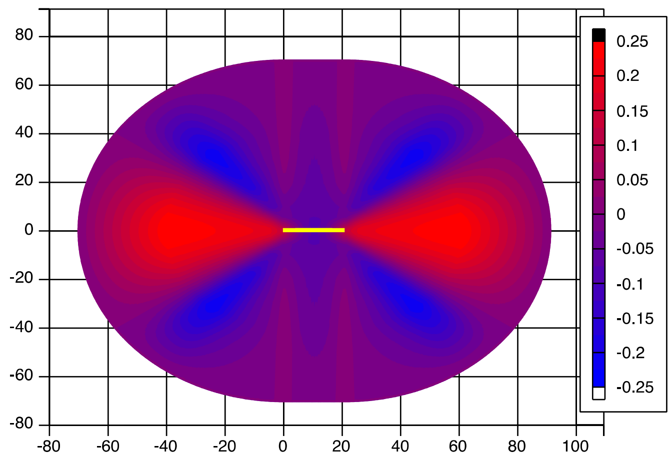

Figure 2.7 **Change in the mean of the natural log of the 5% damped pseudo-spectral acceleration at 3 sec due to the randomization of hypocenters using hypocenter distribution models from Chiou and Youngs [2008] for a moment-magnitude 6.5, strike–slip rupture.**

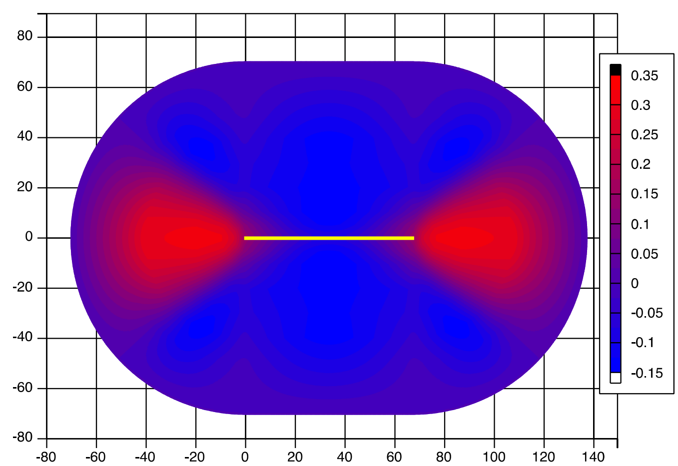

Figure 2.8 **Change in the mean of the natural log of the 5% damped pseudo-spectral acceleration at 3 sec due to the randomization of hypocenters using hypocenter distribution models from Chiou and Youngs [2008] for a moment-magnitude 7, strike–slip rupture.**

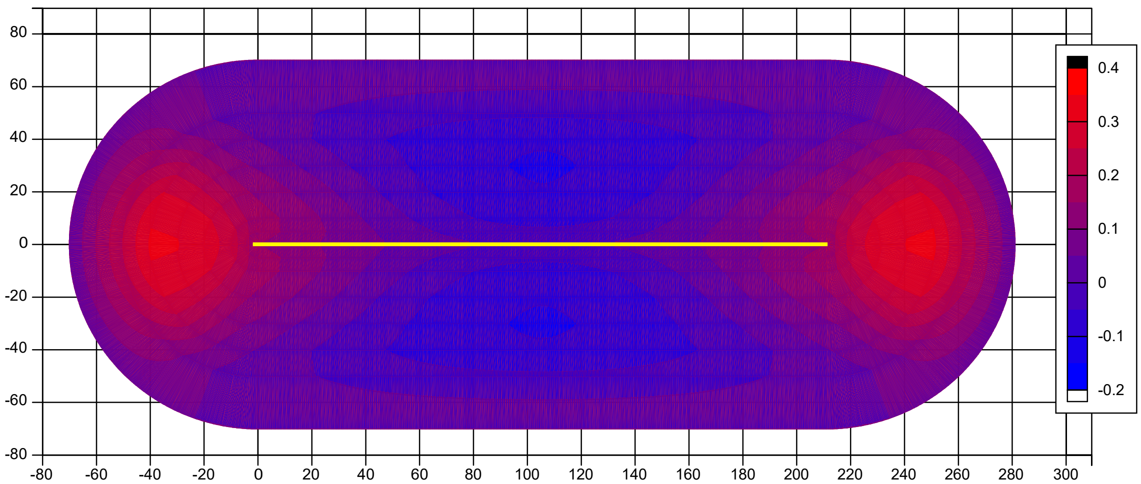

Figure 2.9 **Change in the mean of the natural log of the 5% damped pseudo-spectral acceleration at 3 sec due to the randomization of hypocenters using hypocenter distribution models from Chiou and Youngs [2008] for a moment-magnitude 7.5, strike–slip rupture.**

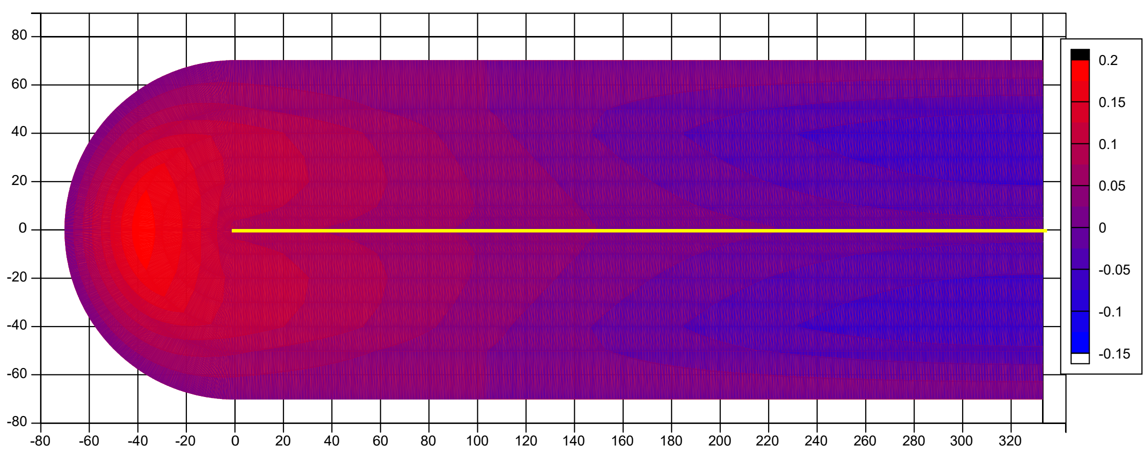

Figure 2.10 **Change in the mean of the natural log of the 5% damped pseudo-spectral acceleration at 3 sec due to the randomization of hypocenters using hypocenter distribution models from Chiou and Youngs [2008] for a moment-magnitude 8, strike–slip rupture.**

The period at which the peak directivity effect is located for each magnitude from the Chiou and Youngs [2014] model is predicted by the relationship between period and coefficient c_{8b} given in Table 2.1. The calculated change in the mean is shown for a magnitude 6.5 rupture at 1, 3 and 5 sec in Figures 2.11–2.13. These figures show that the effect peaks at 3 sec as predicted by this relationship. As the magnitude of the rupture increases, so does the peak calculated change in the mean, thus the amplitude of the peak effect for a magnitude 7 at 5 sec and shown in Figure 2.14, is larger than the peak effect for a magnitude 6.5 rupture at 3 sec and shown in Figure 2.12.

Table 2.1 Coefficient c_{8b} from Chiou and Youngs [2014].

Period	c_{8b}
0.40	4.3745
0.5	4.6099
0.75	5.0376
1	5.3411
1.5	5.7688
2	6.0723
3	6.5
4	6.8035
5	7.0389
7.5	7.4666

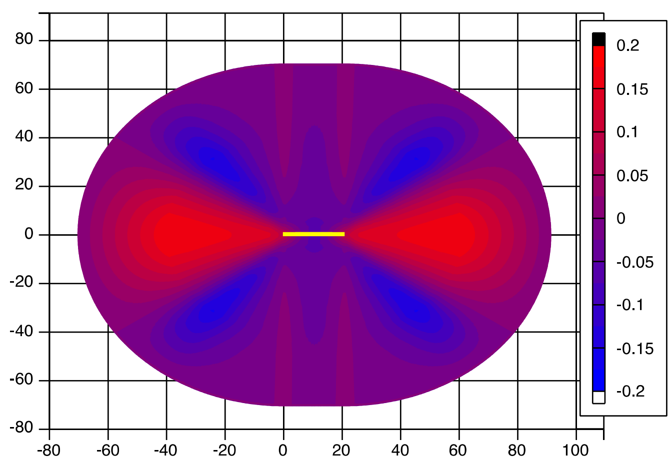

Figure 2.11 **Change in the mean of the natural log of the 5% damped pseudo-spectral acceleration at 1 sec due to the randomization of hypocenters using hypocenter distribution models from Chiou and Youngs [2008] for a moment-magnitude 6.5, strike–slip rupture.**

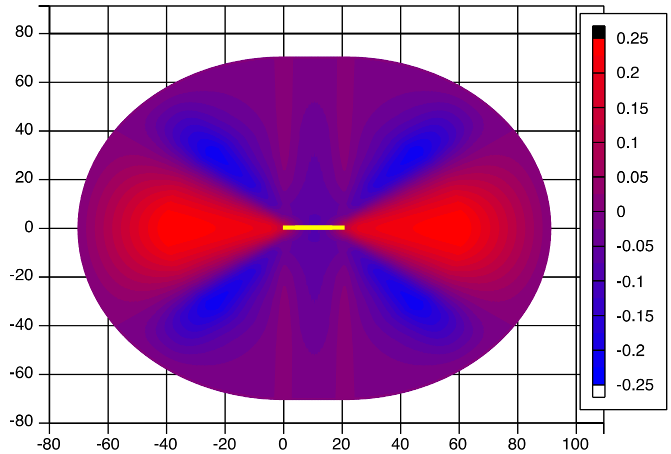

Figure 2.12 **Change in the mean of the natural log of the 5% damped pseudo-spectral acceleration at 3 sec due to the randomization of hypocenters using hypocenter distribution models from Chiou and Youngs [2008] for a moment-magnitude 6.5, strike–slip rupture.**

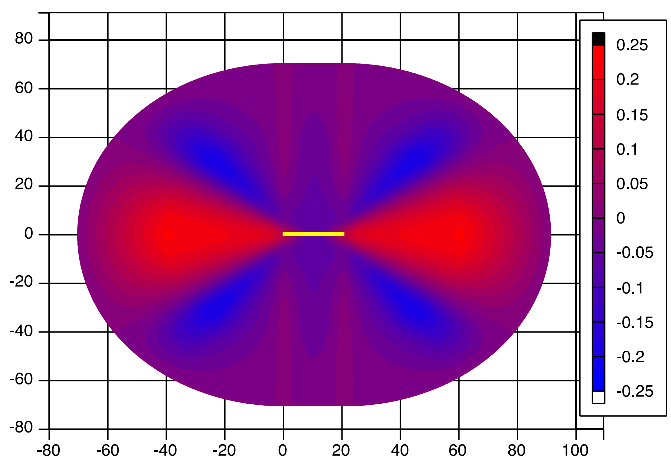

Figure 2.13 **Change in the mean of the natural log of the 5% damped pseudo-spectral acceleration at 5 sec due to the randomization of hypocenters using hypocenter distribution models from Chiou and Youngs [2008] for a moment-magnitude 6.5, strike–slip rupture.**

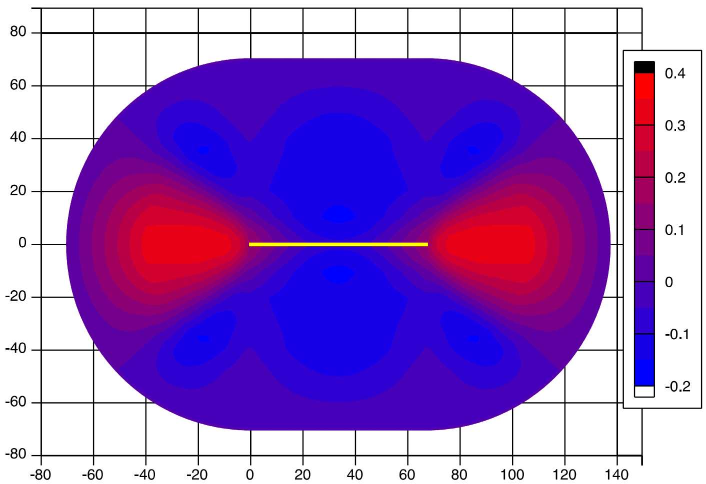

Figure 2.14 **Change in the mean of the natural log of the 5% damped pseudo-spectral acceleration at 5 sec due to the randomization of hypocenters using hypocenter distribution models from Chiou and Youngs [2008] for a moment-magnitude 7, strike–slip rupture.**

2.2.3 Standard Deviation Change Due to Randomization of Hypocenters

The change in the standard deviation due to randomization of hypocenters ($\phi_{i|RandomHypocenters}$) is calculated using Equation (1.5), where the change in pseudo-spectral acceleration is calculated using the Chiou and Youngs [2014] model, for the five strike–slip rupture scenarios detailed in Table 1.1. The calculated change in the standard deviation for 5% damped pseudo-spectral acceleration at 3 sec is shown for moment-magnitudes 7–8 in Figures 2.14–2.16. The results of these calculations are consistent with the DPP values presented in the previous section. There is an increase in the standard deviation at sites off the ends of the rupture and at sites that have an average of approximately 45° from strike.

The calculated change in the standard deviation is shown for a magnitude 6.5 rupture at 1, 3 and 5 sec in Figures 2.20–2.22. These figures show that the effect peaks at 3 sec as predicted by the relationship between period and c_{8b} from Table 2.1. As the magnitude of the rupture increases so does the peak calculated change in the standard deviation, thus the amplitude of the peak effect for a magnitude 7 at 5 sec and shown in Figure 2.23, is larger than the peak effect for a magnitude 6.5 rupture at 3 sec and shown in Figure 2.21.

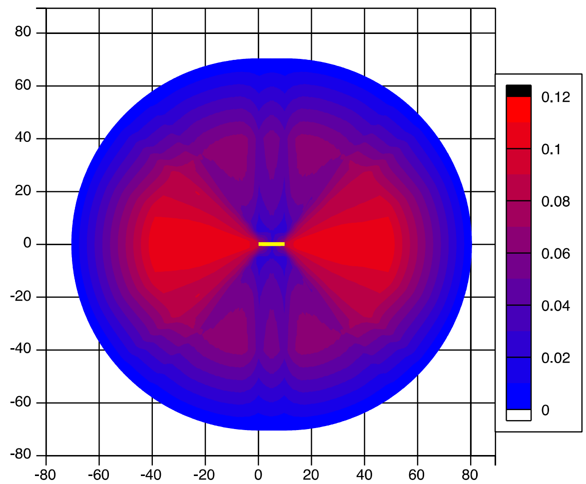

Figure 2.15 **Change in the standard deviation of the natural log of the 5% damped pseudo-spectral acceleration at 3 sec due to the randomization of hypocenters using hypocenter distribution models from Chiou and Youngs [2008] for a moment-magnitude 6, strike–slip rupture.**

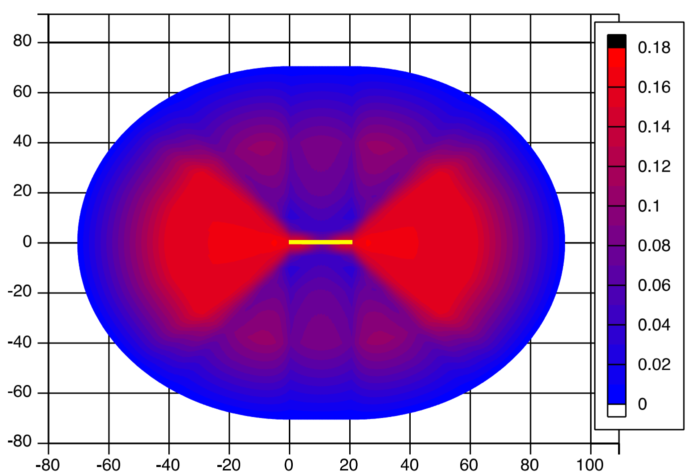

Figure 2.16 **Change in the standard deviation of the natural log of the 5% damped pseudo-spectral acceleration at 3 sec due to the randomization of hypocenters using hypocenter distribution models from Chiou and Youngs [2008] for a moment-magnitude 6.5, strike–slip rupture.**

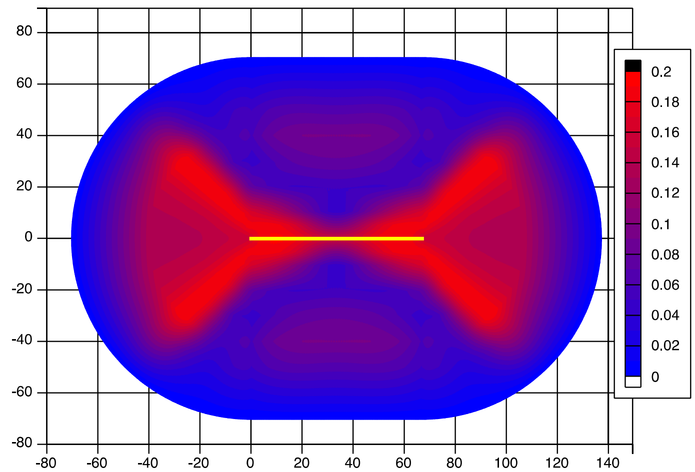

Figure 2.17 **Change in the standard deviation of the natural log of the 5% damped pseudo-spectral acceleration at 3 sec due to the randomization of hypocenters using hypocenter distribution models from Chiou and Youngs [2008] for a moment-magnitude 7, strike–slip rupture.**

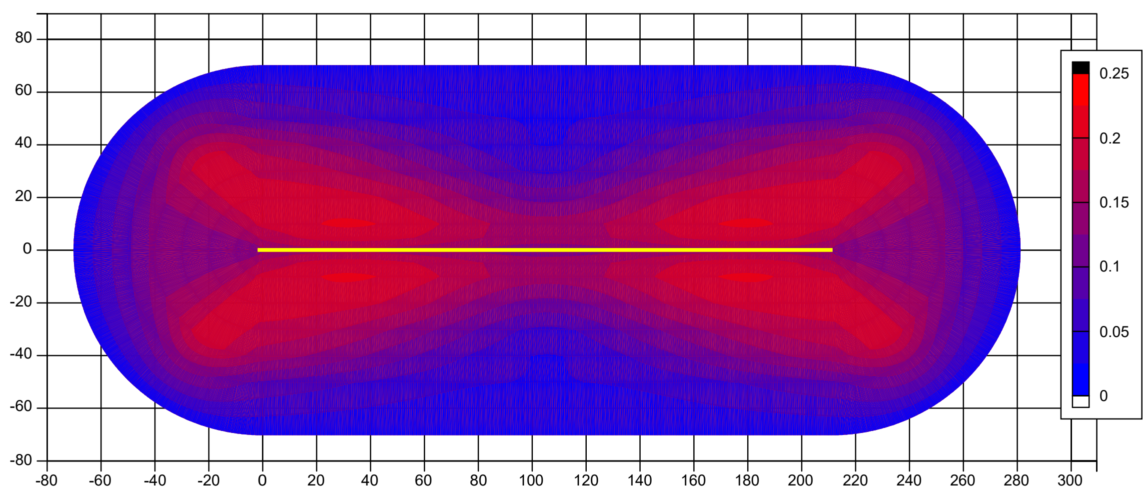

Figure 2.18 **Change in the standard deviation of the natural log of the 5% damped pseudo-spectral acceleration at 3 sec due to the randomization of hypocenters using hypocenter distribution models from Chiou and Youngs [2008] for a moment-magnitude 7.5, strike–slip rupture.**

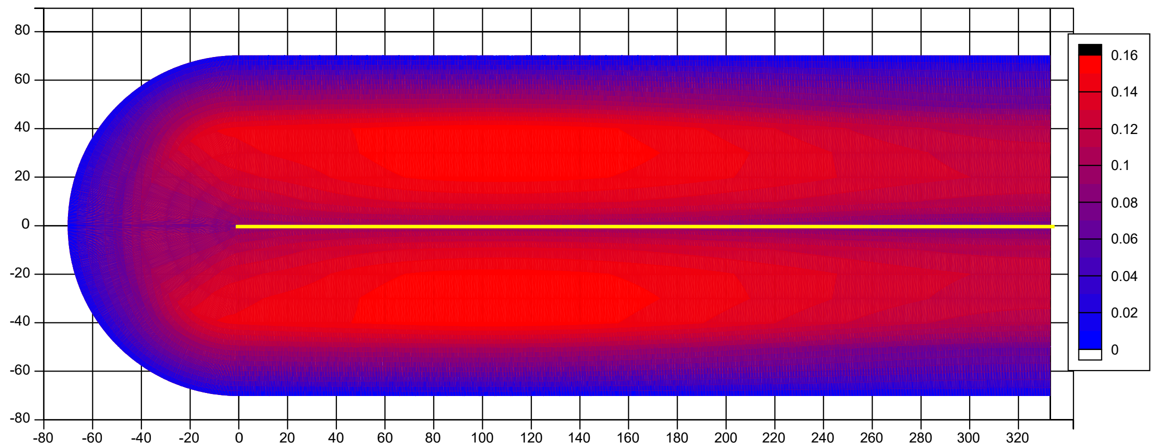

Figure 2.19 **Change in the standard deviation of the natural log of the 5% damped pseudo-spectral acceleration at 3 sec due to the randomization of hypocenters using hypocenter distribution models from Chiou and Youngs [2008] for a moment-magnitude 8, strike–slip rupture.**

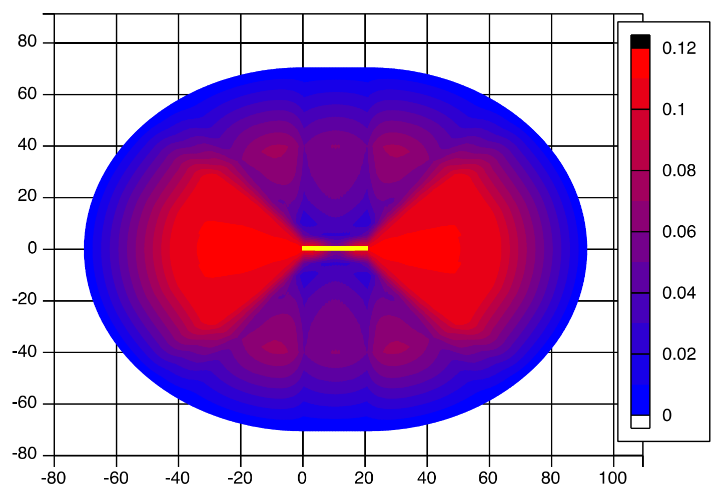

Figure 2.20 **Change in the standard deviation of the natural log of the 5% damped pseudo-spectral acceleration at 1 sec due to the randomization of hypocenters using hypocenter distribution models from Chiou and Youngs [2008] for a moment-magnitude 6.5, strike–slip rupture.**

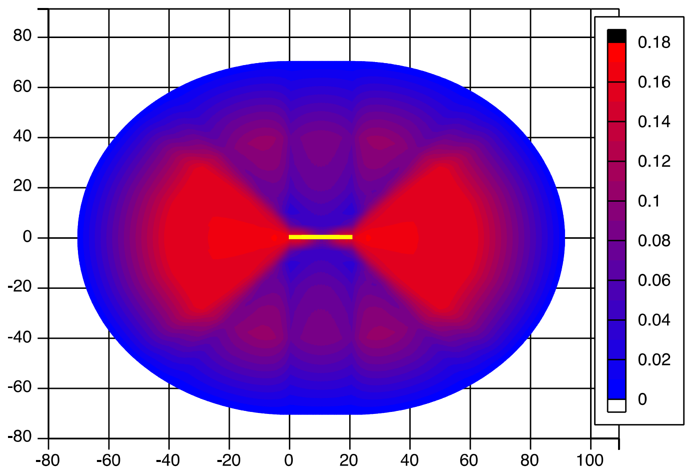

Figure 2.21 **Change in the standard deviation of the natural log of the 5% damped pseudo-spectral acceleration at 3 sec due to the randomization of hypocenters using hypocenter distribution models from Chiou and Youngs [2008] for a moment-magnitude 6.5, strike–slip rupture.**

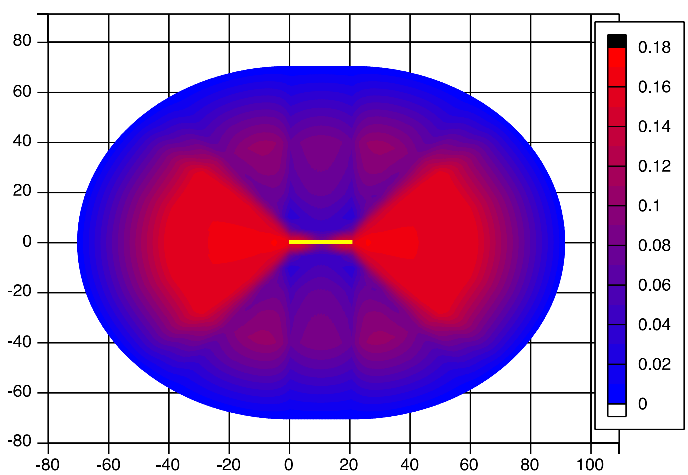

Figure 2.22 **Change in the standard deviation of the natural log of the 5% damped pseudo-spectral acceleration at 5 sec due to the randomization of hypocenters using hypocenter distribution models from Chiou and Youngs [2008] for a moment-magnitude 6.5, strike–slip rupture.**

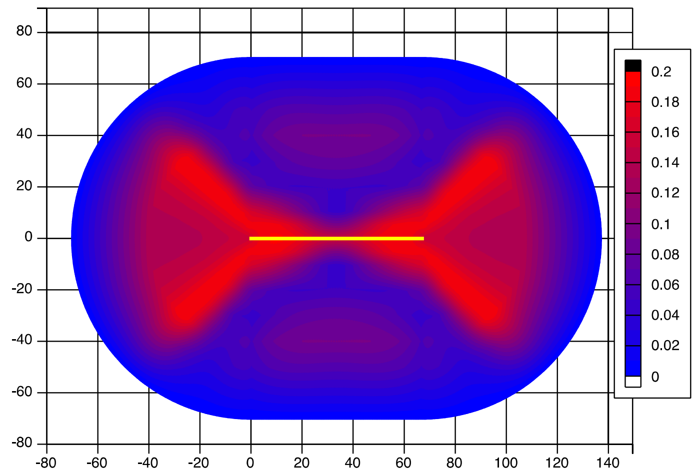

Figure 2.23 **Change in the standard deviation of the natural log of the 5% damped pseudo-spectral acceleration at 5 sec due to the randomization of hypocenters using hypocenter distribution models from Chiou and Youngs [2008] for a moment-magnitude 7, strike–slip rupture.**

2.2.4 Total Standard Deviation Change

The total change in the standard deviation is calculated using Equation (1.7), where $\phi_{i|RandomHypocenters}$ is from Section 2.2.3 and $\phi_{Reduction}$ is shown in Figure 1.2, for the five strike-slip rupture scenarios detailed in Table 1.1. $\phi_{Reduction}$ is not magnitude or distance dependent, but does increase with increasing period. The combined effect of the two cancels out at higher periods and smaller magnitudes, and reducing it slightly below $\phi_{i|RandomHypocenters}$ at smaller periods and larger magnitudes. This is demonstrated for 5% damped pseudo-spectral acceleration at 3 sec for moment-magnitude 6–8 ruptures shown in Figures 2.24–2.28. The standard deviation for the moment-magnitude 6 rupture is zero at every site. For the larger magnitudes, the change in standard deviation is smaller than shown in Section 2.2.3 and though the peak effect still increases with increasing magnitude, it does so at a smaller rate than previously.

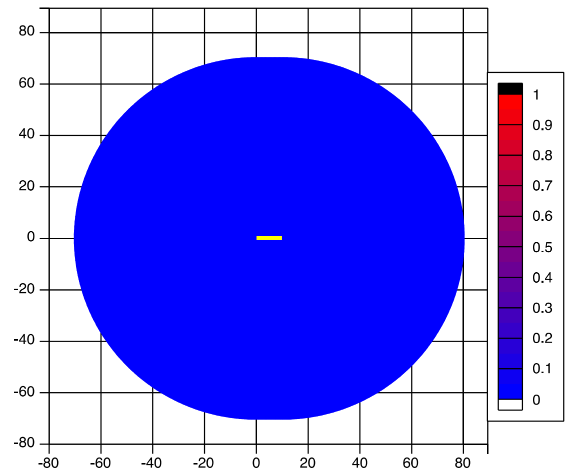

Figure 2.24 **Total change in the standard deviation of the natural log of the 5% damped pseudo-spectral acceleration at 3 sec using hypocenter distribution models from Chiou and Youngs [2008] for a moment-magnitude 6, strike–slip rupture.**

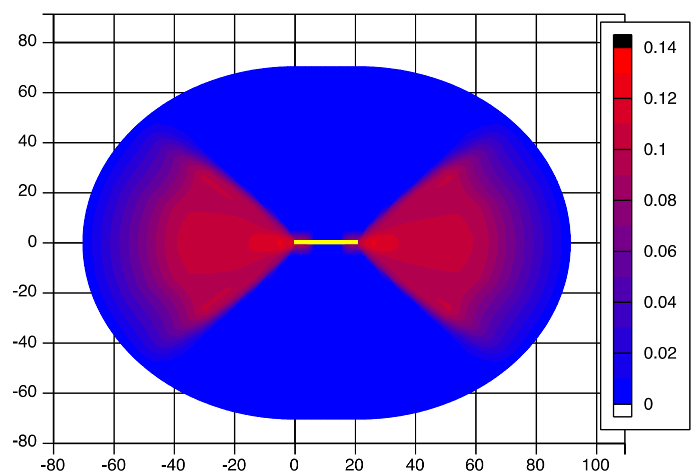

Figure 2.25 **Total change in the standard deviation of the natural log of the 5% damped pseudo-spectral acceleration at 3 sec using hypocenter distribution models from Chiou and Youngs [2008] for a moment-magnitude 6.5, strike–slip rupture.**

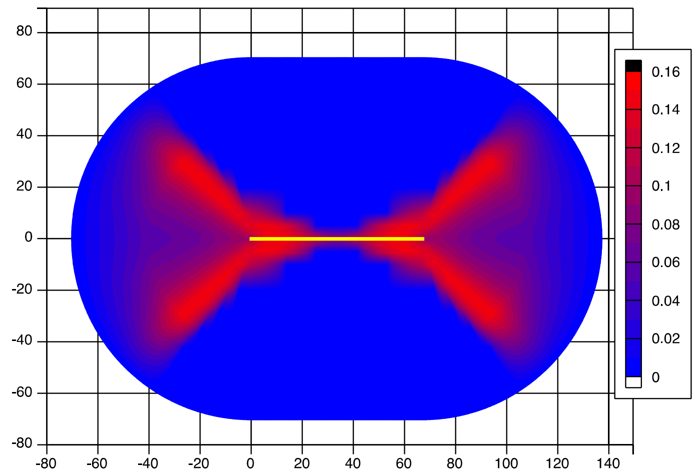

Figure 2.26 **Total change in the standard deviation of the natural log of the 5% damped pseudo-spectral acceleration at 3 sec using hypocenter distribution models from Chiou and Youngs [2008] for a moment-magnitude 7, strike–slip rupture.**

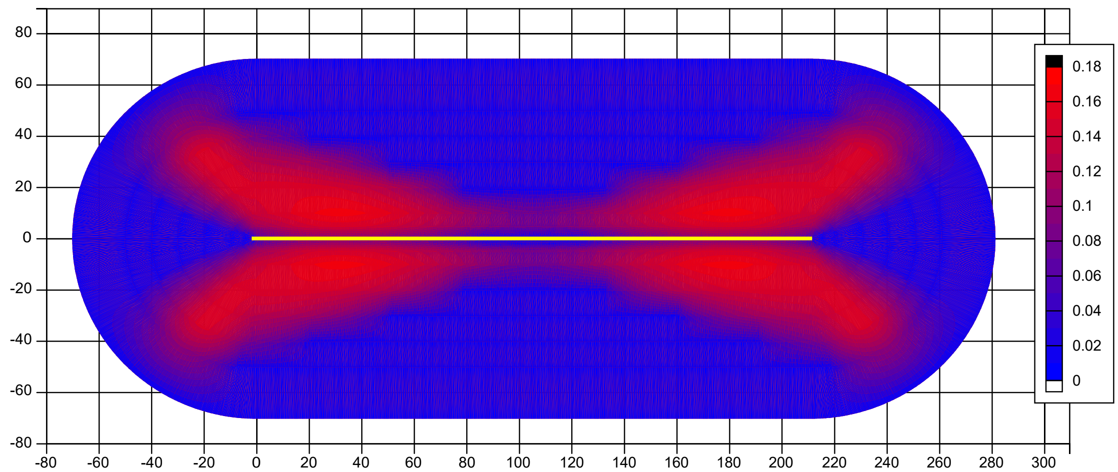

Figure 2.27 **Total change in the standard deviation of the natural log of the 5% damped pseudo-spectral acceleration at 3 sec using hypocenter distribution models from Chiou and Youngs [2008] for a moment-magnitude 7.5, strike–slip rupture.**

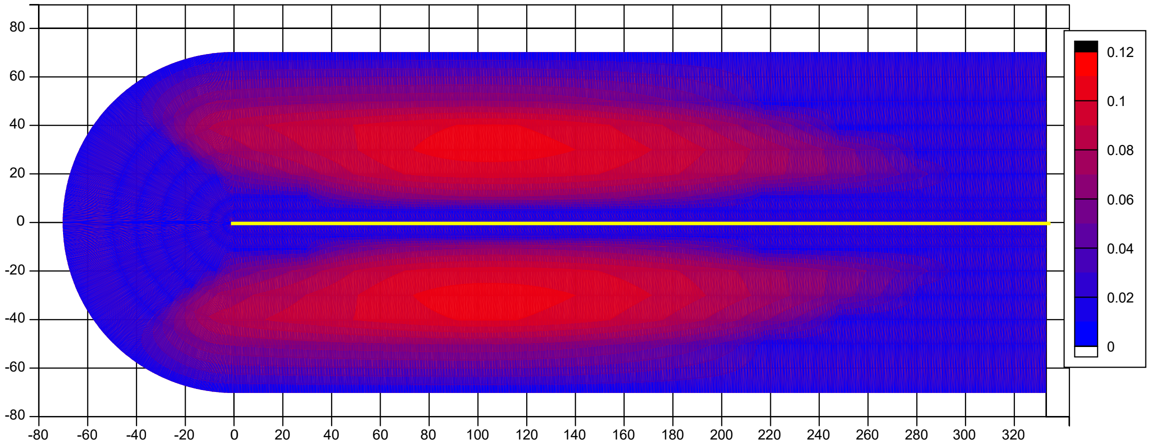

Figure 2.28 Total change in the standard deviation of the natural log of the 5% damped pseudo-spectral acceleration at 3 sec using hypocenter distribution models from Chiou and Youngs [2008] for a moment-magnitude 8, strike–slip rupture.

2.3 REVERSE RESULTS

2.3.1 Directivity Parameter DPP

The length E, isochrones velocity ratio ($\hat{c}'$), average shear-wave radiation ($\overline{FS}$), and DPP are presented in Figures 2.29—2.32 for two moments-magnitude 6.5 reverse ruptures. The first rupture has a hypocenter located in the middle of the rupture, and the second has a hypocenter located 1 km from the left-hand edge of the rupture and 14 km down-dip, as shown in the figures.

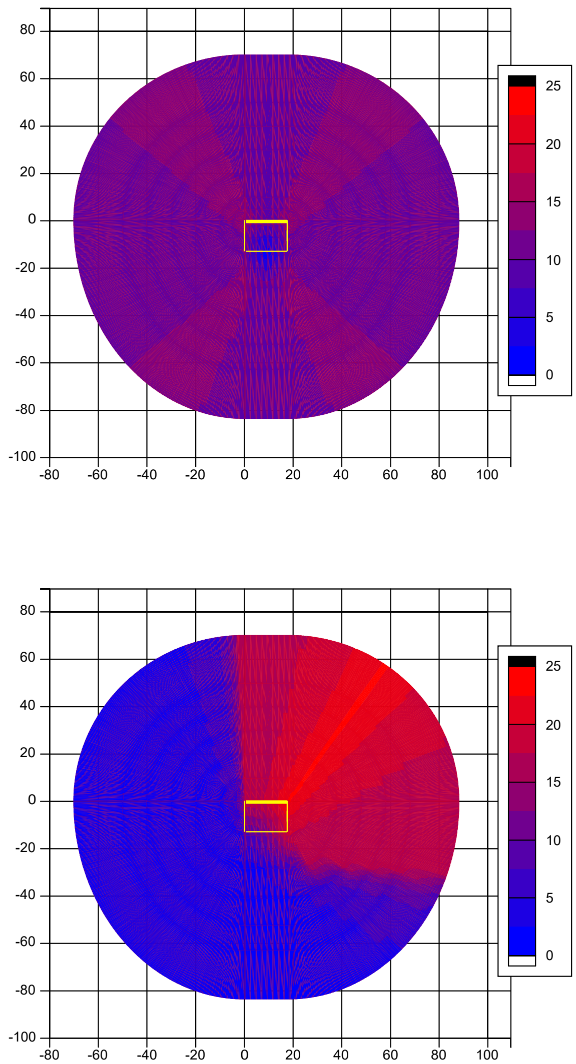

Figure 2.29 **The length of the fault from the hypocenter to the direct point (E) in kilometers for two moment-magnitude 6.5, dip-slip ruptures where the hypocenter of the upper figure is located at the center of the rupture and that of the lower is located 1 km from the left edge of the rupture length and 14 km down-dip.**

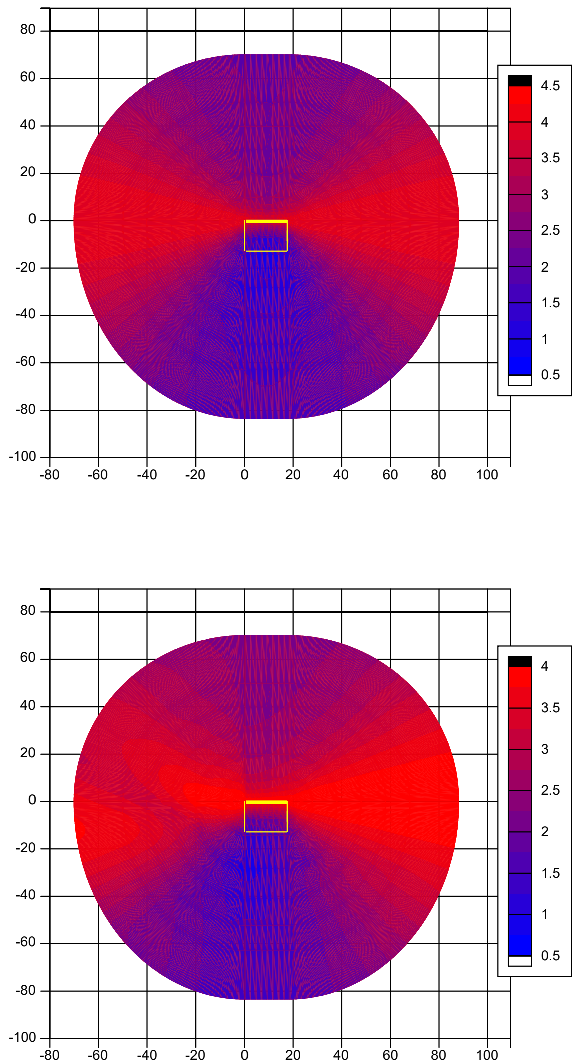

Figure 2.30 **The isochrone velocity ratio ($\hat{c}'$) along the length of the fault from the hypocenter to the direct point for two moment-magnitude 6.5, dip-slip ruptures where the hypocenter of the upper figure is located at the center of the rupture and that of the lower is located 1 km from the left edge of the rupture length and 14 km down-dip.**

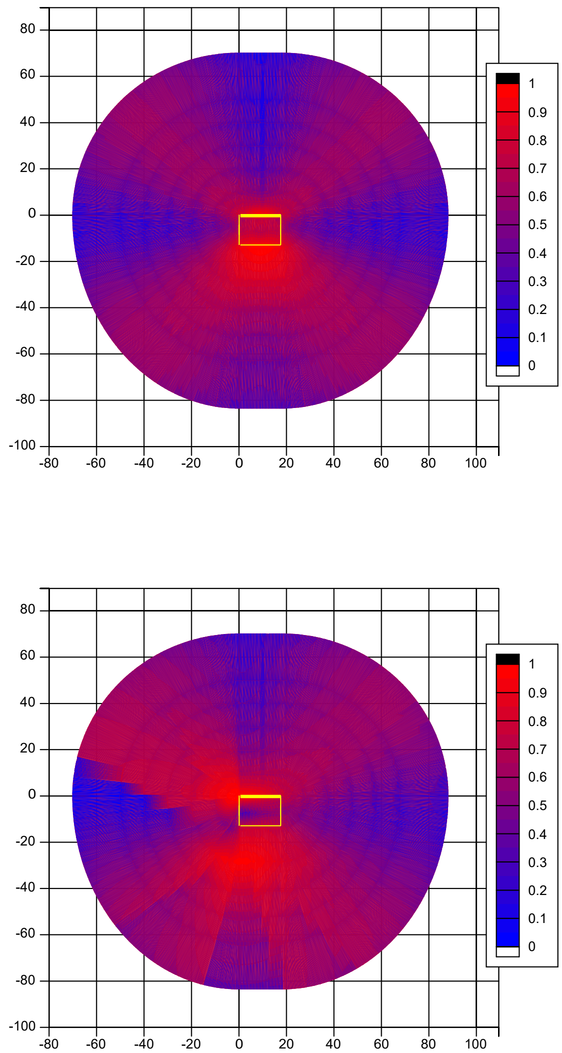

Figure 2.31 The average shear-wave radiation pattern ($\overline{FS}$) along the length of the fault from the hypocenter to the direct point for two moment-magnitude 6.5, dip-slip ruptures where the hypocenter of the upper figure is located at the center of the rupture and that of the lower is located 1 km from the left edge of the rupture length and 14 km down-dip.

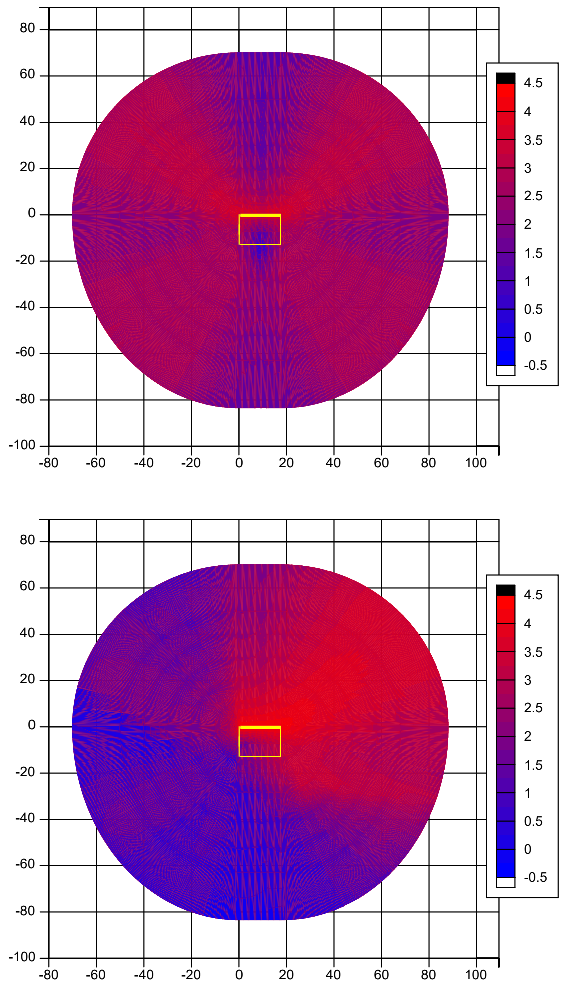

Figure 2.32 **The direct point parameter (DPP) for two moment-magnitude 6.5, dip-slip ruptures where the hypocenter of the upper figure is located at the center of the rupture and that of the lower is located 1 km from the left edge of the rupture length and 14 km down-dip.**

These two example hypocenters show the center and the extremes of the DPP distributions. A study of the three sites around the rupture demonstrate how the parameters $\hat{c}'$, $\overline{FS}$, and E effect DPP and its distribution. Similarly to the strike–slip results at sites off the very ends of the rupture, $\hat{c}'$ and $\overline{FS}$ are similar and high for both hypocenters, but E varies from 0 to 12 km; this change in E causes the DPP value to vary slightly but is generally moderate. At sites roughly 45° from the end of the rupture, the greatest variability of DPP values are seen at those sites where $\overline{FS}$ and E are positively correlated; thus very small DPP values are calculated for sites near hypocenters, and moderate DPP values are calculated for more distant hypocenters. As shown in the histogram of DPP values in Figure 2.33c, most of the DPP values are moderate, but there is a tail down to very low DPP values corresponding to those hypocenters where $\overline{FS}$ and E are small. For sites off the sides of the rupture, $\overline{FS}$ and E are inversely correlated, resulting in less little variability; see Figures 2.33(b) and 2.33(a). Lastly, sites on the footwall side of the rupture have a larger $\hat{c}'$ than hanging wall sites, resulting in larger DPP values as shown in Figures 2.33(b) and 2.33(a).

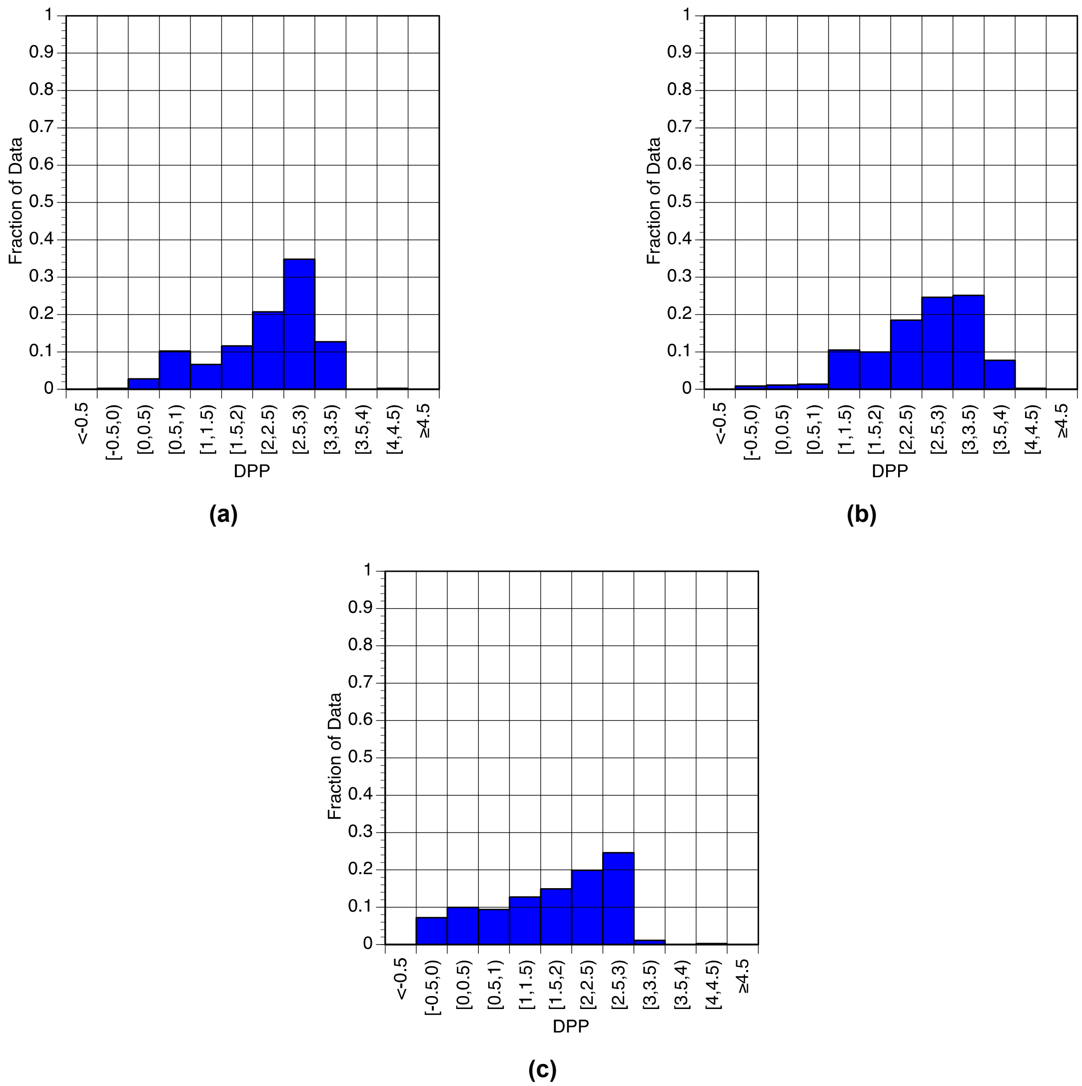

Figure 2.33 Histogram of direct point parameter (DPP) for three sites 20 km from moment-magnitude 6.5, dip-slip ruptures where the hypocenters have been randomly distributed using hypocenter distribution models from Chiou and Youngs [2008]. The location of the sites are shown in Figure 2.24 where the site a is located 14.7 km to the left and 19.12 km down from the left edge of the top of rupture and sites b and c are located clockwise from site a.

2.3.2 Mean Change

The change in the mean for the four reverse rupture scenarios detailed in Table 1.1 is calculated using Equation (1.4), where the change in pseudo-spectral acceleration is calculated using the Chiou and Youngs [2014] model. The change in the mean for 5% damped pseudo-spectral acceleration at 3 sec is shown for moment magnitudes of 6–7.5 in Figures 2.34–2.37. The results of these calculations are consistent with the DPP values presented in the previous section. There is an increase in the mean for those sites off the ends of the rupture, those that are approximately

45° off the end of the rupture, and footwall sites. There is a decrease in the mean for those sites on the hanging wall.

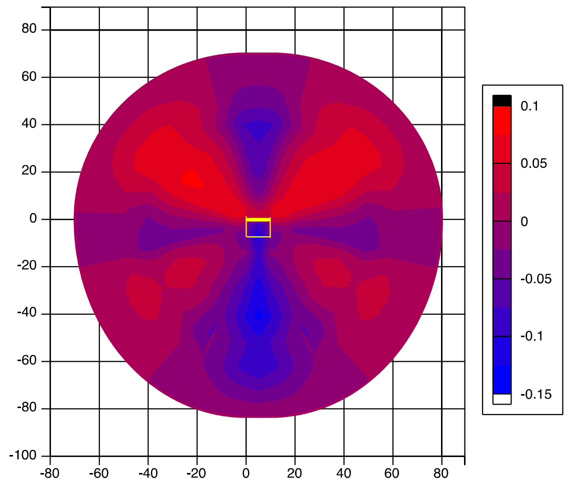

Figure 2.34 **Change in the mean of the natural log of the 5% damped pseudo-spectral acceleration at 3 sec due to the randomization of hypocenters using hypocenter distribution models from Chiou and Youngs [2008] for a moment-magnitude 6, reverse rupture.**

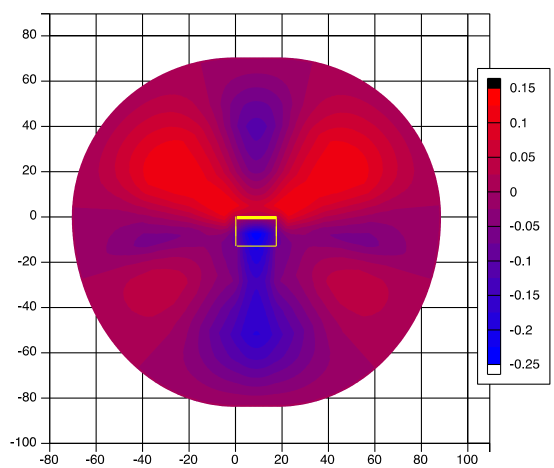

Figure 2.35 **Change in the mean of the natural log of the 5% damped pseudo-spectral acceleration at 3 sec due to the randomization of hypocenters using hypocenter distribution models from Chiou and Youngs [2008] for a moment-magnitude 6.5, reverse rupture.**

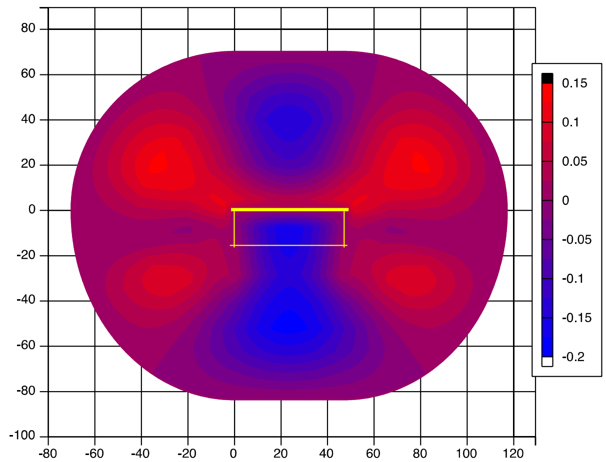

Figure 2.36 **Change in the mean of the natural log of the 5% damped pseudo-spectral acceleration at 3 sec due to the randomization of hypocenters using hypocenter distribution models from Chiou and Youngs [2008] for a moment-magnitude 7, reverse rupture.**

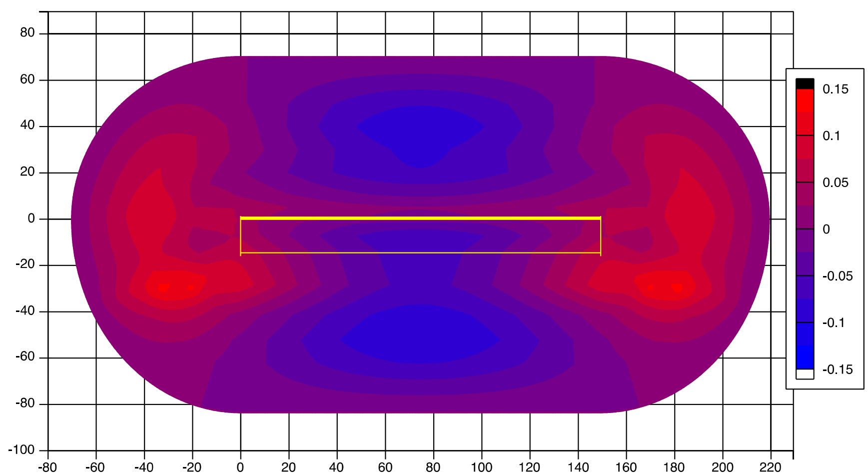

Figure 2.37 **Change in the mean of the natural log of the 5% damped pseudo-spectral acceleration at 3 sec due to the randomization of hypocenters using hypocenter distribution models from Chiou and Youngs [2008] for a moment-magnitude 7.5, reverse rupture.**

The calculated change in the mean is shown for a magnitude 6.5 rupture at 1, 3 and 5 sec in Figures 2.38–2.40. These figures show that the effect peaks at 3 sec as predicted by the relationship between period and c_{8b} from Table 2.1. As the magnitude of the rupture increases, so does the peak calculated change in the mean; thus the amplitude of the peak effect for a magnitude 7 at 5 sec (see Figure 2.41) is larger than the peak effect for a magnitude 6.5 rupture at 3 sec (see Figure 2.39).

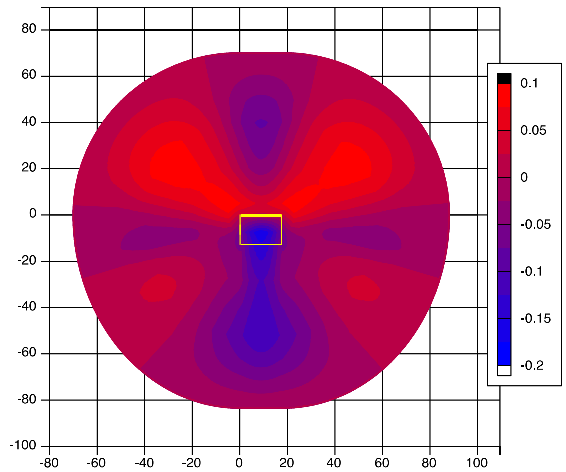

Figure 2.38 **Change in the mean of the natural log of the 5% damped pseudo-spectral acceleration at 1 sec due to the randomization of hypocenters using hypocenter distribution models from Chiou and Youngs [2008] for a moment-magnitude 6.5, reverse rupture.**

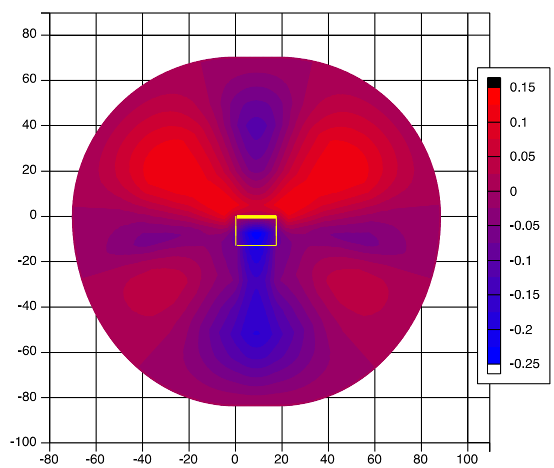

Figure 2.39 **Change in the mean of the natural log of the 5% damped pseudo-spectral acceleration at 3 sec due to the randomization of hypocenters using hypocenter distribution models from Chiou and Youngs [2008] for a moment-magnitude 6.5, reverse rupture.**

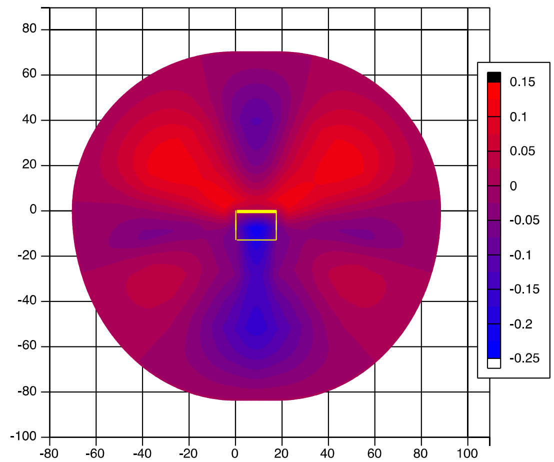

Figure 2.40 **Change in the mean of the natural log of the 5% damped pseudo-spectral acceleration at 5 sec due to the randomization of hypocenters using hypocenter distribution models from Chiou and Youngs [2008] for a moment-magnitude 6.5, reverse rupture.**

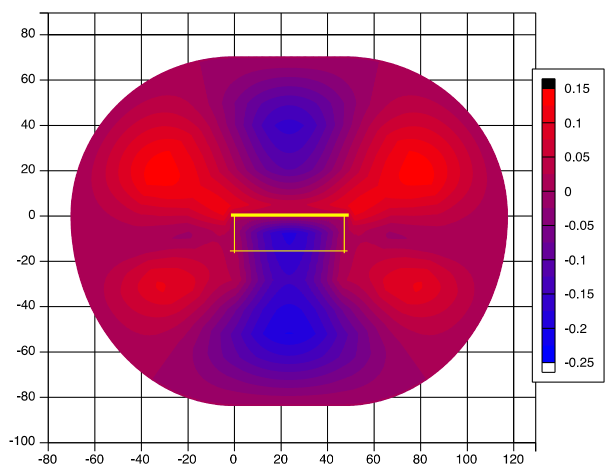

Figure 2.41 **Change in the mean of the natural log of the 5% damped pseudo-spectral acceleration at 5 sec due to the randomization of hypocenters using hypocenter distribution models from Chiou and Youngs [2008] for a moment-magnitude 7, reverse rupture.**

2.3.3 Standard Deviation Change Due to Randomization of Hypocenters

The change in the standard deviation due to randomization of hypocenters ($\phi_{i|RandomHypocenters}$) is calculated for the four reverse rupture scenarios detailed in Table 1.1 using Equation (1.5), where the change in pseudo-spectral acceleration is calculated using the Chiou and Youngs [2014] model,. The change in the mean for 5% damped pseudo-spectral acceleration at 3 sec is shown for moment magnitudes of 6–7.5 in Figures 2.42–2.45. The results of these calculations are consistent with the DPP values presented in the previous section. The change in standard deviation is largest over the hanging wall side of the rupture. This is the area where sites experience both shear wave maxima and minima, resulting in large variability.

The calculated change in the standard deviation is shown for a magnitude 6.5 rupture at 1, 3 and 5 sec shown in Figures 2.45–2.47. These figures show that the effect peaks at 3 sec as predicted by the relationship between period and c_{8b} from Table 2.1. In contrast to the strike–slip results and mean results, as the magnitude of the rupture increases, the peak calculated change in the standard deviation does not increase. The amplitude of the peak effect for a magnitude 7 at 5 sec (see Figure 2.48) is the same as the peak effect for a magnitude 6.5 rupture at 3 sec (see Figure 2.46).

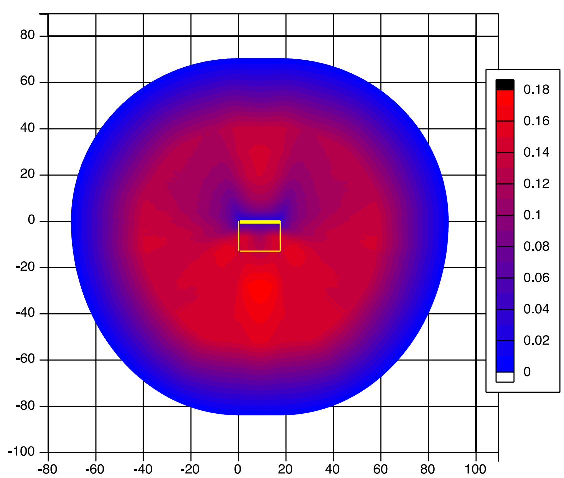

Figure 2.42 **Change in the standard deviation of the natural log of the 5% damped pseudo-spectral acceleration at 3 sec due to the randomization of hypocenters using hypocenter distribution models from Chiou and Youngs [2008] for a moment-magnitude 6.5, reverse rupture.**

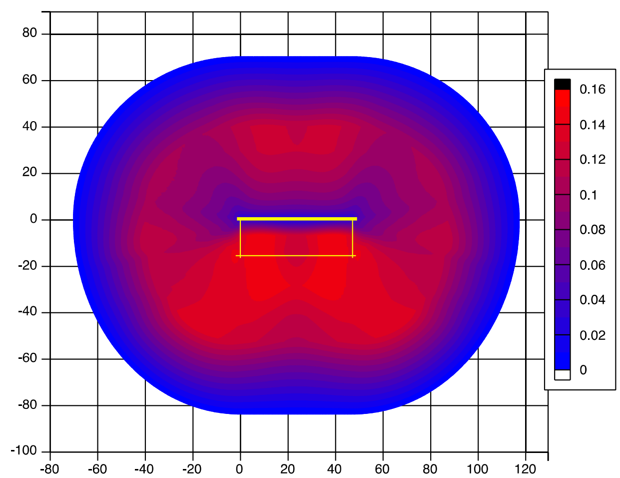

Figure 2.43 **Change in the standard deviation of the natural log of the 5% damped pseudo-spectral acceleration at 3 sec due to the randomization of hypocenters using hypocenter distribution models from Chiou and Youngs [2008] for a moment-magnitude 7, reverse rupture.**

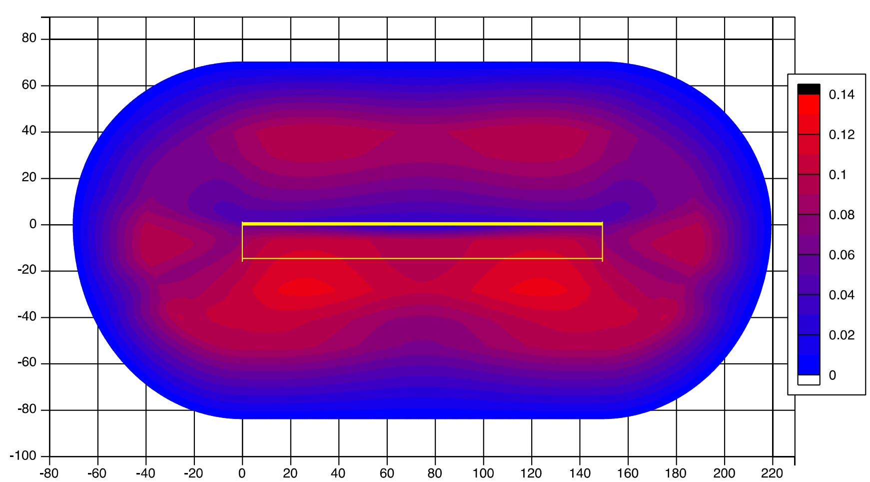

Figure 2.44 **Change in the standard deviation of the natural log of the 5% damped pseudo-spectral acceleration at 3 sec due to the randomization of hypocenters using hypocenter distribution models from Chiou and Youngs [2008] for a moment-magnitude 7.5, reverse rupture.**

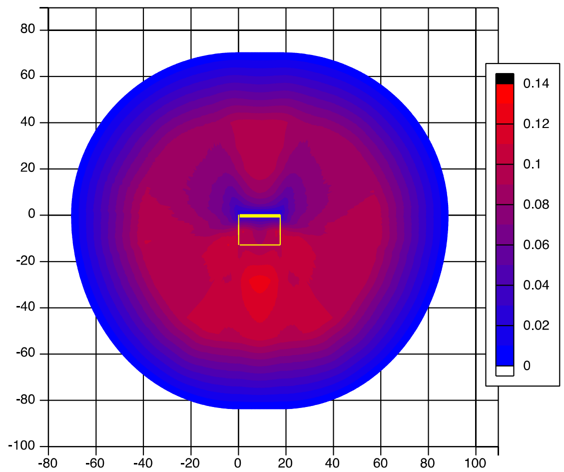

Figure 2.45 **Change in the standard deviation of the natural log of the 5% damped pseudo-spectral acceleration at 1 sec due to the randomization of hypocenters using hypocenter distribution models from Chiou and Youngs [2008] for a moment-magnitude 6.5, reverse rupture.**

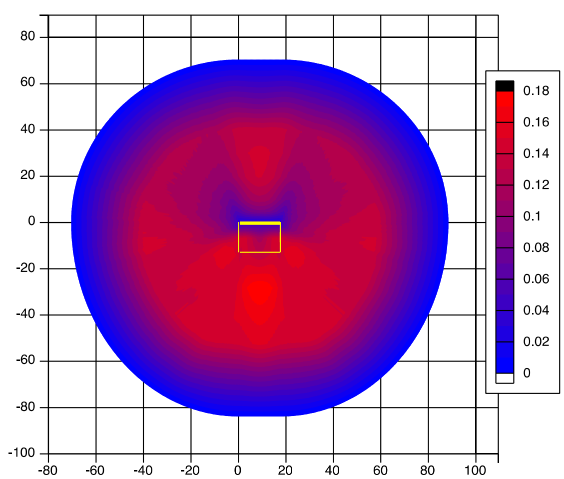

Figure 2.46 **Change in the standard deviation of the natural log of the 5% damped pseudo-spectral acceleration at 3 sec due to the randomization of hypocenters using hypocenter distribution models from Chiou and Youngs [2008] for a moment-magnitude 6.5, reverse rupture.**

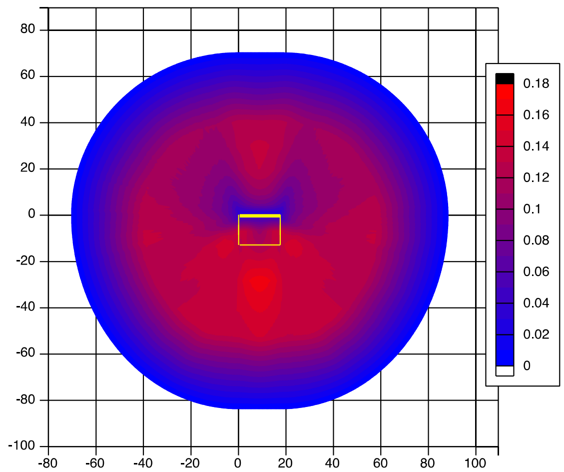

Figure 2.47 **Change in the standard deviation of the natural log of the 5% damped pseudo-spectral acceleration at 5 sec due to the randomization of hypocenters using hypocenter distribution models from Chiou and Youngs [2008] for a moment-magnitude 6.5, reverse rupture.**

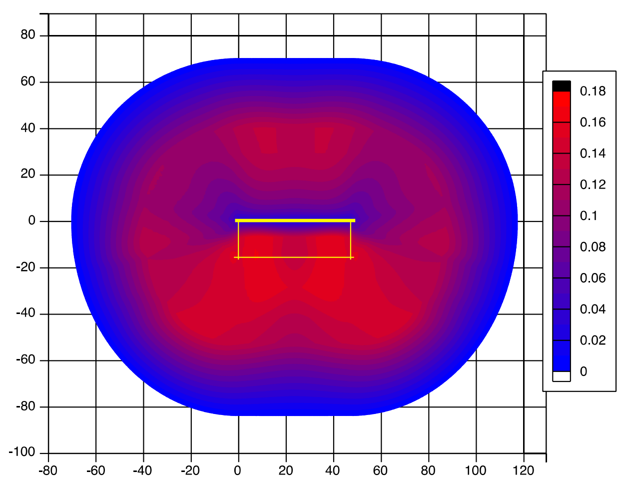

Figure 2.48 **Change in the standard deviation of the natural log of the 5% damped pseudo-spectral acceleration at 5 sec due to the randomization of hypocenters using hypocenter distribution models from Chiou and Youngs [2008] for a moment-magnitude 7, reverse rupture.**

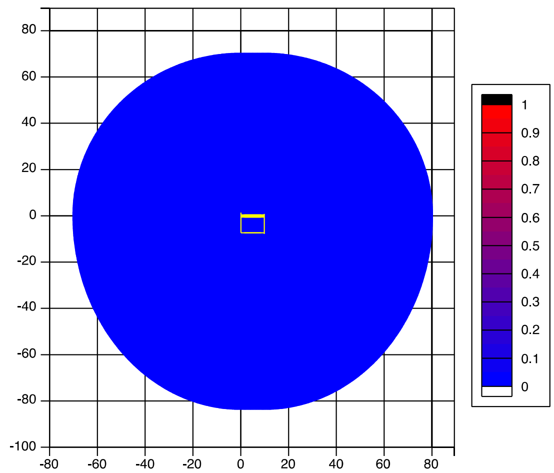

Figure 2.49 **Total change in the standard deviation of the natural log of the 5% damped pseudo-spectral acceleration at 3 sec using hypocenter distribution models from Chiou and Youngs (2008) for a moment-magnitude 6, reverse rupture.**

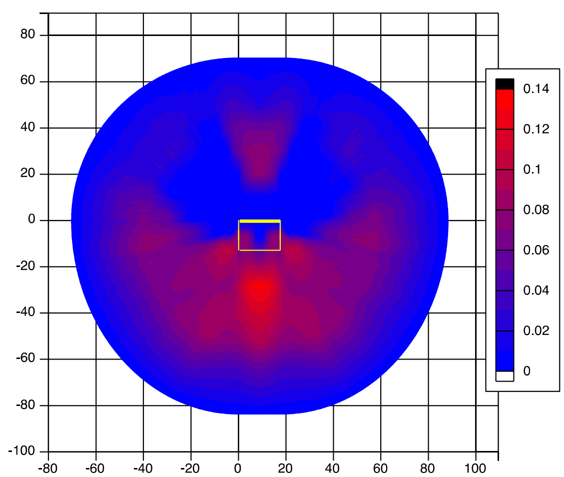

Figure 2.50 **Total change in the standard deviation of the natural log of the 5% damped pseudo-spectral acceleration at 3 sec using hypocenter distribution models from Chiou and Youngs [2008] for a moment-magnitude 6.5, reverse rupture.**

2.3.4 Total Standard Deviation Change

The total change in the standard deviation is calculated using Equation (1.7) for the four reverse rupture scenarios detailed in Table 1.1, where $\phi_{i|RandomHypocenters}$ is from Section 2.2.3 and $\phi_{Reduction}$ is shown in Figure 1.2. As shown in Figure 1.2, the ϕ_2 reduction is larger than the change in standard deviation for periods of 5 and greater and for the magnitude 6 change in standard deviation. This results in a zero change in the standard deviation at long periods and small magnitudes. For periods less than 5, the maximum total change in standard deviation is on the order of 0.1–0.17 or less for all magnitudes. The peak total change in standard deviation for each magnitude occurs at a period of 3 sec. The total change in standard deviation for 5% damped pseudo-spectral acceleration at 3 sec is shown for magnitudes 6–7.5 in Figures 2.49–2.52.

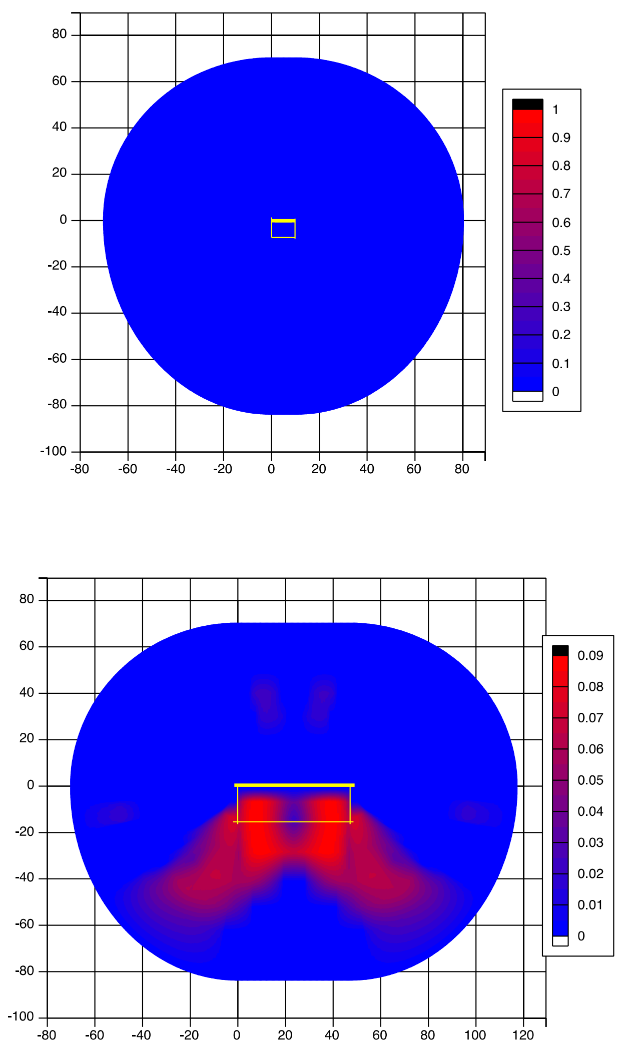

Figure 2.51 Total change in the standard deviation of the natural log of the 5% damped pseudo-spectral acceleration at 3 sec using hypocenter distribution models from Chiou and Youngs [2008] for a moment-magnitude 7, reverse rupture.

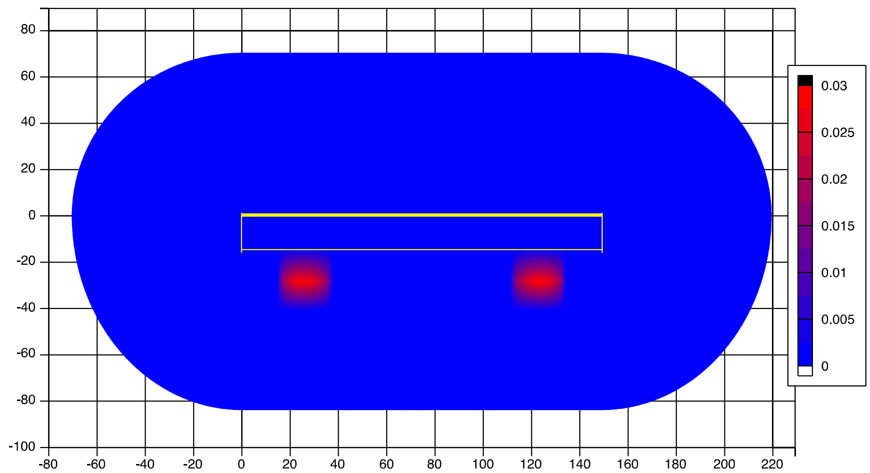

Figure 2.52 **Total change in the standard deviation of the natural log of the 5% damped pseudo-spectral acceleration at 3 sec using hypocenter distribution models from Chiou and Youngs [2008] for a moment-magnitude 7.5, reverse rupture.**

3 Models of Change in Ground Motion Mean and Standard Deviation

3.1 BASIC MODEL

The basic model for the directivity adjustment is the same for both strike–slip and reverse ruptures for both the mean and sigma. The basic model for the adjustment is given by:

$$Adjustment = \frac{c_{8,revised}}{c_{8,original}} * e^{b_M(Mag - c_{8b})^2} * Taper\_Dist * Taper\_Mag * Dir\_Factor \tag{3.1}$$

The first term of the model is the ratio of a revised c_8 coefficient developed by Brian Chiou in 2014 (Personal communication) with the original c_8 coefficient having a value of 0.2154 [Chiou and Youngs 2014]. This term reduces the directivity effect to zero at periods less than 0.5 sec. The second term creates a peak in the directivity effect at a period of c_{8b} as a function of magnitude. The form of the peak as well as the c_{8b} coefficients are from Chiou and Youngs [2014] and are given in Table 3.1.

Table 3.1 Coefficient c_8 and c_{8b} from Chiou and Youngs [2014].

Period	c_8 revised	c_{8b}
0.40	0	4.3745
0.5	0.0991	4.6099
0.75	0.1982	5.0376
1	0.2154	5.3411
1.5	0.2154	5.7688
2	0.2154	6.0723
3	0.2154	6.5
4	0.2154	6.8035
5	0.2154	7.0389
7.5	0.2154	7.4666
10	0.2154	7.77

Two tapers are applied to the directivity model by Chiou and Youngs [2014]. These tapers are used as a basis for the tapers on the change in mean and standard deviation. The distance taper is as follows:

$$Taper\_Dist = max\left(1 - \frac{max\left(Rrup - 40, 0\right)}{30}, 0\right) \tag{3.2}$$

where *Rrup* is the rupture distance in kilometers. The magnitude taper is as follows:

$$Taper\_Mag = min\left(\frac{max\left(Mag - 5.5, 0\right)}{0.8}, 1\right) \tag{3.3}$$

where *Mag* is the moment magnitude of the rupture.

3.2 STRIKE–SLIP MODEL

3.2.1 Mean Model

The *Dir_Factor* term for the change in mean of 5% damped pseudo-spectral acceleration for strike–slip ruptures is as follows:

$$Dir\_Factor_{SS} = b_0 + b_1\left(\max\left(RyRatio * \overline{\cos 2\theta}\right), -0.5\right) + b_2\left(\max\left(RyRatio * \overline{\cos 2\theta}\right), -0.5\right)^2 + b_3\left(\max\left(RyRatio * \overline{\cos 2\theta}\right), -0.5\right)^3 \tag{3.4}$$

where *RyRatio* and $\overline{cos2\theta}$ are as follows.

RyRatio is a measure of where the site is along the length of the rupture and is given by:

$$RyRatio = \min\left(\frac{|Ry|}{Length / 2}, 1\right) \tag{3.5}$$

where *Ry* is the site coordinate parallel to the strike of the surface projection of the rupture where zero is the center of the top of rupture in kilometers. For bending faults, the generalized coordinate system 2 is used to calculate *Ry* [Spudich and Chiou 2015], and *Length* is the length of the fault in kilometers.

The average value of $\cos 2\theta$ evaluated over the length of the surface projection of the top of rupture is $\overline{cos2\theta}$, and where θ is the angle between the ray from a point on the surface of rupture to the site and the ray from the same point along the strike. This is calculated using the following equation:

$$\overline{cos2\theta} = \frac{\left(\left(Ry + Length/2\right) - 2|Rx| * ArcTangent\left(\frac{Ry + Length/2}{|Rx|}\right)\right) - \left(\left(Ry - Length/2\right) - 2|Rx| * ArcTangent\left(\frac{Ry - Length/2}{|Rx|}\right)\right)}{Length} \tag{3.6}$$

where *Rx* is the site coordinate perpendicular to the strike of the surface projection of the top of rupture where zero is the center of the top of rupture and the positive direction is over the hanging wall (if any) in kilometers, and *Ry*, and *Length* are as described above.

The distance and magnitude tapers from Chiou and Youngs [2014] are modified to better fit the results. The peak change in the mean has a peak value at approximately 40 km from the rupture and decreases towards the rupture. Thus the distance taper is changed to the following:

$$Taper\_Dist = if \begin{cases} Rrup < r_0 & r_1\left(\dfrac{(Rrup - r_0)}{r_0}\right) + 1 \\ else & max\left(1 - \dfrac{max(Rrup - 40, 0)}{30}, 0\right) \end{cases} \tag{3.7}$$

where *Rrup* is the rupture distance in kilometers.

The peak change in the mean increases with magnitude, thus the magnitude taper is changed to the following:

$$Taper\_Mag = if \begin{cases} Mag < 6.3 & \dfrac{max(Mag - 5.5, 0)}{0.8} \\ else & 1 + m_1(Mag - 6.3) + m_2(Mag - 6.3)^2 \end{cases} \tag{3.8}$$

where *Mag* is the moment magnitude of the rupture.

Coefficients for the model of the change in mean for strike–slip ruptures were estimated using a least-squares regressions and are given in Table 3.2. The model and data for 5% damped pseudo-spectral acceleration at 3 sec are shown with respect to the combined parameter $RyRatio * \overline{\cos 2\theta}$ for moment-magnitudes 6–8 shown in Figures 3.1–3.5.

Table 3.2 Coefficients for model of change in mean for strike–slip ruptures.

Coefficient	Value	Standard error
b_0	-0.110972	0.000245
b_1	0.0345899	0.000279
b_2	0.433312	0.001190
b_3	-0.128870	0.000815
r_o	16.7488	0.065292
r_1	0.574546	0.001269
m_1	0.948640	0.006477
m_2	-0.436357	0.003069
b_M	-0.269988	0.000415
Sigma	0.015801	

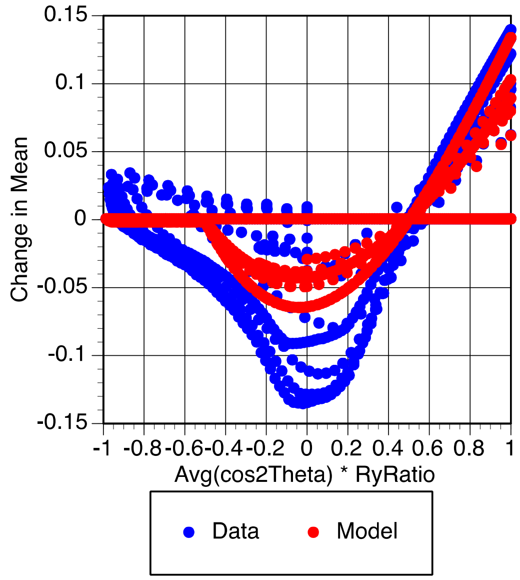

Figure 3.1 **Data and model of change in the mean of the natural log of the 5% damped pseudo-spectral acceleration at 3 sec due to the randomization of hypocenters using Chiou and Youngs [2008] hypocenter distribution models for a moment-magnitude 6, strike–slip rupture.**

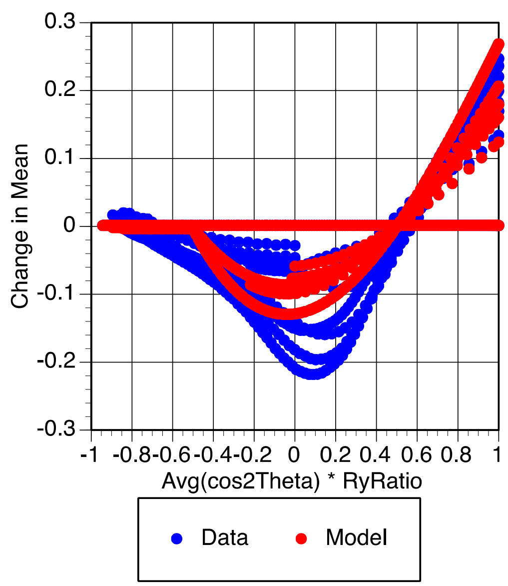

Figure 3.2 **Data and model of change in the mean of the natural log of the 5% damped pseudo-spectral acceleration at 3 sec due to the randomization of hypocenters using Chiou and Youngs [2008] hypocenter distribution models for a moment-magnitude 6.5, strike–-slip rupture.**

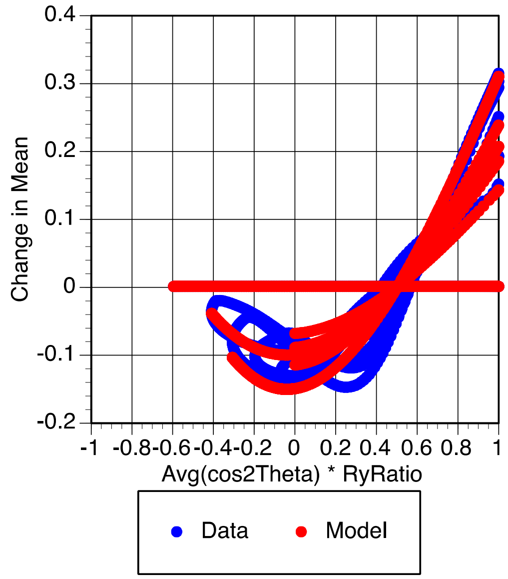

Figure 3.3 **Data and model of change in the mean of the natural log of the 5% damped pseudo-spectral acceleration at 3 sec due to the randomization of hypocenters using Chiou and Youngs [2008] hypocenter distribution models for a moment-magnitude 7, strike–slip rupture.**

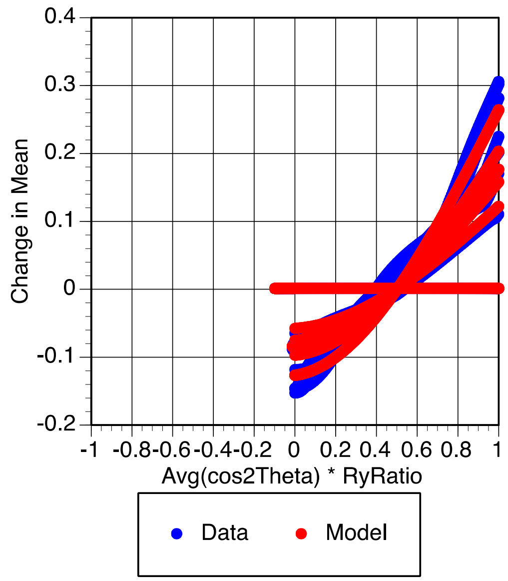

Figure 3.4 **Data and model of change in the mean of the natural log of the 5% damped pseudo-spectral acceleration at 3 sec due to the randomization of hypocenters using Chiou and Youngs [2008] hypocenter distribution models for a moment-magnitude 7.5, strike–slip rupture.**

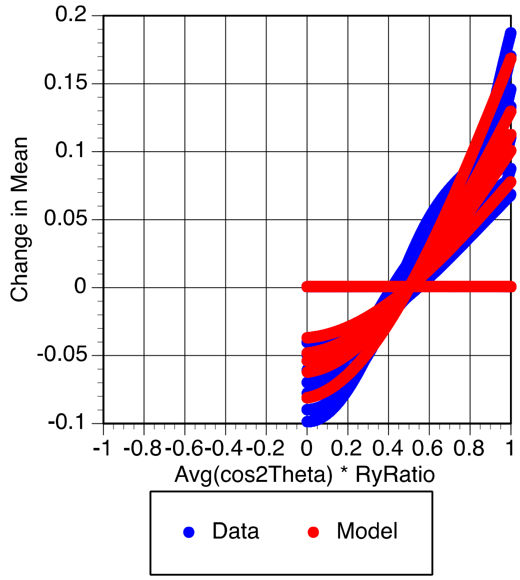

Figure 3.5 Data and model of change in the mean of the natural log of the 5% damped pseudo-spectral acceleration at 3 sec due to the randomization of hypocenters using Chiou and Youngs [2008] hypocenter distribution models for a moment-magnitude 8, strike–slip rupture.

3.2.2 Standard Deviation Model

The *Dir_Factor* term and tapers for the change in standard deviation of 5% damped pseudo-spectral acceleration for strike–slip ruptures are the same as for the median and are given in Equations (3.4), (3.7) and (3.8), respectively. Coefficients for the model for the change in standard deviation for strike slip were estimated using a least-squares regressions and are given in Table 3.3. The model and data for 5% damped pseudo-spectral acceleration at 3 sec are shown with respect to the combined parameter $RyRatio * \overline{\cos 2\theta}$ for moment-magnitudes 6–8 shown in Figures 3.6–3.10.

Table 3.3 Coefficients for model of change in standard deviation for strike–slip ruptures.

Coefficient	Value	Standard error
b_0	0.0160638	0.000218
b_1	0.102589	0.001127
b_2	0.174049	0.001653
b_3	-0.273383	0.002450
r_o	17.4688	0.211929
r_1	0.627373	0.003879
m_1	0.578942	0.022945
m_2	-0.308831	0.010811
b_M	-0.0554069	0.000640
Sigma	0.0311712	

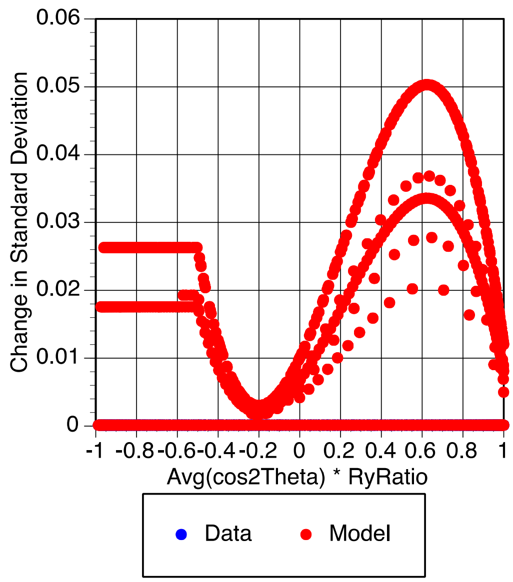

Figure 3.6 Data and model of change in the standard deviation of the natural log of the 5% damped pseudo-spectral acceleration at 3 sec due to the randomization of hypocenters using Chiou and Youngs [2008] hypocenter distribution models for a moment-magnitude 6, strike–slip rupture.

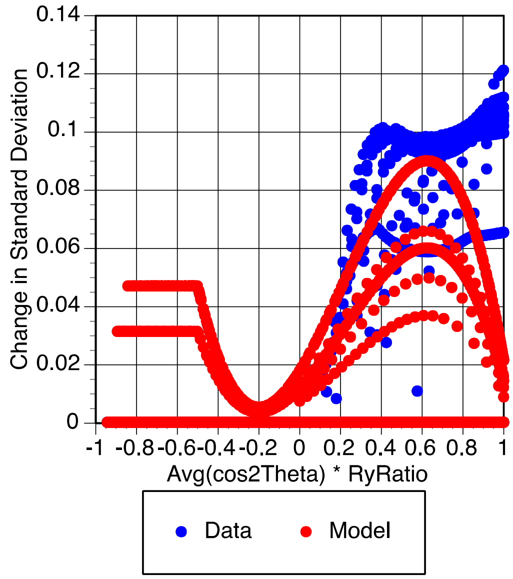

Figure 3.7 **Data and model of change in the standard deviation of the natural log of the 5% damped pseudo-spectral acceleration at 3 sec due to the randomization of hypocenters using Chiou and Youngs [2008] hypocenter distribution models for a moment-magnitude 6.5, strike–slip rupture.**

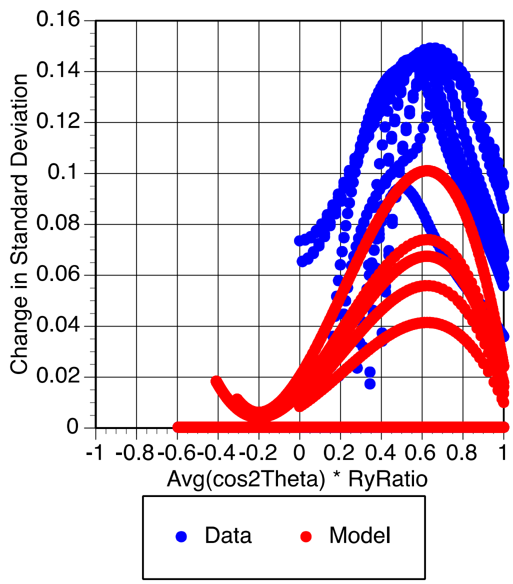

Figure 3.8 **Data and model of change in the standard deviation of the natural log of the 5% damped pseudo-spectral acceleration at 3 sec due to the randomization of hypocenters using Chiou and Youngs [2008] hypocenter distribution models for a moment-magnitude 7, strike–slip rupture.**

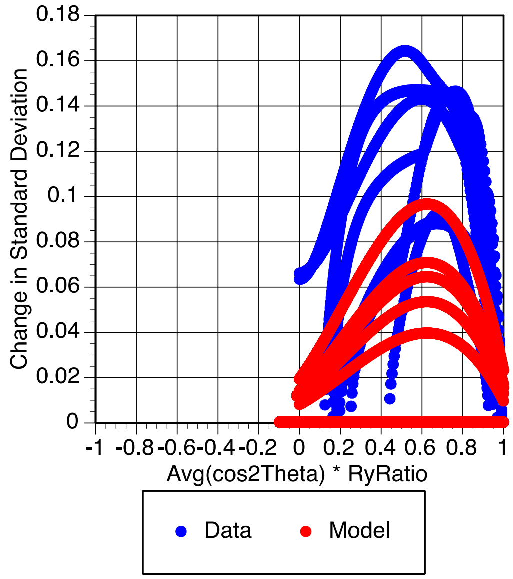

Figure 3.9 **Data and model of change in the standard deviation of the natural log of the 5% damped pseudo-spectral acceleration at 3 sec due to the randomization of hypocenters using Chiou and Youngs [2008] hypocenter distribution models for a moment-magnitude 7.5, strike—slip rupture.**

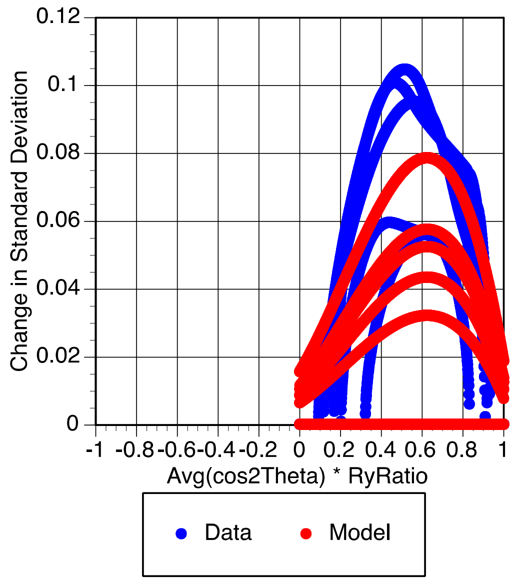

Figure 3.10 **Data and model of change in the standard deviation of the natural log of the 5% damped pseudo-spectral acceleration at 3 sec due to the randomization of hypocenters using Chiou and Youngs [2008] hypocenter distribution models for a moment-magnitude 8, strike–slip rupture.**

3.3 REVERSE MODEL

3.3.1 Mean Model

The *Dir_Factor* term for the change in mean of 5% damped pseudo-spectral acceleration for reverse ruptures is as follows:

$$Dir\_Factor_{RV} = \left\{ \begin{array}{l} b_0 + b_1\left(RyRatio * \overline{sin2\theta}' * HW \right) + b_2\left(RyRatio * \overline{sin2\theta}' * HW \right)^2 + b_3\left(RyRatio * \overline{sin2\theta}' * HW \right)^3 + \\ b_4\overline{cos2\phi} + b_5\overline{cos2\phi}^2 + b_6\overline{cos2\phi}^3 + \\ b_7\left(RyRatio * \overline{cos2\theta}' \right) + b_8\left(RyRatio * \overline{cos2\theta}' \right)^2 + b_9\left(RyRatio * \overline{cos2\theta}' \right)^3 \end{array} \right\} \tag{3.9}$$

where *RyRatio* is defined using Equation (3.5), and HW is -1 on the hanging-wall side of the rupture and 1 elsewhere; $\overline{cos2\phi}$, $\overline{cos2\theta}'$, and $\overline{sin2\theta}'$ are defined below.

$\overline{cos2\phi}$ is the average value of $\cos 2\phi$ evaluated in the plane perpendicular to rupture over the width of the rupture, and where ϕ is the angle between the ray from a point on the rupture to the site and the ray from the same point up dip. This is calculated using the following equation:

$$\overline{cos2\phi} = \frac{\left((Rx\sin\delta) - 2\left|Rx\cos\delta\right| * ArcTangent\left(\frac{Rx\sin\delta}{\left|Rx\cos\delta\right|} \right) \right) - \left((Rx\sin\delta - Width) - 2\left|Rx\cos\delta\right| * ArcTangent\left(\frac{Rx\sin\delta - Width}{\left|Rx\cos\delta\right|} \right) \right)}{Width} \tag{3.10}$$

where *Rx* is the site coordinate perpendicular to the strike of the surface projection of the top of rupture where zero is the center of the top of rupture and the positive direction is over the hanging wall (if any) in kilometers. *Ry* is the site coordinate parallel to the strike of the surface projection of the rupture where zero is the center of the top of rupture in kilometers, δ is the dip, and *Width* is the width of the rupture in kilometers. For bending faults, the generalized coordinate system 2 is used to calculate *Rx* and *Ry* [Spudich and Chiou 2015].

The average value of $\overline{cos2\theta}$ evaluated on the line halfway down-dip of the rupture projected onto the surface is $\overline{cos2\theta}'$. This is calculated using Equation (3.6) and exchanging *Rx* with coordinate Rx' calculated from the center of the fault. Rx' is calculated as follows:

$$Rx' = Rx + Width * cos\,\delta \tag{3.11}$$

where *Rx* is defined above, δ is the dip, and *Width* is the width of the rupture in kilometers.

The average value of $\overline{sin2\theta}$ evaluated on the line halfway down-dip of the rupture projected onto the surface is $\overline{sin2\theta}'$. This is calculated as follows

$$\overline{sin2\theta}' = \left| \frac{|Rx'| * ln\left(\left(Ry + \frac{Length}{2}\right)^2 + Rx'^2\right) - |Rx'| * ln\left(\left(Ry - \frac{Length}{2}\right)^2 + Rx'^2\right)}{Length} \right| \tag{3.12}$$

where Rx' and Ry are defined above, and *Length* is the length of the rupture in kilometers.

The distance and magnitude tapers from Chiou and Youngs [2014] are modified to better fit the results. The change in the mean becomes closer to zero at sites close to the rupture. Thus the distance taper is changed to the following:

$$Taper\_Dist = if \begin{cases} Rrup < r_0 & r_1\left(\frac{(Rrup - r_0)}{r_0}\right) + 1 \\ else & max\left(1 - \frac{max(Rrup - 40, 0)}{30}, 0\right) \end{cases} \tag{3.13}$$

where *Rrup* is the rupture distance in kilometers.

The peak change in the mean increases with magnitude and the magnitude taper is changed to allow for this. The updated magnitude taper is given by:

$$Taper\_Mag = if \begin{cases} Mag < 6.3 & \frac{max(Mag - 5.5, 0)}{0.8} \\ else & 1 + m_1(Mag - 6.3) + m_2(Mag - 6.3)^2 \end{cases} \tag{3.14}$$

where *Mag* is the moment magnitude of the rupture.

Coefficients for the model for the change in mean for reverse ruptures were estimated using a least-squares regressions and are given in Table 3.4. The model and data for 5% damped pseudo-spectral acceleration at 3 sec are shown with respect to the combined parameters $RyRatio * \overline{sin2\theta}'$, $\overline{cos2\phi}$, and $RyRatio * \overline{cos2\theta}'$ for moment-magnitudes 6–7.5 in Figures 3.11–3.14.

Table 3.4 Coefficients for model of change in mean for reverse ruptures.

Coefficient	Value	Standard error
b_0	-0.0670606	0.000429
b_1	-0.0309605	0.000476
b_2	0.0743133	0.000486
b_3	0.0640140	0.000647
b_4	-0.0520015	0.000505
b_5	0.0844005	0.000734
b_6	0.0940033	0.000997
b_7	0.0422176	0.000426
b_8	0.0284827	0.000612
b_9	0.00423869	0.000678
r_o	6.43713	0.078280
r_1	0.652545	0.013126
m_1	1.46839	0.028011
m_2	-0.657629	0.018571
b_M	-0.269943	0.001484
Sigma	0.0244068	

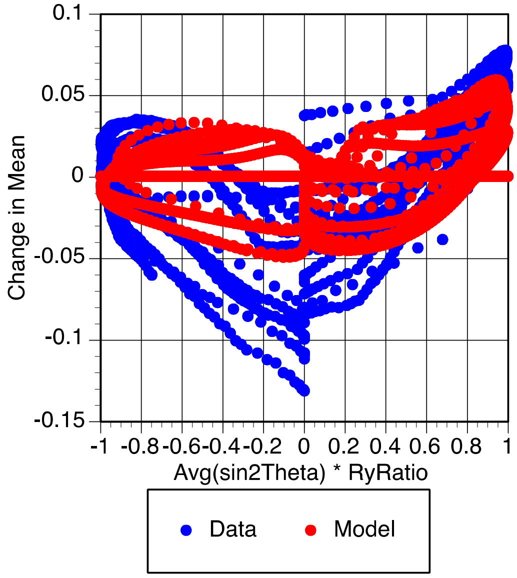

(a)

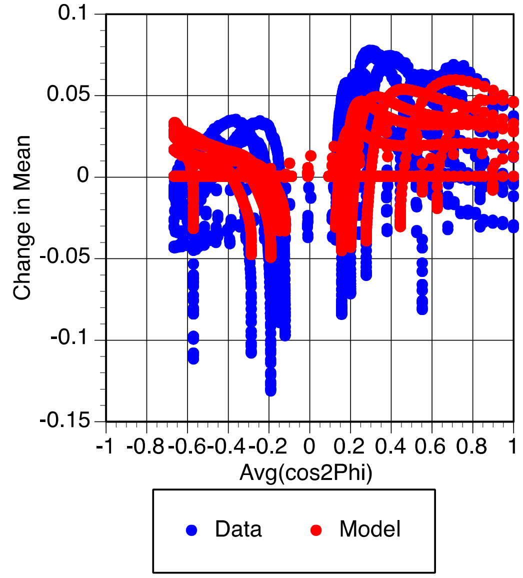

(b)

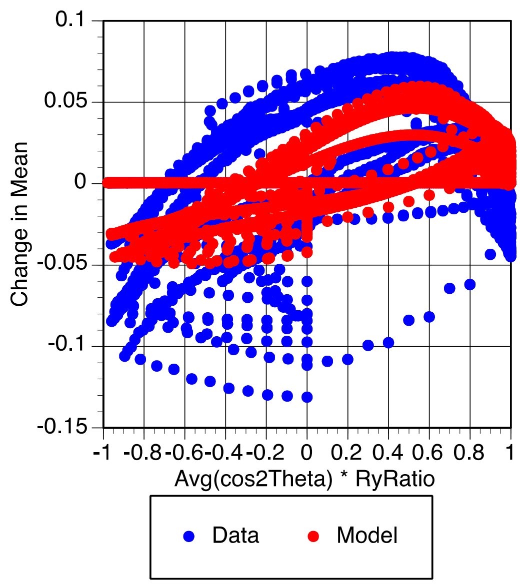

(c)

Figure 3.11 Data and model of change in the mean of the natural log of the 5% damped pseudo-spectral acceleration at 3 sec due to the randomization of hypocenters using Chiou and Youngs [2008] hypocenter distribution models for a moment-magnitude 6, reverse rupture.

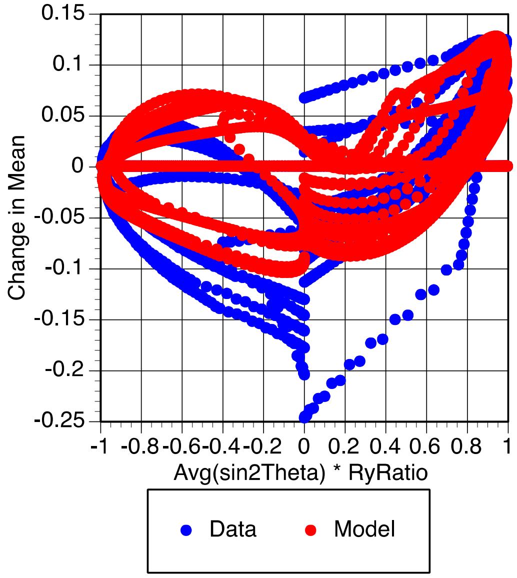

(a)

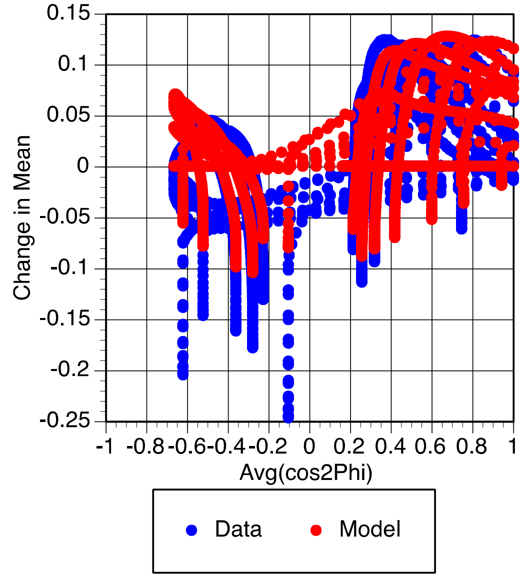

(b)

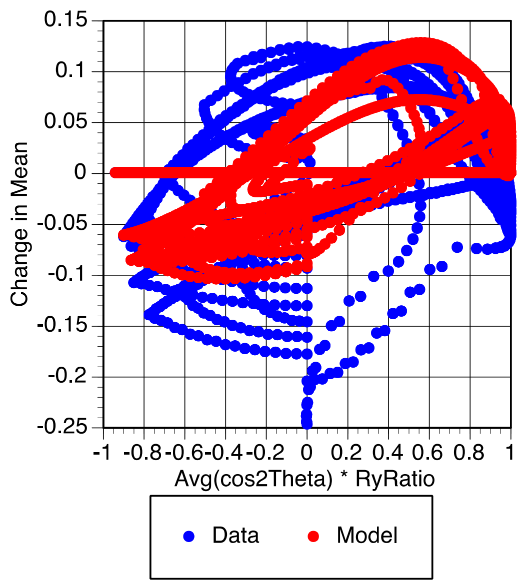

(c)

Figure 3.12 Data and model of change in the mean of the natural log of the 5% damped pseudo-spectral acceleration at 3 sec due to the randomization of hypocenters using Chiou and Youngs [2008] hypocenter distribution models for a moment-magnitude 6.5, reverse rupture.

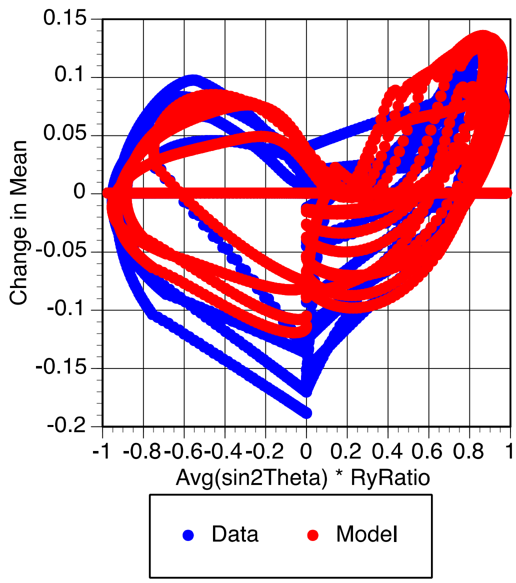

(a)

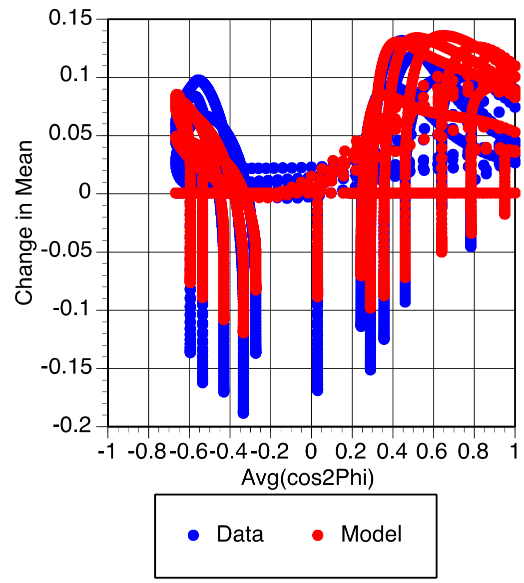

(b)

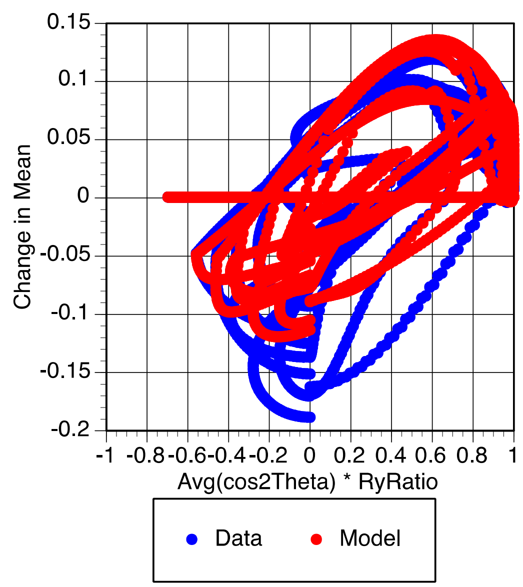

(c)

Figure 3.13 Data and model of change in the mean of the natural log of the 5% damped pseudo-spectral acceleration at 3 sec due to the randomization of hypocenters using Chiou and Youngs [2008] hypocenter distribution models for a moment-magnitude 7, reverse rupture.

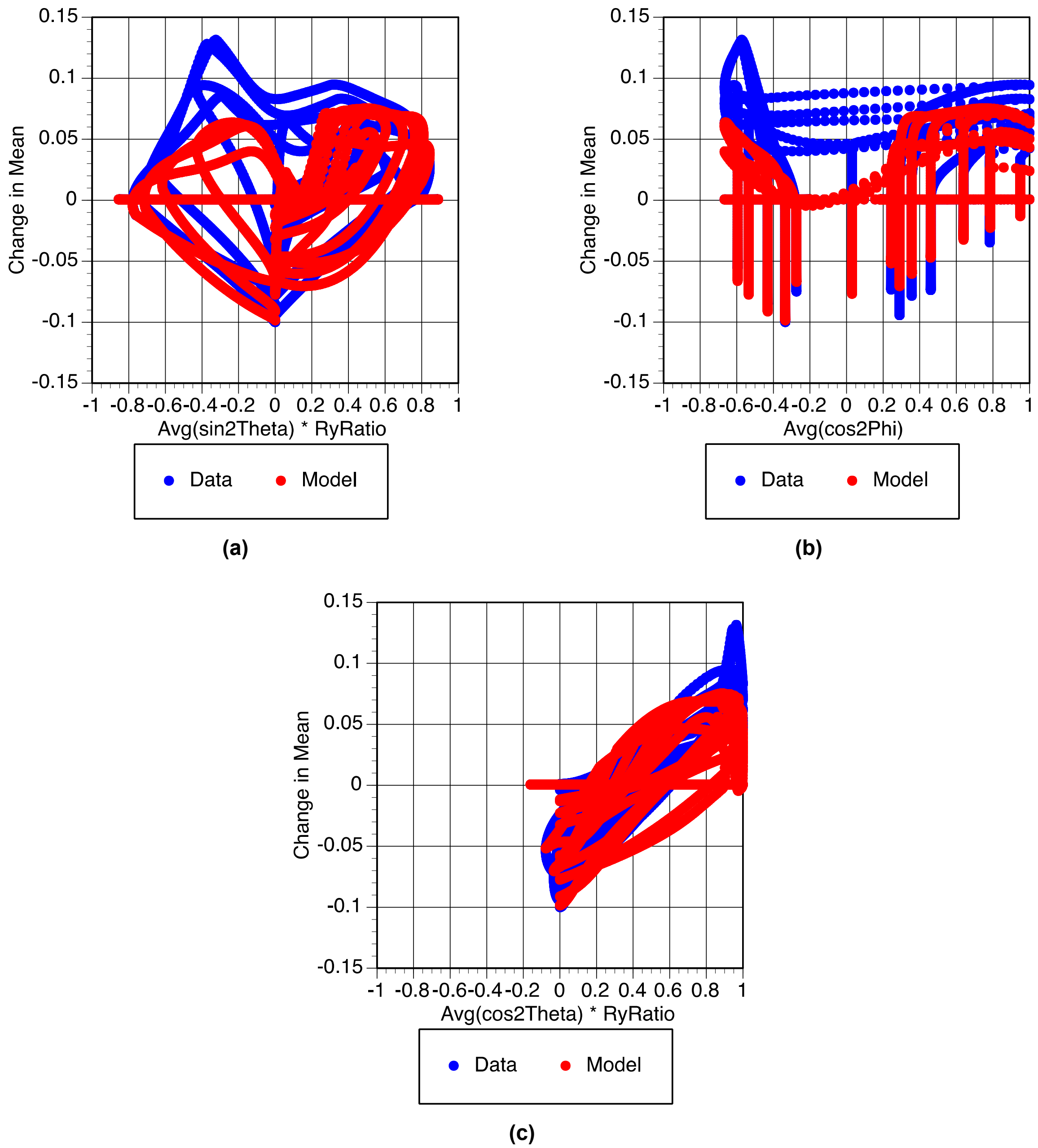

Figure 3.14 **Data and model of change in the mean of the natural log of the 5% damped pseudo-spectral acceleration at 3 sec due to the randomization of hypocenters using Chiou and Youngs [2008] hypocenter distribution models for a moment-magnitude 7.5, reverse rupture.**

3.3.2 Standard Deviation Model

The change in the standard deviation with the ϕ_2 reduction is zero for periods of 5 sec and greater and for small magnitudes. For the other magnitudes and periods, the peak effect is approximately 0.2 at 3 sec. When combined with the total standard deviation from published GMPEs, this increases the variability by 0.03. Given the small increase in the standard deviation and limited periods and magnitudes to which it would be applied, the change in standard deviation to account for the effect of directivity for reverse ruptures is negligibly small and can be ignored for most engineering applications.

A model is developed for engineering applications that wish to include an equation for the change in standard deviation for reverse ruptures. This model smooths out the increase in standard deviation so that it can be applied to a broader range of periods and magnitudes than it is calculated for. The *Dir_Factor* term and distance taper for the change in standard deviation of 5% damped pseudo-spectral acceleration for reverse ruptures are the same as for the mean and are given in Equations (3.9) and (3.12), respectively. The magnitude taper is the same as that used by Chiou and Youngs [2014] and is given in Equation (3.3).

Coefficients for the model for the change in standard deviation for reverse ruptures were estimated using a least-squares regressions and are given in Table 3.5. The model and data for 5% damped pseudo-spectral acceleration at 3 sec are shown with respect to the combined parameters $RyRatio * \overline{\cos 2\theta}$ and $\left(1 - RyRatio\right) * \overline{\cos 2\phi}$ for moment-magnitudes 6–7.5 in Figures 3.15–3.18. These figures show the maximum misfit between the data and the model.

Table 3.5 Coefficients for model of change in standard deviation for reverse ruptures.

Coefficient	Value	Standard error
b_0	0.0622329	0.000561
b_1	0.00164904	0.000928
b_2	-0.00823970	0.000622
b_3	-0.00421270	0.001025
b_4	0.0160663	0.000941
b_5	-0.0145000	0.001132
b_6	-0.00926689	0.001770
b_7	0.0115074	0.000829
b_8	-0.00179300	0.000696
b_9	-0.0104468	0.001198
r_o	3.5	0
r_1	0.680677	0.017850
m_1	-0.724118	0.012627
m_2	0.100161	0.010090
b_M	0.0443404	0.001382
Sigma	0.0265229	

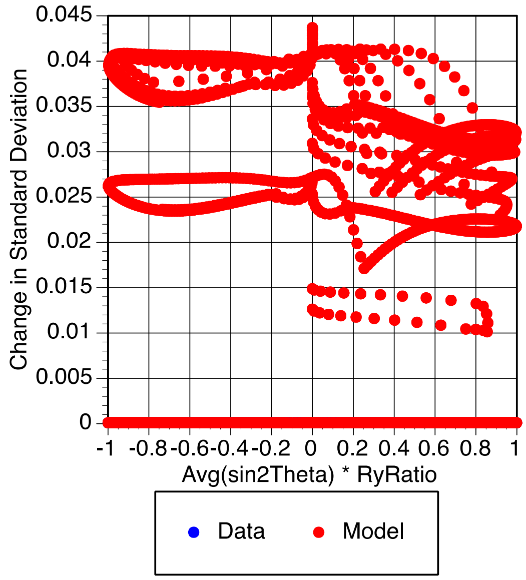

(a)

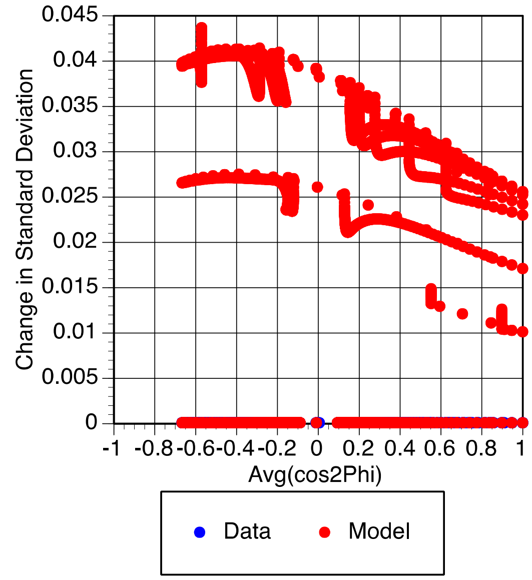

(b)

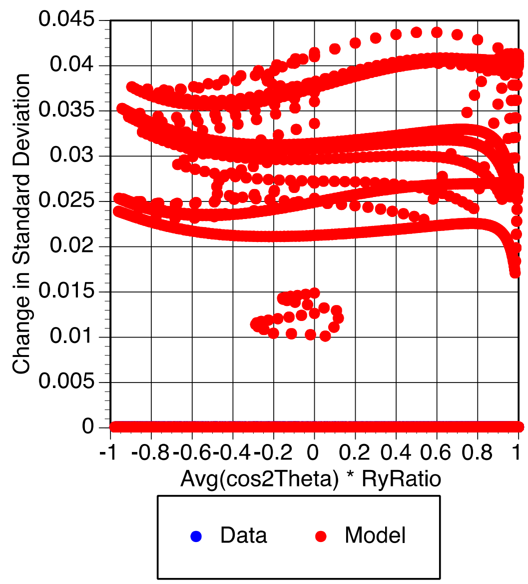

(c)

Figure 3.15 **Data and model of change in the standard deviation of the natural log of the 5% damped pseudo-spectral acceleration at 3 sec due to the randomization of hypocenters using Chiou and Youngs [2008] hypocenter distribution models for a moment-magnitude 6, reverse rupture.**

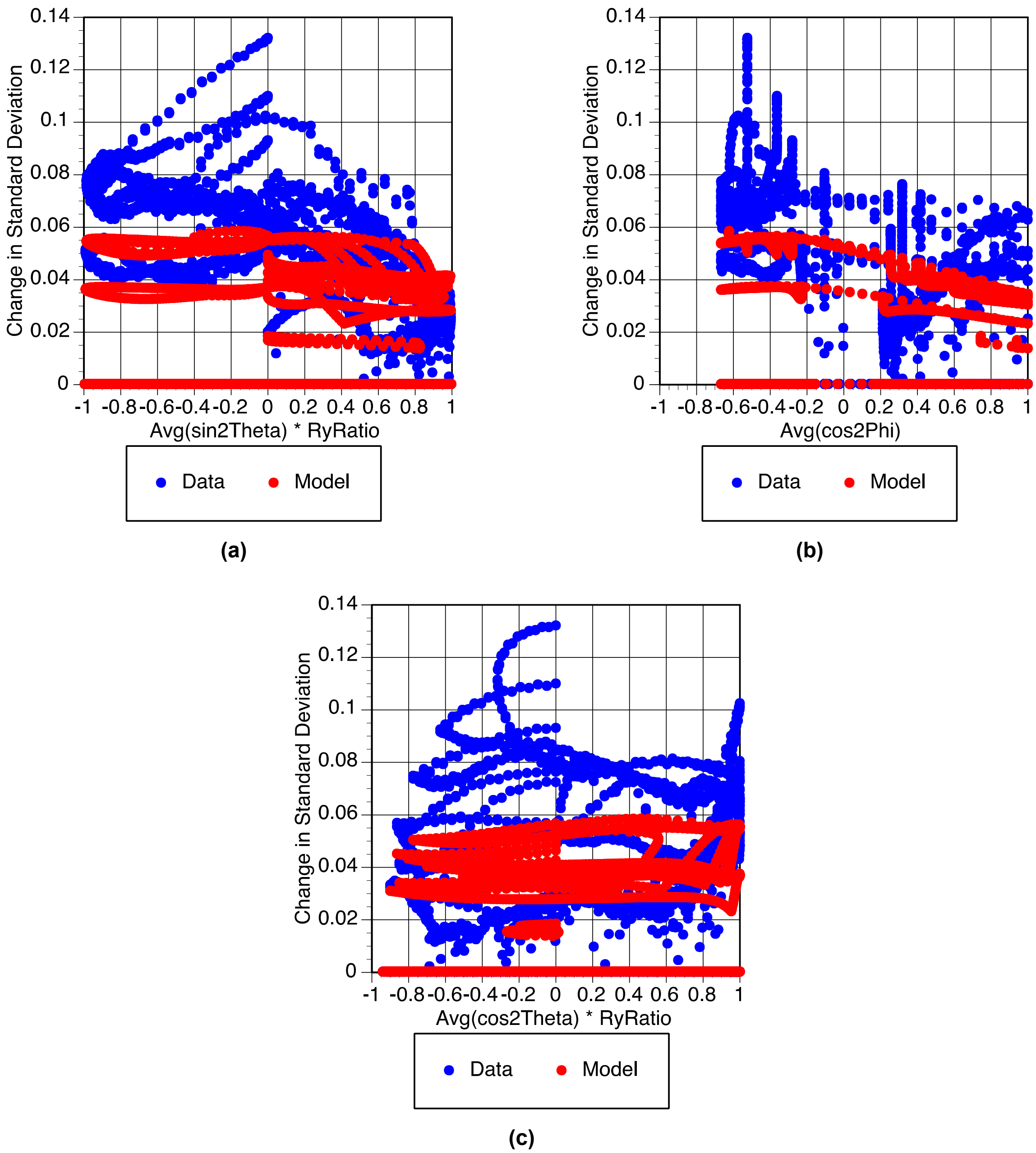

Figure 3.16 **Data and model of change in the standard deviation of the natural log of the 5% damped pseudo-spectral acceleration at 3 sec due to the randomization of hypocenters using Chiou and Youngs [2008] hypocenter distribution models for a moment-magnitude 6.5, reverse rupture.**

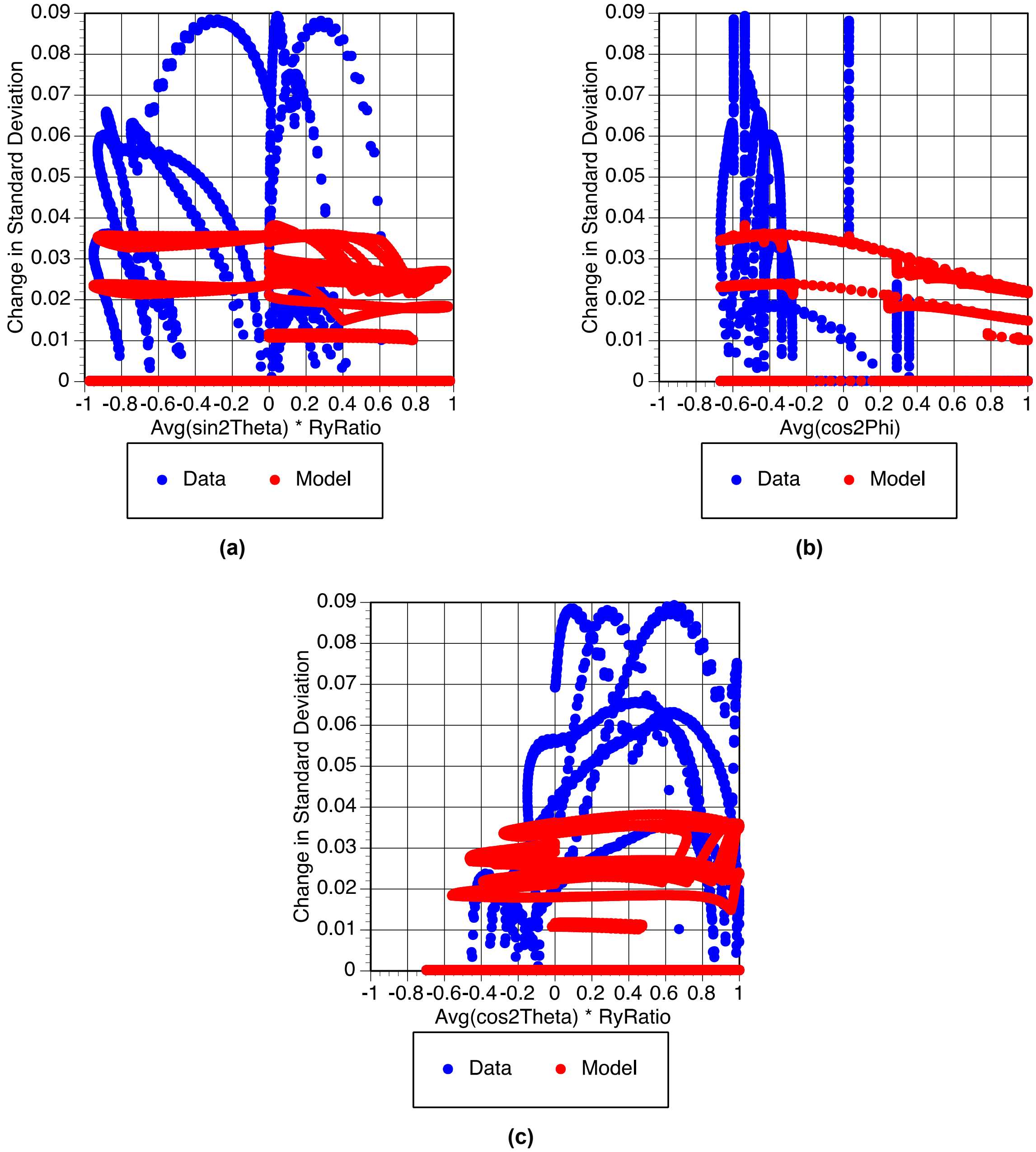

Figure 3.17 **Data and model of change in the standard deviation of the natural log of the 5% damped pseudo-spectral acceleration at 3 sec due to the randomization of hypocenters using Chiou and Youngs [2008] hypocenter distribution models for a moment-magnitude 7, reverse rupture.**

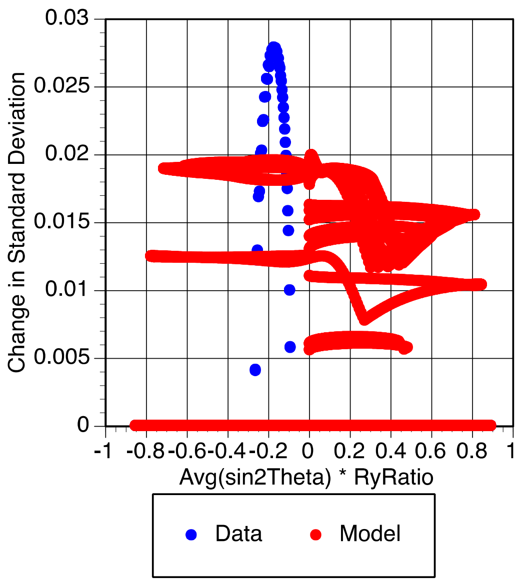

(a)

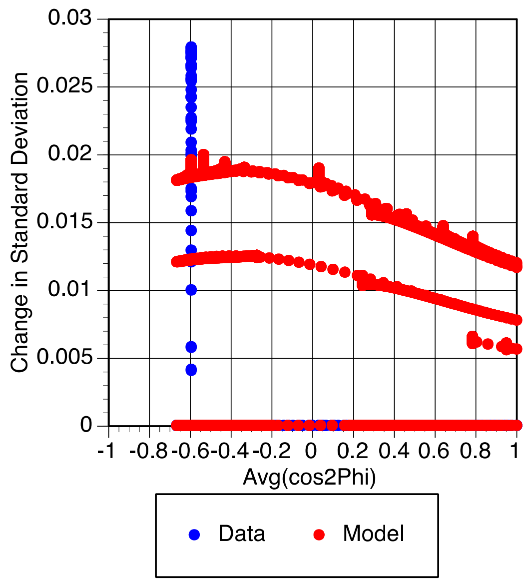

(b)

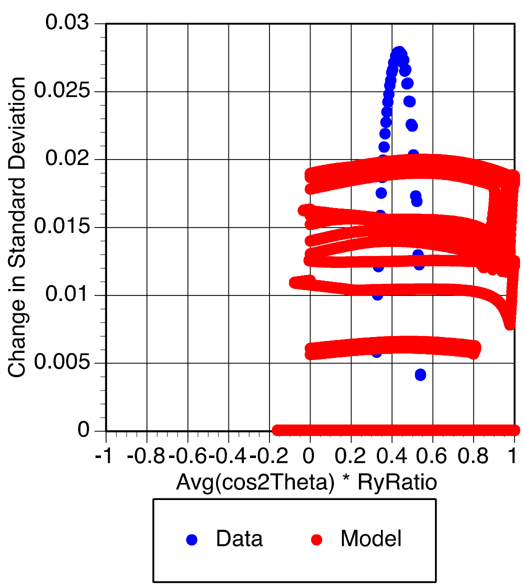

(c)

Figure 3.18 Data and model of change in the standard deviation of the natural log of the 5% damped pseudo-spectral acceleration at 3 sec due to the randomization of hypocenters using Chiou and Youngs [2008] hypocenter distribution models for a moment-magnitude 7.5, reverse rupture.

4 Effect of Hypocenter Distribution

4.1 ALTERNATIVE HYPOCENTER DISTRIBUTIONS

Hypocenter distribution models from Chiou and Youngs [2008] were used for the results in Sections 4.2 and 4.3. An analysis of hypocenter locations was performed to determine if the hypocenter distribution model should be updated. The analysis, given in electronic Appendix D, shows that the along-strike hypocenter distribution was clustered too close to the center for strike–slip ruptures, and that the along-strike distribution should be closer to uniform or favor unilateral ruptures. A sensitivity analysis of the strike-slip and reverse models was performed to determine what effect the updated hypocenter distribution model or a uniform distribution model would have on the results. Figures of all of the 1, 3 and 5 sec results using the uniform hypocenter distribution are shown in electronic Appendix B. Figures of all of the 1, 3 and 5 sec results using the electronic Appendix D hypocenter distribution are shown in electronic Appendix C. Selected results are shown in the following sections.

4.1.1 Strike-Slip Hypocenter Distributions

Three hypocenter distributions were used along the strike: Chiou and Youngs [2008], uniform, and the distribution given in electronic Appendix D. These distributions are shown in Figure 4.1. Two down-dip hypocenter distributions were used: Chiou and Youngs [2008] and uniform. These distributions are shown in Figure 4.2.

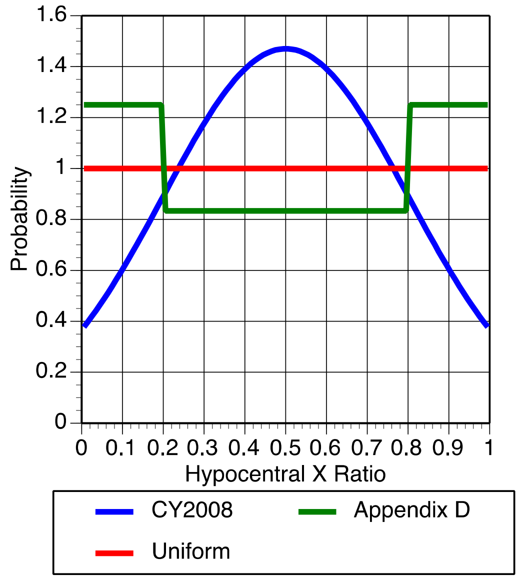

Figure 4.1 Hypocenter distributions along strike for strike–slip ruptures.

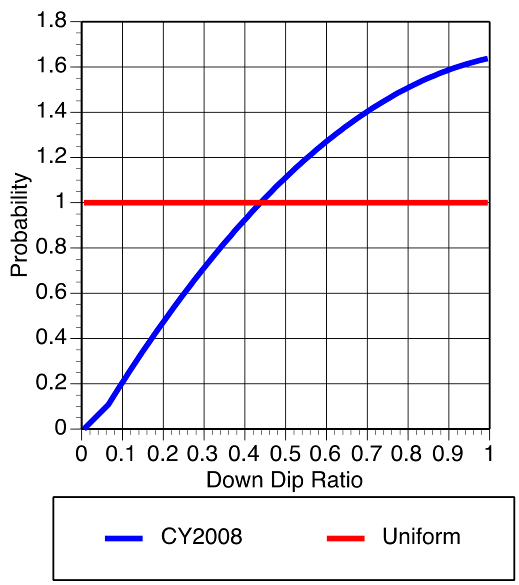

Figure 4.2 Hypocenter distributions down-dip for strike–slip ruptures.

4.1.2 Reverse Hypocenter Distributions

Two hypocenter distributions were used along the strike: Chiou and Youngs [2008] and uniform. These distributions are shown in Figure 4.3. Two down-dip hypocenter distributions were used: Chiou and Youngs [2008] and uniform. These distributions are shown in Figure 4.4.

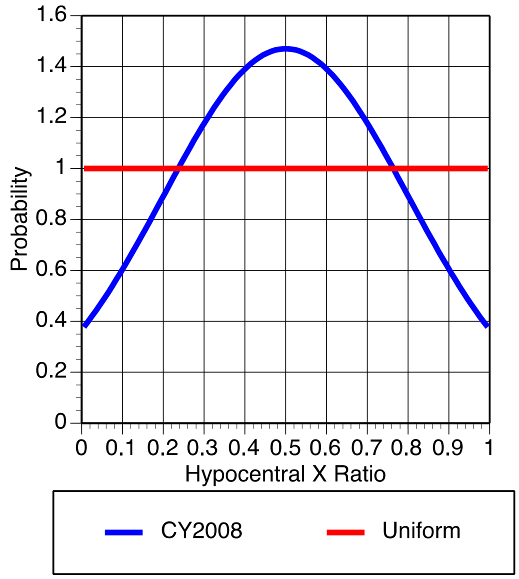

Figure 4.3 Hypocenter distributions along strike for reverse ruptures.

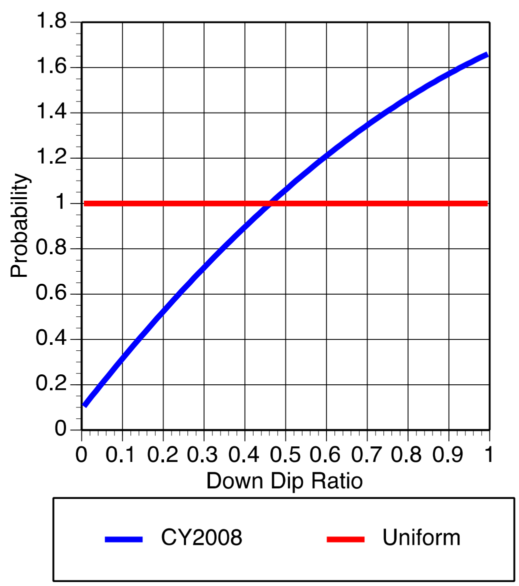

Figure 4.4 Hypocenter distributions down-dip for reverse ruptures.

4.2 STRIKE–SLIP RESULTS

4.2.1 Mean Results

The change in the mean of 5% damped pseudo-spectral acceleration was calculated for strike–slip ruptures using a uniform hypocenter distribution and the hypocenter distribution from electronic Appendix D. Compared with the change calculated using the Chiou and Youngs

[2008] hypocenter distribution, the largest effect was found using the Chiou and Youngs [2008] hypocenter distribution and the smallest for the hypocenter distribution from electronic Appendix D. This is demonstrated for 5% damped pseudo-spectral acceleration at 3 sec for a moment-magnitude 6.5 strike–slip earthquake shown in Figures 4.5– 4.7.

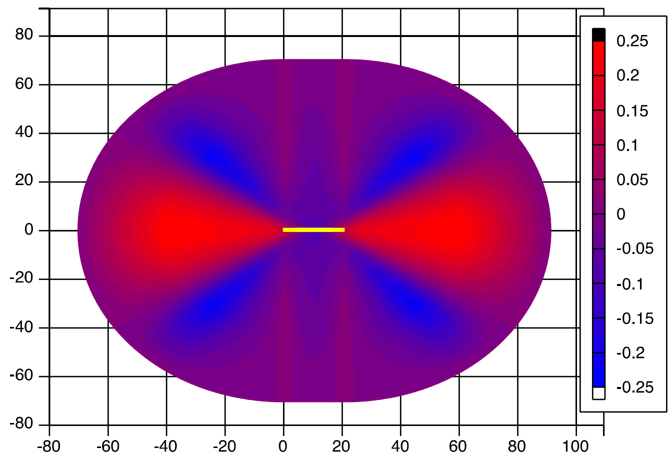

Figure 4.5 **Change in the mean of the natural log of the 5% damped pseudo-spectral acceleration at 3 sec due to the randomization of hypocenters using hypocenter distribution models from Chiou and Youngs [2008] for a moment-magnitude 6.5, strike–slip rupture.**

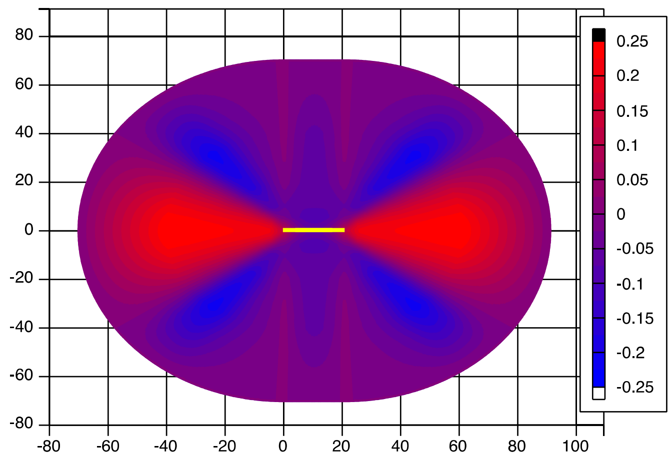

Figure 4.6 **Change in the mean of the natural log of the 5% damped pseudo-spectral acceleration at 3 sec due to the randomization of hypocenters using a uniform hypocenter distribution for a moment-magnitude 6.5, strike–slip rupture.**

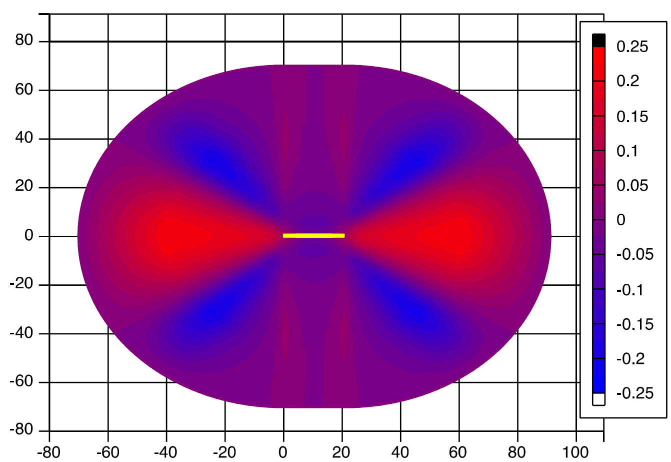

Figure 4.7 **Change in the mean of the natural log of the 5% damped pseudo-spectral acceleration at 3 sec due to the randomization of hypocenters using hypocenter distribution model from Appendix D for a moment-magnitude 6.5, strike–slip rupture.**

4.2.2 Additional Mean Models

Coefficients were estimated for the change in the mean of 5% damped pseudo-spectral acceleration for strike–slip ruptures using both a uniform hypocenter distribution and the hypocenter distribution from electronic Appendix D. The coefficients can be found in Tables 4.1 and 4.2. The models are compared with the model calculated using the Chiou and Youngs [2008] hypocenter distribution for a site 20 km off the end of a moment-magnitude 7.5 strike–slip rupture with a *Rx* value of 0 km. The comparison is shown in Figure 4.8.

Table 4.1 Coefficients for model of change in mean using a uniform hypocenter distribution for strike–slip ruptures

Coefficient	Value	Standard error
b_0	-0.103586	0.000215
b_1	0.0119421	0.000276
b_2	0.358110	0.001024
b_3	-0.0200015	0.000784
r_o	17.4501	0.064851
r_1	0.680090	0.001381
m_1	0.959704	0.005838
m_2	-0.571625	0.002972
b_M	-0.269678	0.000456
Sigma	0.0142550	

Table 4.2 Coefficients for model of change in mean using Appendix D hypocenter distribution for strike–slip ruptures.

Coefficient	Value	Standard error
b_0	-0.080707	0.000221
b_1	-0.0130894	0.000287
b_2	0.270306	0.001033
b_3	0.0358174	0.000798
r_o	19.0763	0.085385
r_1	0.770570	0.001680
m_1	1.37281	0.008674
m_2	-0.807316	0.004450
b_M	-0.269628	0.000565
Sigma	0.0155178	

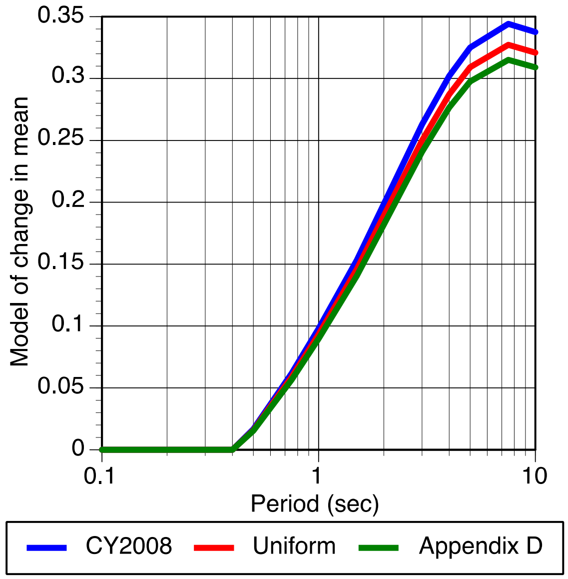

Figure 4.8 Model of change in the mean of the natural log of the 5% damped pseudo-spectral acceleration due to the randomization of hypocenters using Chiou and Youngs [2008] hypocenter distribution models, uniform hypocenter distribution model, and hypocenter distribution model from Appendix D for a site 20 km from the end of a moment-magnitude 7.5, strike–slip rupture with a *Rx* value of 0 km.

4.2.3 Standard Deviation Results

The change in the standard deviation of 5% damped pseudo-spectral acceleration for strike–slip ruptures was calculated using a uniform hypocenter distribution and the hypocenter distribution from electronic Appendix D. Compared with the change calculated using the Chiou and Youngs [2008] hypocenter distribution, the largest effect is seen for the hypocenter distribution from electronic Appendix D and smallest for the Chiou and Youngs [2008] hypocenter distribution. This is demonstrated for 5% damped pseudo-spectral acceleration at 3 sec for a moment-magnitude 6.5 strike–slip earthquake in Figures 4.9–4.11.

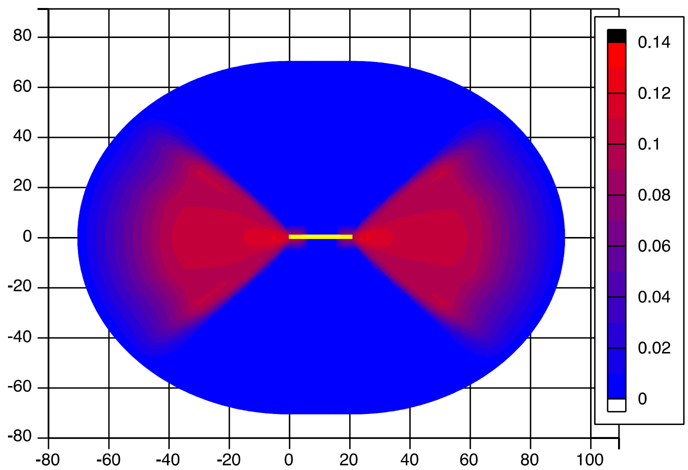

Figure 4.9 **Change in the standard deviation of the natural log of the 5% damped pseudo-spectral acceleration at 3 sec due to the randomization of hypocenters using hypocenter distribution models from Chiou and Youngs [2008] for a moment-magnitude 6.5, strike–slip rupture with ϕ_2 reduction.**

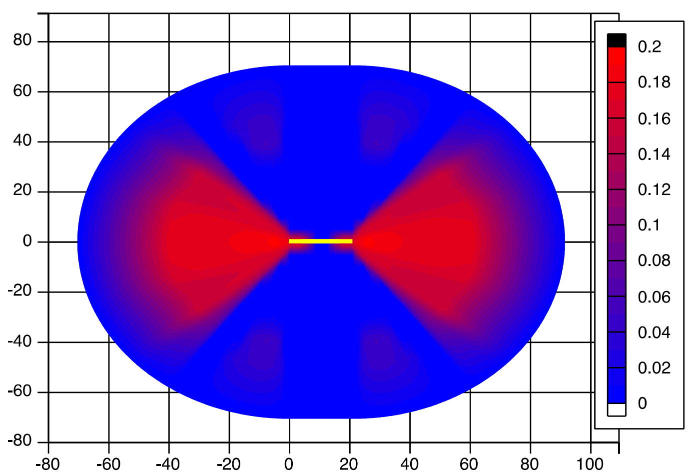

Figure 4.10 **Change in the standard deviation of the natural log of the 5% damped pseudo-spectral acceleration at 3 sec due to the randomization of hypocenters using a uniform hypocenter distribution for a moment-magnitude 6.5, strike–slip rupture with ϕ_2 reduction.**

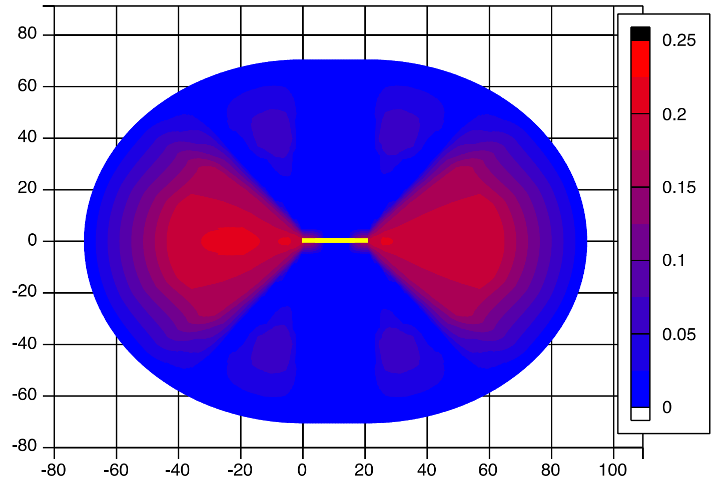

Figure 4.11 **Change in the standard deviation of the natural log of the 5% damped pseudo-spectral acceleration at 3 sec due to the randomization of hypocenters using hypocenter distributions model from Appendix D for a moment-magnitude 6.5, strike–slip rupture with ϕ_2 reduction.**

4.2.4 Additional Standard Deviation Models

Coefficients were estimated for the change in the standard deviation of 5% damped pseudo-spectral acceleration for strike–slip ruptures using both a uniform hypocenter distribution and the hypocenter distribution from electronic Appendix D. The coefficients can be found in Tables 4.3 and 4.4. The models are compared with the model calculated using the Chiou and Youngs [2008] hypocenter distribution for a site 20 km off the end of a moment-magnitude 7.5 strike–slip rupture with a *Rx* value of 0 km. The comparison is shown in Figure 4.12.

Table 4.3 **Coefficients for model of change in standard deviation using a uniform hypocenter distribution for strike–slip ruptures.**

Coefficient	Value	Standard error
b_0	0.0113618	0.000202
b_1	0.141932	0.001270
b_2	0.303622	0.002162
b_3	-0.408713	0.002918
r_o	13.3528	0.076369
r_1	0.747826	0.002984
m_1	0.838457	0.020591
m_2	-0.398519	0.009572
b_M	-0.111522	0.000629
Sigma	0.0360734	

Table 4.4 Coefficients for model of change in standard deviation using Appendix D hypocenter distribution for strike–slip ruptures.

Coefficient	Value	Standard error
b_0	0.00657229	0.000195
b_1	0.154046	0.001278
b_2	0.351609	0.002308
b_3	-0.446410	0.002964
r_o	13.1910	0.068559
r_1	0.748240	0.002748
m_1	0.741209	0.018492
m_2	-0.315181	0.008461
b_M	-0.129245	0.000621
Sigma	0.0369480	

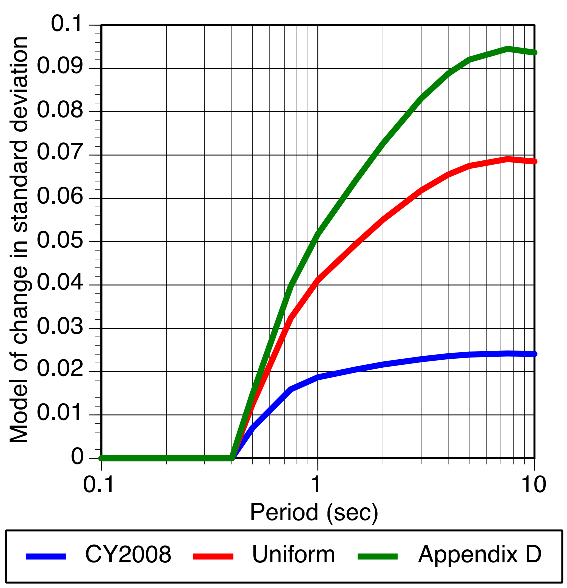

Figure 4.12 Model of change in the standard deviation of the natural log of the 5% damped pseudo-spectral acceleration due to the randomization of hypocenters using Chiou and Youngs [2008] hypocenter distribution models, uniform hypocenter distribution model, and hypocenter distribution model from Appendix D for a site 20 km from the end of a moment-magnitude 7.5, strike–slip rupture with a *Rx* value of 0 km.

4.3 REVERSE RESULTS

4.3.1 Mean Results

The change in the mean of 5% damped pseudo-spectral acceleration for reverse ruptures was calculated using a uniform hypocenter distribution. Compared with the change calculated using the Chiou and Youngs [2008] hypocenter distribution, the effect is largest for the Chiou and Youngs [2008] hypocenter distribution. This is demonstrated for 5% damped pseudo-spectral acceleration at 3 sec for a moment-magnitude 6.5 reverse earthquake shown in Figures 4.13 and 4.14.

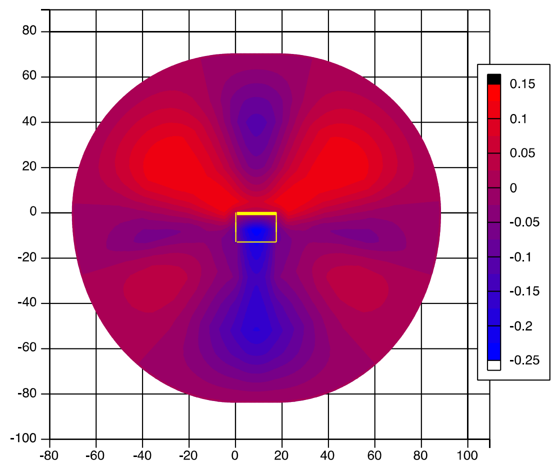

Figure 4.13 Change in the mean of the natural log of the 5% damped pseudo-spectral acceleration at 3 sec due to the randomization of hypocenters using hypocenter distribution models from Chiou and Youngs [2008] for a moment-magnitude 6.5, reverse rupture.

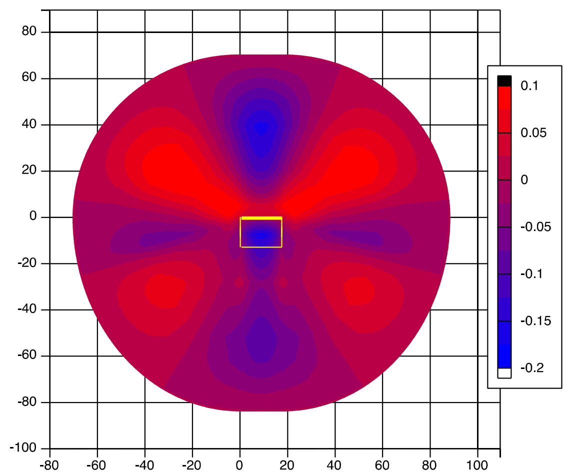

Figure 4.14 Change in the mean of the natural log of the 5% damped pseudo-spectral acceleration at 3 sec due to the randomization of hypocenters using a uniform hypocenter distribution a moment-magnitude 6.5, reverse rupture.

4.3.2 Additional Mean Model

Coefficients were estimated for the change in the mean of 5% damped pseudo-spectral acceleration for reverse ruptures using a uniform hypocenter distribution. The coefficients can be found in Table 4.5. The model is compared with the model calculated using the Chiou and Youngs [2008] hypocenter distribution for a site over the hanging wall with a rupture distance of 20 km and *Ry* value of 0 km. The comparison is shown in Figure 4.15.

Table 4.5 Coefficients for model of change in mean using uniform hypocenter distribution for reverse ruptures.

Coefficient	Value	Standard error
b_0	-0.0559015	0.000396
b_1	-0.0339914	0.000422
b_2	0.0686994	0.000479
b_3	0.0609142	0.000588
b_4	0.00549400	0.000365
b_5	0.0646359	0.000617
b_6	0.0107670	0.000701
b_7	0.0433411	0.000401
b_8	0.00376510	0.000509
b_9	0.0186525	0.000568
r_o	47.3150	0.302286
r_1	0.546951	0.003090
m_1	1.57341	0.029154
m_2	-0.434900	0.018083
b_M	-0.270149	0.001336
Sigma	0.0186421	

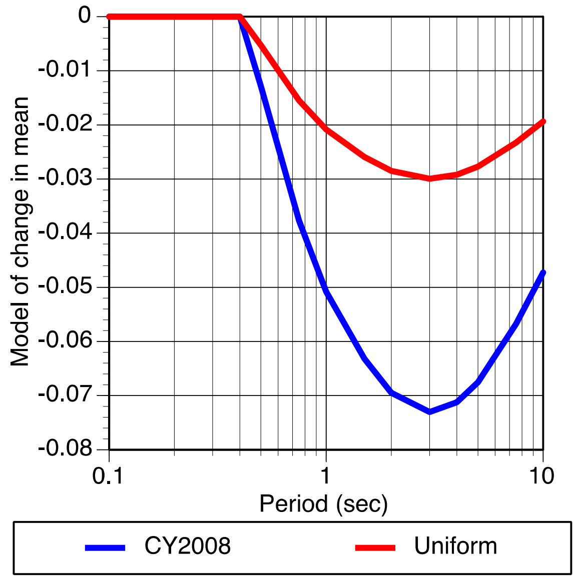

Figure 4.15 **Model of change in the mean of the natural log of the 5% damped pseudo-spectral acceleration due to the randomization of hypocenters using Chiou and Youngs [2008] hypocenter distribution models and uniform hypocenter distribution model for a site over the hanging wall of a moment-magnitude 6.5, reverse rupture, with a rupture distance of 20 km and a *Ry* value of 0 km.**

4.3.3 Standard Deviation Results

The change in the standard deviation of 5% damped pseudo-spectral acceleration for reverse ruptures was calculated using a uniform hypocenter distribution. Compared with the change calculated using the Chiou and Youngs [2008] hypocenter distribution, the effect is largest for the uniform hypocenter distribution. This is demonstrated for 5% damped pseudo-spectral acceleration at 3 sec for a moment-magnitude 6.5 reverse earthquake shown in Figures 4.16 and 4.17.

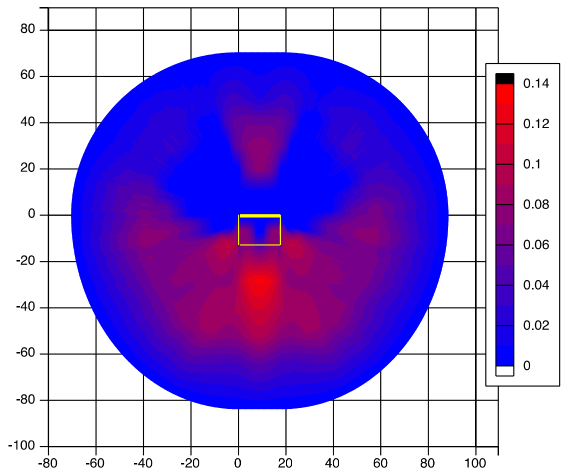

Figure 4.16 **Change in the standard deviation of the natural log of the 5% damped pseudo-spectral acceleration at 3 sec due to the randomization of hypocenters using hypocenter distribution models from Chiou and Youngs [2008] for a moment-magnitude 6.5, reverse rupture with ϕ_2 reduction.**

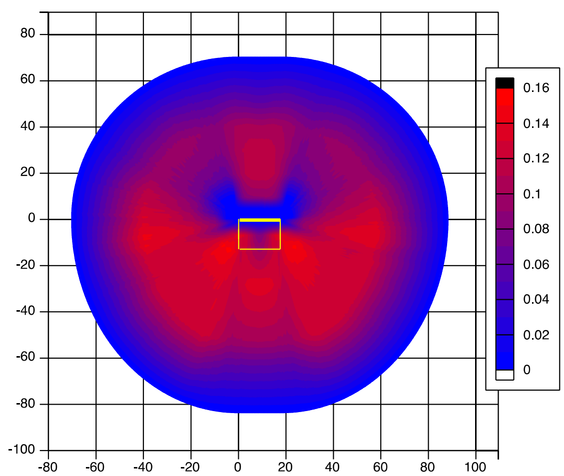

Figure 4.17 **Change in the standard deviation of the natural log of the 5% damped pseudo-spectral acceleration at 3 sec due to the randomization of hypocenters using a uniform hypocenter distribution for a moment-magnitude 6.5, reverse rupture with ϕ_2 reduction.**

4.3.4 Additional Standard Deviation Model

Coefficients were estimated for the change in the standard deviation of 5% damped pseudo-spectral acceleration for reverse ruptures using a uniform hypocenter distribution. The coefficients can be found in Table 4.6. The model is compared with the model calculated using the Chiou and Youngs [2008] hypocenter distribution for a site over the hanging wall with a rupture distance of 20 km and *Ry* value of 0 km. The comparison is shown in Figure 4.18.

Table 4.6 Coefficients for model of change in standard deviation using uniform hypocenter distribution for reverse ruptures.

Coefficient	Value	Standard error
b_0	0.0792172	0.000759
b_1	0.0143492	0.001223
b_2	-0.00618220	0.000846
b_3	-0.0208327	0.001319
b_4	0.0183605	0.001217
b_5	-0.0123780	0.001454
b_6	-0.00522741	0.002243
b_7	0.0193431	0.001117
b_8	0.00155917	0.000895
b_9	-0.0120129	0.001567
r_o	11.1623	0.245612
r_1	0.378549	0.012649
m_1	-0.543070	0.012361
m_2	-0.0602970	0.009931
b_M	0.00752281	0.001375
Sigma	0.0319598	

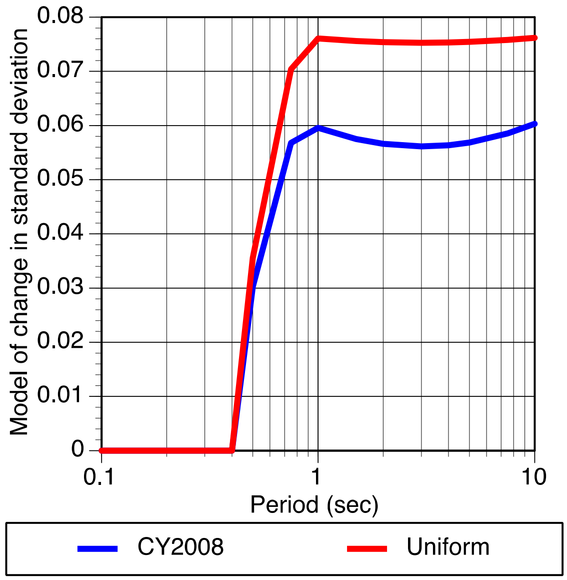

Figure 4.18 **Model of change in the standard deviation of the natural log of the 5% damped pseudo-spectral acceleration due to the randomization of hypocenters using Chiou and Youngs [2008] hypocenter distribution models and uniform hypocenter distribution model for a site over the hanging wall of a moment-magnitude 6.5, reverse rupture, with a rupture distance of 20 km and a *Ry* value of 0 km.**

5 Preferred Models

5.1 PREFERRED STRIKE–SLIP MODELS

The preferred strike–slip rupture models are those developed using the along-strike hypocenter distribution from Appendix D and the down-dip hypocenter distribution from Chiou and Youngs [2008]. The coefficients for these models are found in Tables 4.2 and 4.4. The model for the change in the mean of the natural log of the 5% damped pseudo-spectral acceleration at 3 sec is shown for moment-magnitudes 6 through 8 in Figures 5.1–5.5. The model for the change in the standard deviation of the natural log of the 5% damped pseudo-spectral acceleration at 3 sec is shown for moment-magnitudes 6 through 8 in Figures 5.6–5.10.

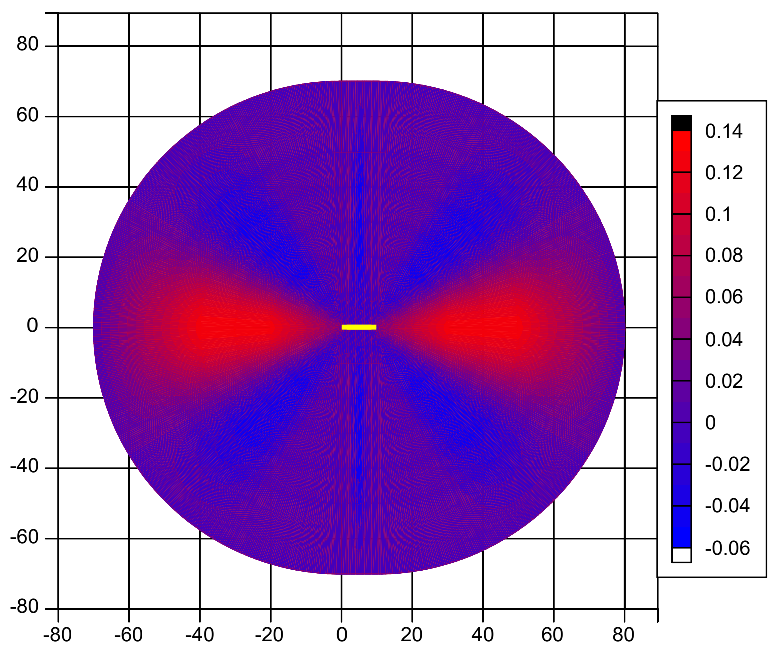

Figure 5.1 Model of change in the mean of the natural log of the 5% damped pseudo-spectral acceleration at 3 sec due to the randomization of hypocenters using hypocenter distribution model from Appendix D for a moment-magnitude 6, strike–slip rupture.

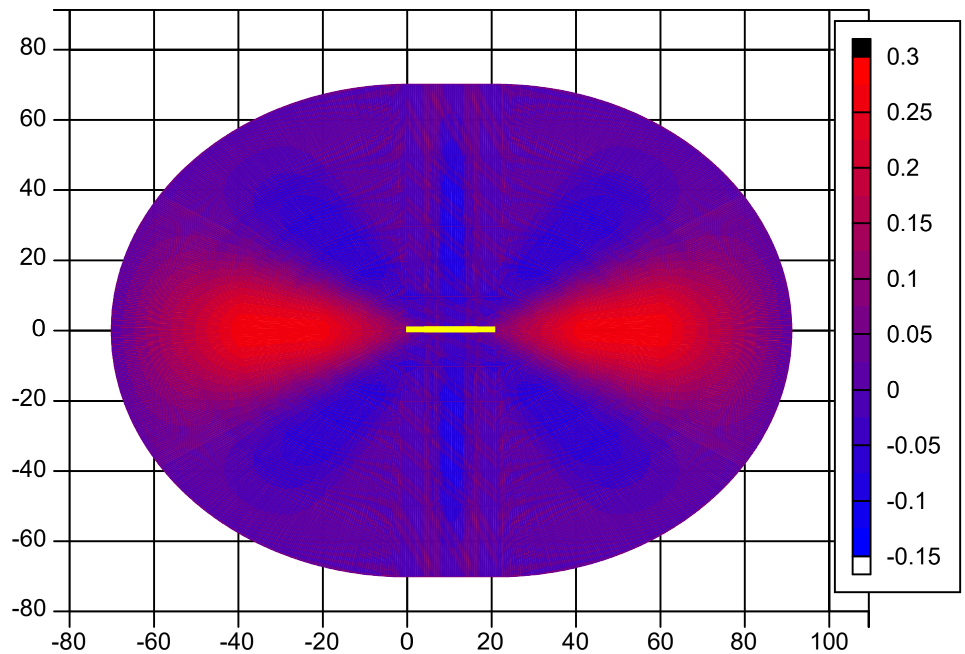

Figure 5.2 **Model of change in the mean of the natural log of the 5% damped pseudo-spectral acceleration at 3 sec due to the randomization of hypocenters using hypocenter distribution model from Appendix D for a moment-magnitude 6.5, strike–slip rupture.**

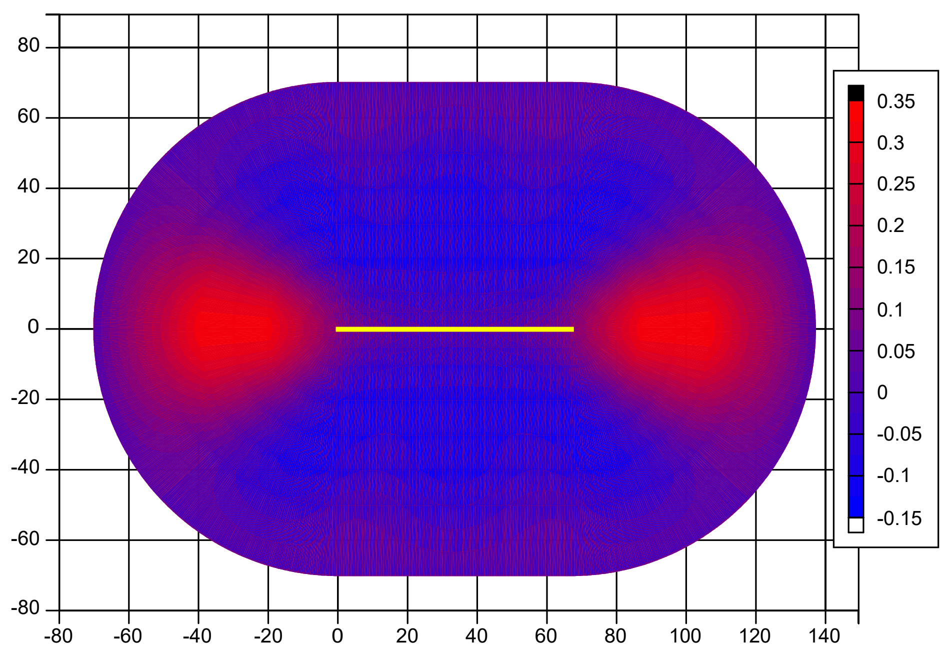

Figure 5.3 **Model of change in the mean of the natural log of the 5% damped pseudo-spectral acceleration at 3 sec due to the randomization of hypocenters using hypocenter distribution model from Appendix D for a moment-magnitude 7, strike–slip rupture.**

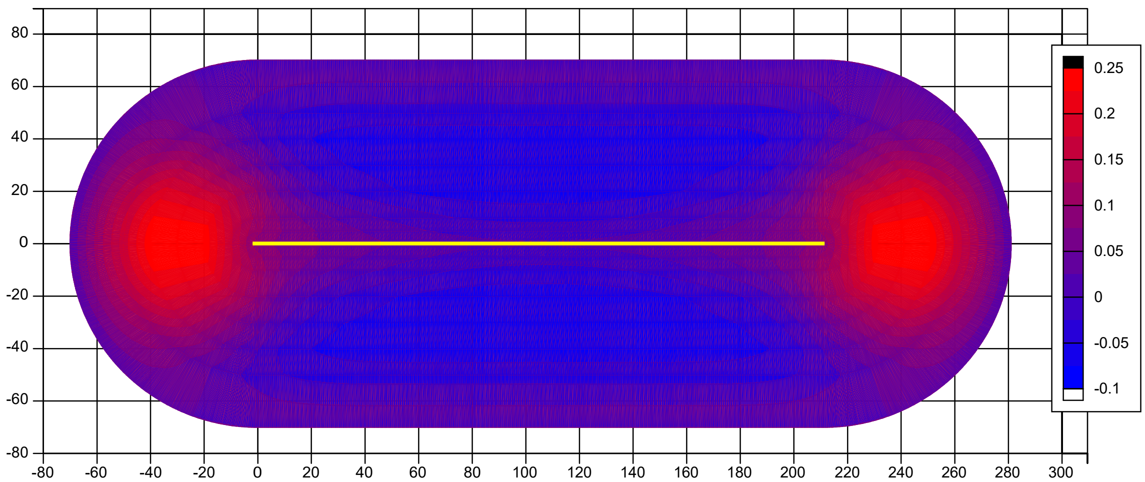

Figure 5.4 **Model of change in the mean of the natural log of the 5% damped pseudo-spectral acceleration at 3 sec due to the randomization of hypocenters using hypocenter distribution model from Appendix D for a moment-magnitude 7.5, strike–slip rupture.**

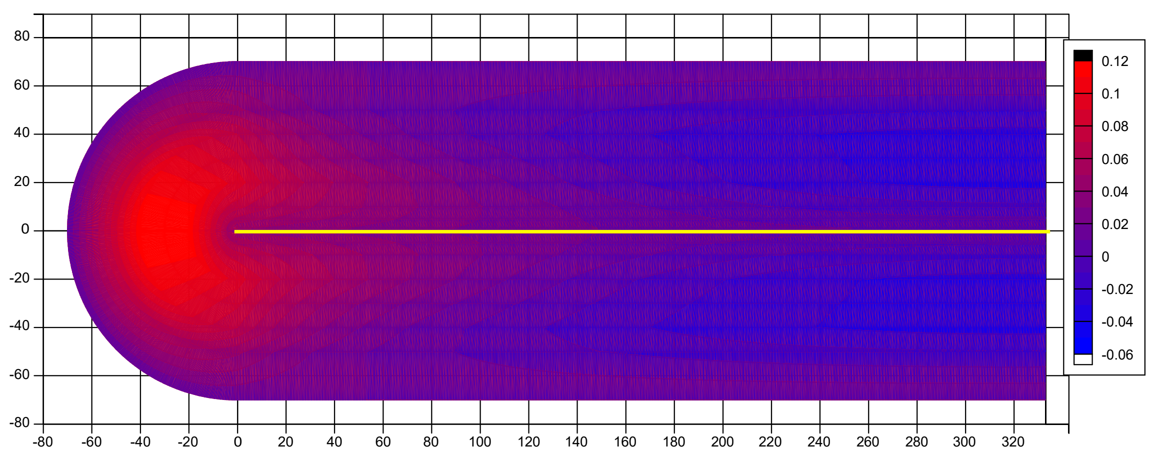

Figure 5.5 **Model of change in the mean of the natural log of the 5% damped pseudo-spectral acceleration at 3 sec due to the randomization of hypocenters using hypocenter distribution model from Appendix D for a moment-magnitude 8, strike–slip rupture.**

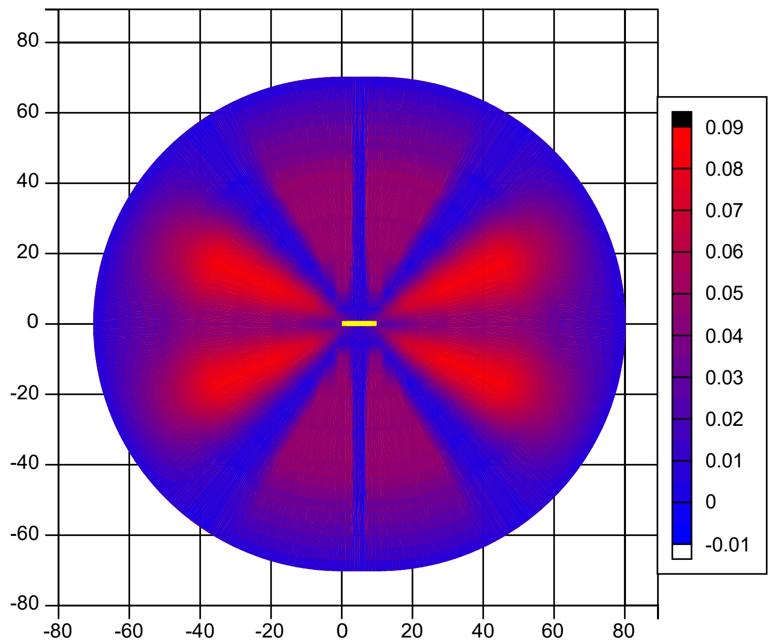

Figure 5.6 **Model of change in the standard deviation of the natural log of the 5% damped pseudo-spectral acceleration at 3 sec due to the randomization of hypocenters using hypocenter distribution model from Appendix D for a moment-magnitude 6, strike–slip rupture.**

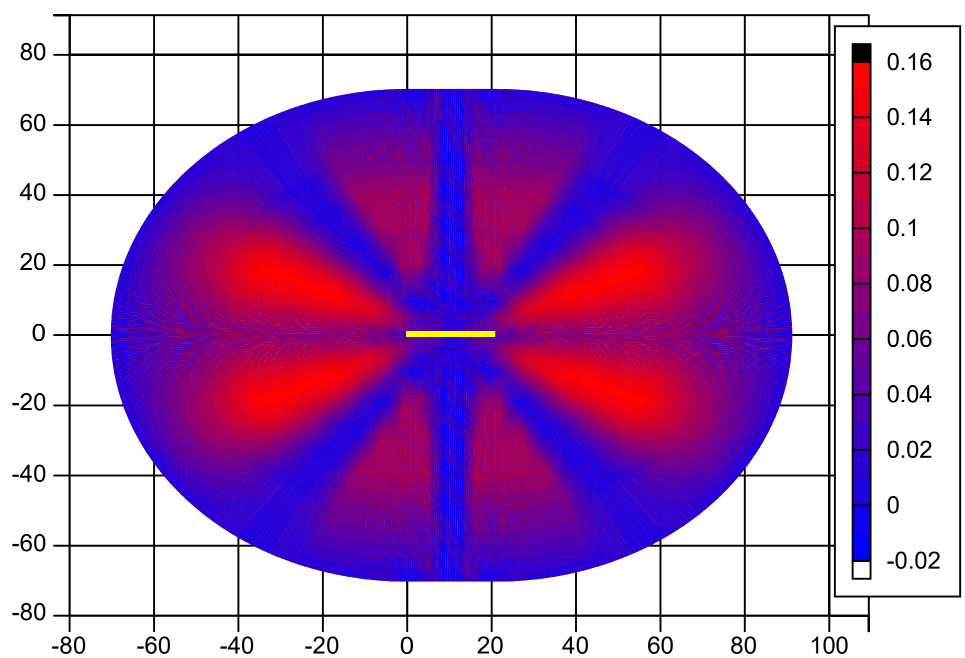

Figure 5.7 **Model of change in the standard deviation of the natural log of the 5% damped pseudo-spectral acceleration at 3 sec due to the randomization of hypocenters using hypocenter distribution model from Appendix D for a moment-magnitude 6.5, strike–slip rupture.**

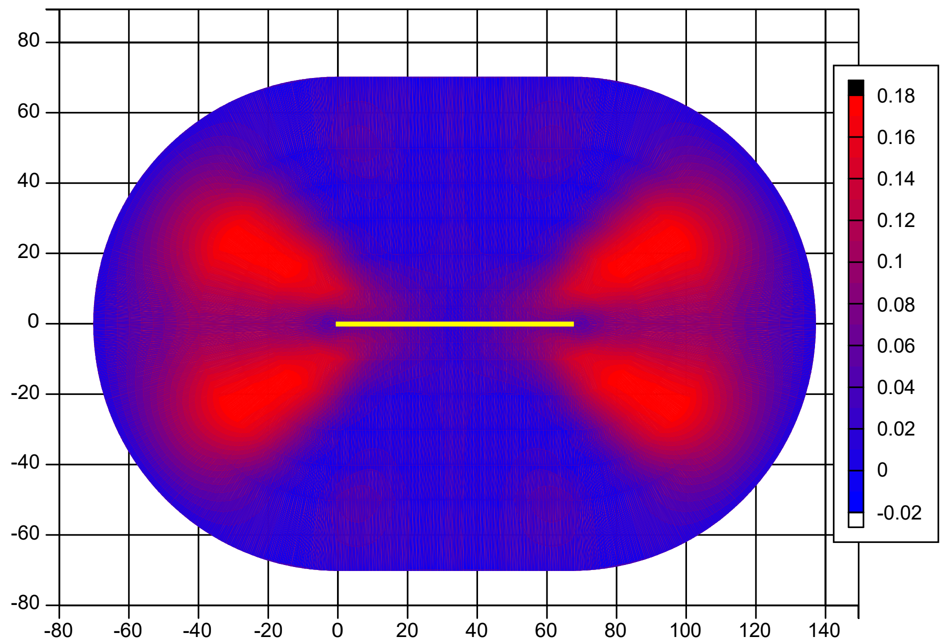

Figure 5.8 **Model of change in the standard deviation of the natural log of the 5% damped pseudo-spectral acceleration at 3 sec due to the randomization of hypocenters using hypocenter distribution model from Appendix D for a moment-magnitude 7, strike–slip rupture.**

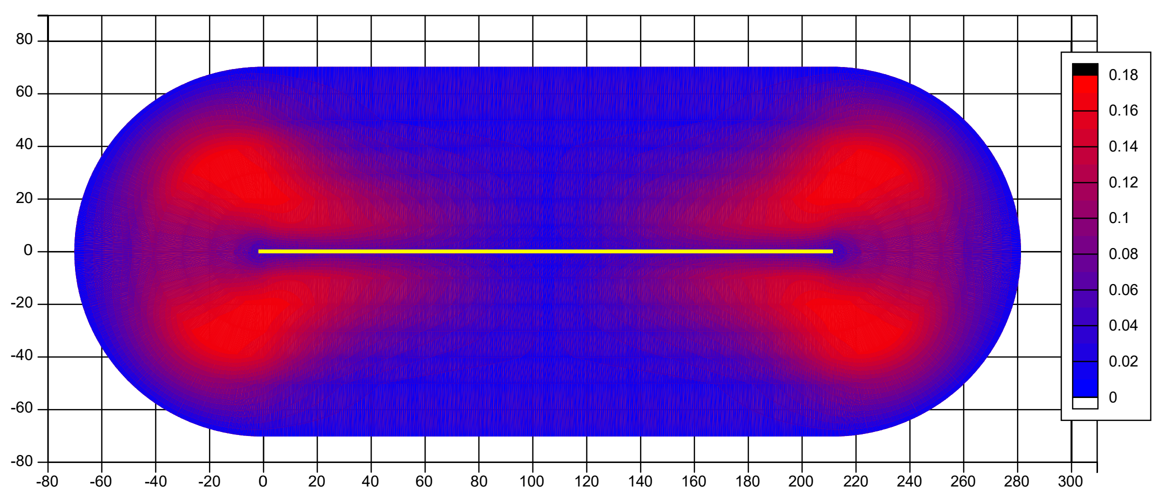

Figure 5.9 **Model of change in the standard deviation of the natural log of the 5% damped pseudo-spectral acceleration at 3 sec due to the randomization of hypocenters using hypocenter distribution model from Appendix D for a moment-magnitude 7.5, strike–slip rupture.**

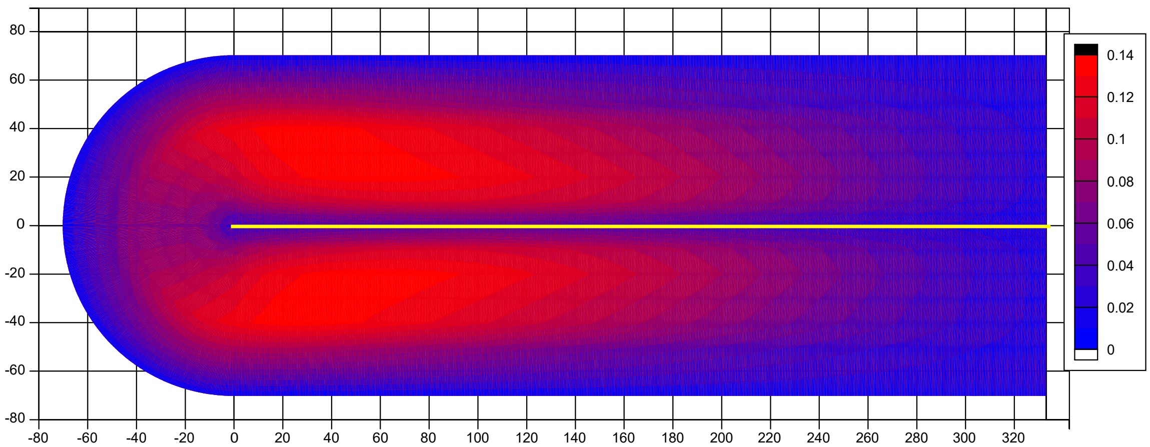

Figure 5.10 Model of change in the standard deviation of the natural log of the 5% damped pseudo-spectral acceleration at 3 sec due to the randomization of hypocenters using hypocenter distribution model from Appendix D for a moment-magnitude 8, strike–slip rupture.33.

5.2 PREFERRED REVERSE MODELS

The preferred reverse rupture models are those developed using the along-strike and down-dip hypocenter distributions from Chiou and Youngs [2008]. The coefficients for these models are found in Tables 3.4 and 3.5. The model for the change in the mean of the natural log of the 5% damped pseudo-spectral acceleration at 3 sec is shown for moment-magnitudes 6–7.5 in Figures 5.11–5.14. The model for the change in the standard deviation of the natural log of the 5% damped pseudo-spectral acceleration at 3 sec is shown for moment-magnitudes 6–7.5 in Figures 5.15–5.18.

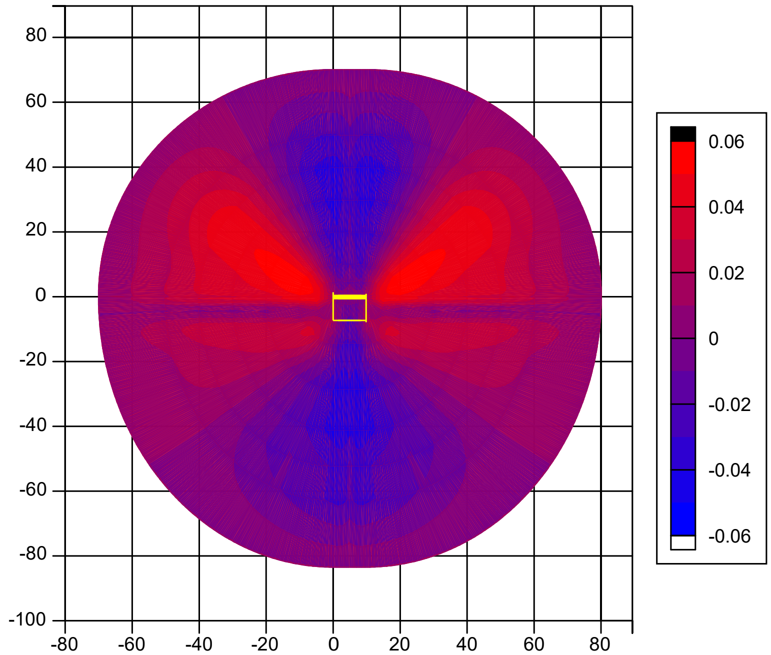

Figure 5.11 **Model of change in the mean of the natural log of the 5% damped pseudo-spectral acceleration at 3 sec due to the randomization of hypocenters using hypocenter distribution model from Chiou and Youngs [2008] for a moment-magnitude 6, reverse rupture.**

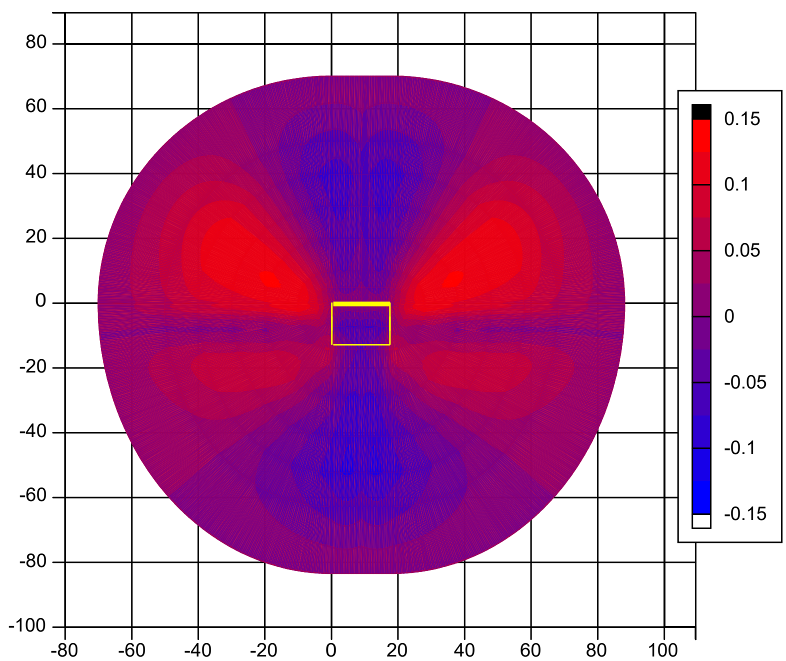

Figure 5.12 **Model of change in the mean of the natural log of the 5% damped pseudo-spectral acceleration at 3 sec due to the randomization of hypocenters using hypocenter distribution model from Chiou and Youngs [2008] for a moment-magnitude 6.5, reverse rupture.**

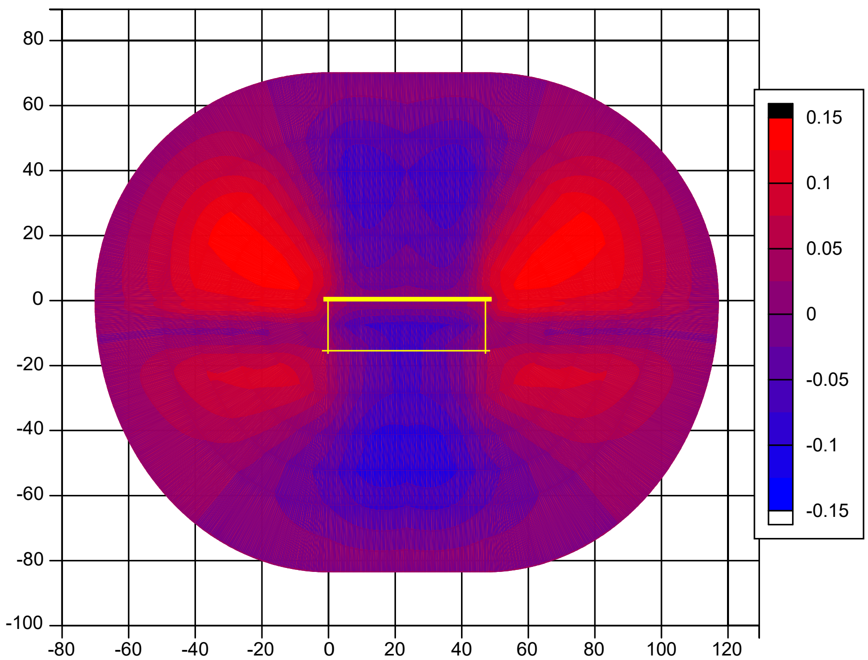

Figure 5.13 **Model of change in the mean of the natural log of the 5% damped pseudo-spectral acceleration at 3 sec due to the randomization of hypocenters using hypocenter distribution model from Chiou and Youngs [2008] for a moment-magnitude 7, reverse rupture.**

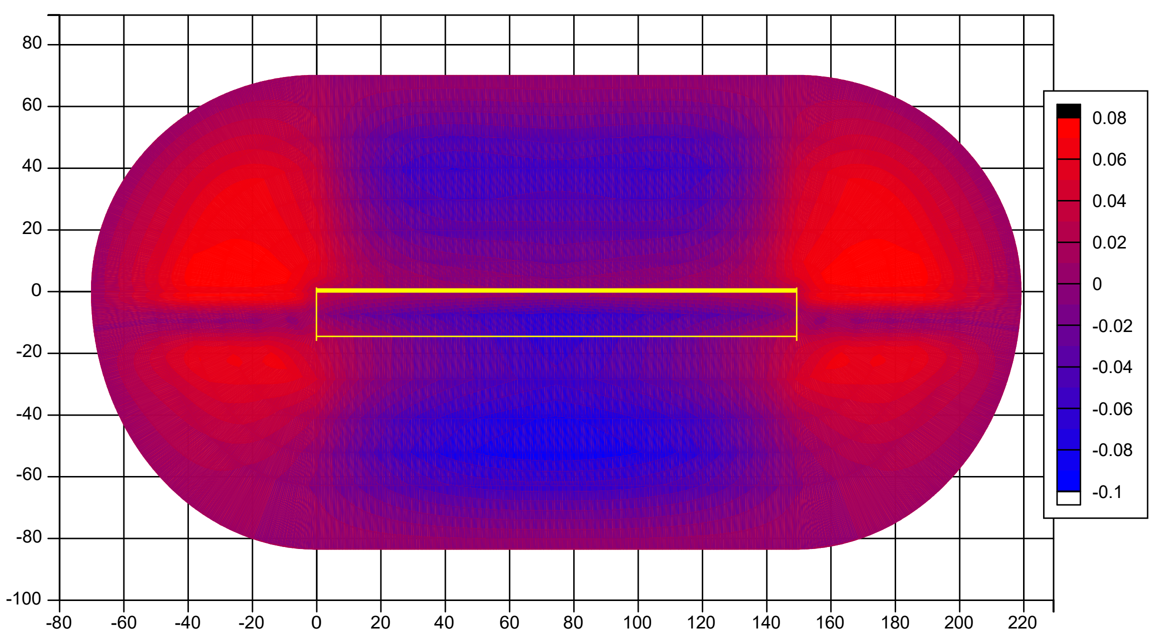

Figure 5.14 **Model of change in the mean of the natural log of the 5% damped pseudo-spectral acceleration at 3 sec due to the randomization of hypocenters using hypocenter distribution model from Chiou and Youngs [2008] for a moment-magnitude 7.5, reverse rupture.**

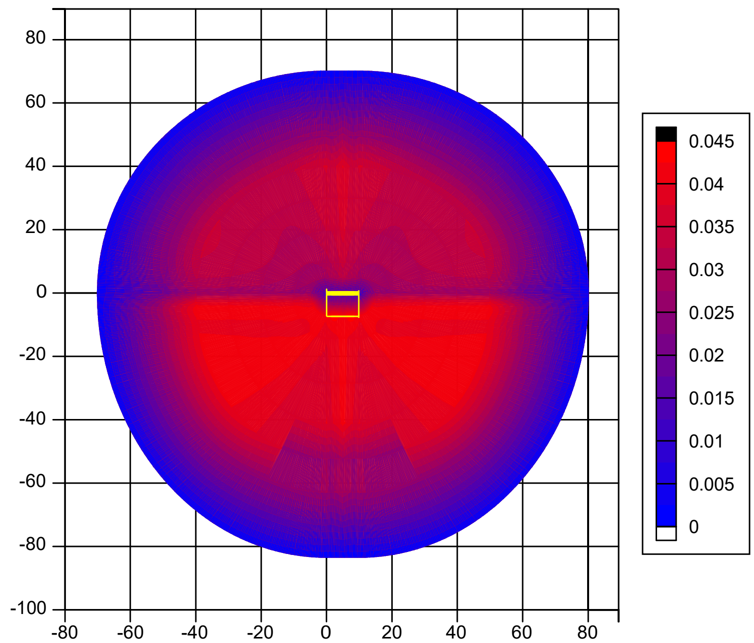

Figure 5.15 **Model of change in the standard deviation of the natural log of the 5% damped pseudo-spectral acceleration at 3 sec due to the randomization of hypocenters using hypocenter distribution model from Chiou and Youngs [2008] for a moment-magnitude 6, reverse rupture.**

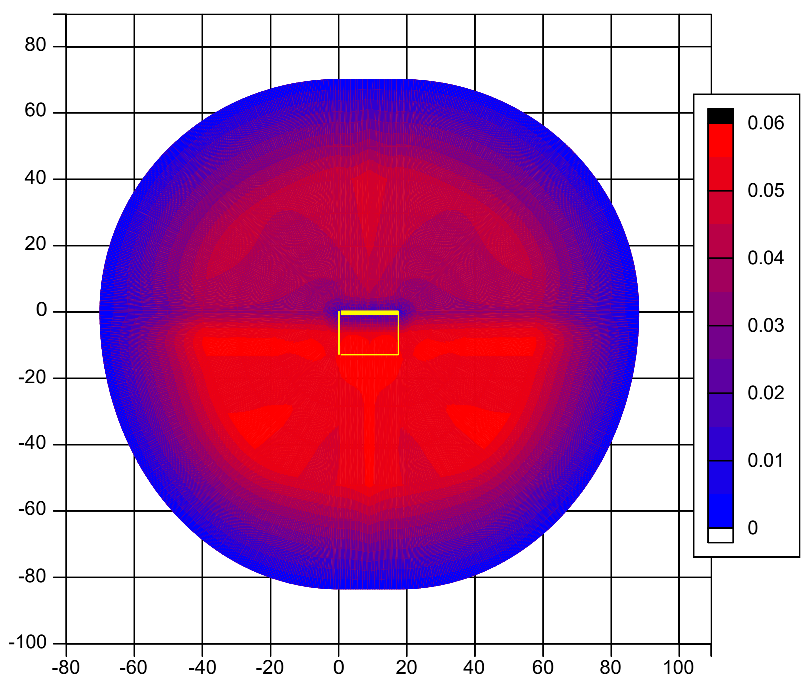

Figure 5.16 **Model of change in the standard deviation of the natural log of the 5% damped pseudo-spectral acceleration at 3 sec due to the randomization of hypocenters using hypocenter distribution model from Chiou and Youngs [2008] for a moment-magnitude 6.5, reverse rupture.**

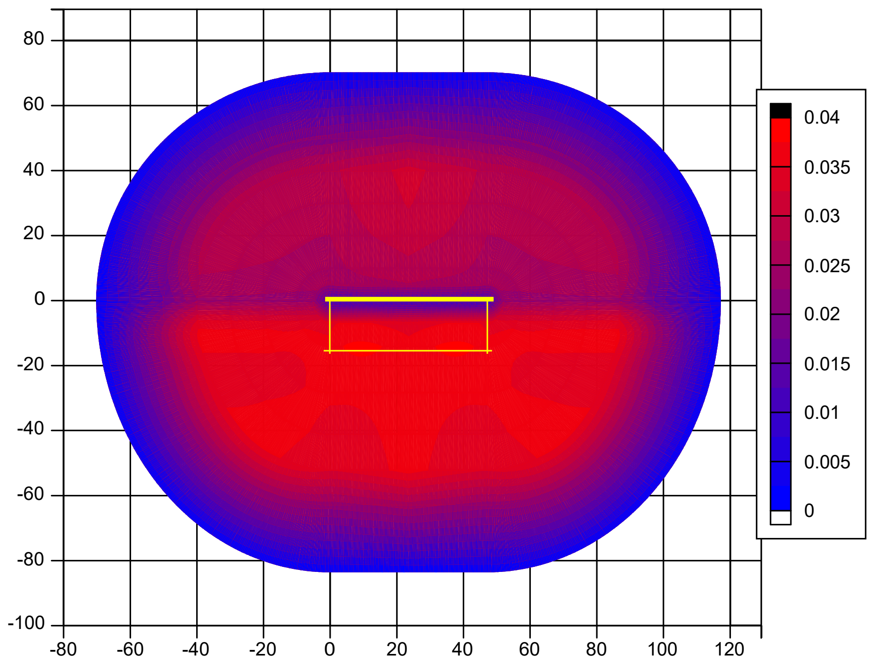

Figure 5.17 **Model of change in the standard deviation of the natural log of the 5% damped pseudo-spectral acceleration at 3 sec due to the randomization of hypocenters using hypocenter distribution model from Chiou and Youngs [2008] for a moment-magnitude 7, reverse rupture.**

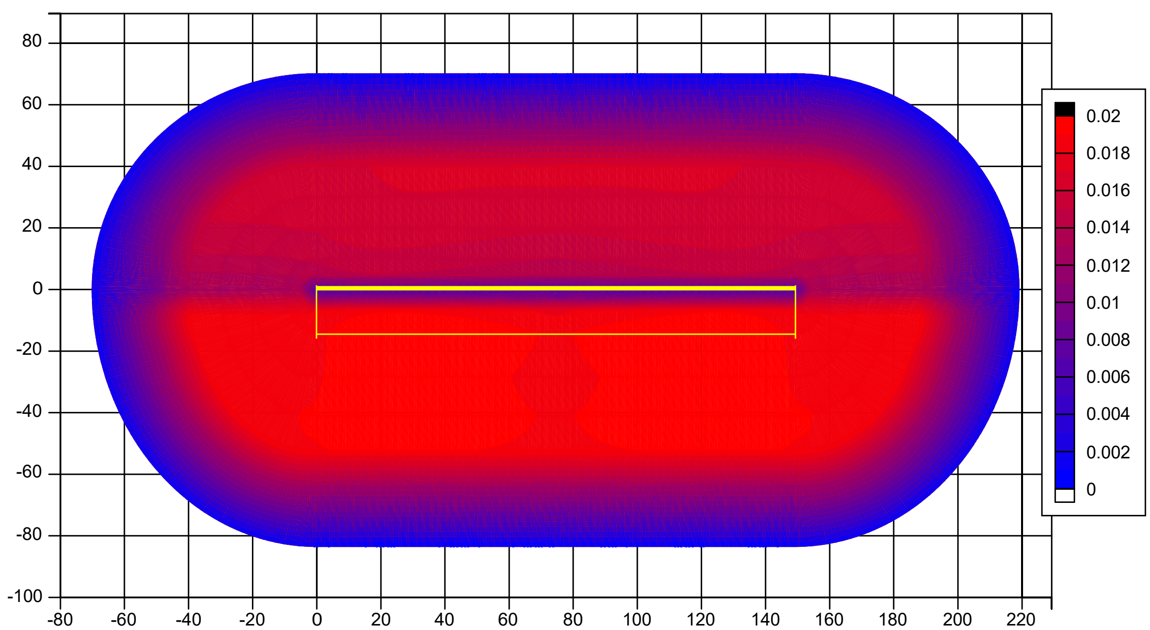

Figure 5.18 **Model of change in the standard deviation of the natural log of the 5% damped pseudo-spectral acceleration at 3 sec due to the randomization of hypocenters using hypocenter distribution model from Chiou and Youngs [2008].**

5.3 EXAMPLE APPLICATION

Example calculations are performed at three sites around a strike–slip fault with a length of 150 km and a width of 12 km. The locations of the three sites with respect to the fault are shown in Figure 5.19. The change in the mean of the natural log of the 5% damped pseudo-spectral acceleration is calculated using the preferred model for a moment-magnitude of 7.3 at the three sites; see Figure 5.20. The change in the standard deviation of the natural log of the 5% damped pseudo-spectral acceleration is calculated and presented in Figure 5.21. The change in the mean and standard deviation peaks for each site at a period of 5 sec.

Example hazard calculations are performed at the three sites assuming the fault has a slip rate of 5 mm/yr and modeling the earthquake recurrence using Youngs and Coppersmith [1985] with an average characteristic magnitude of 7.3. The hazard curves calculated for 5% damped pseudo-spectral acceleration at 3 sec are shown in Figure 5.22. There is a very slight decrease in the hazard at the site located near the middle of the rupture, a slight increase in the hazard at the site located at the very end of the rupture, and an increase in the hazard at the site located 15 km off the end of the rupture.

The uniform hazard spectrum (UHS) at all three sites with and without the preferred directivity model are calculated for an annual probability of exceedance of 10^{-4} and shown in Figure 5.23. The effect of the preferred directivity model on the 10^{-4} UHS is calculated by dividing the UHS calculated with the preferred model by the UHS calculated without the preferred model; see Figure 5.24. The change in the UHS is similar to that calculated for a full rupture of the fault using the average characteristic magnitude.

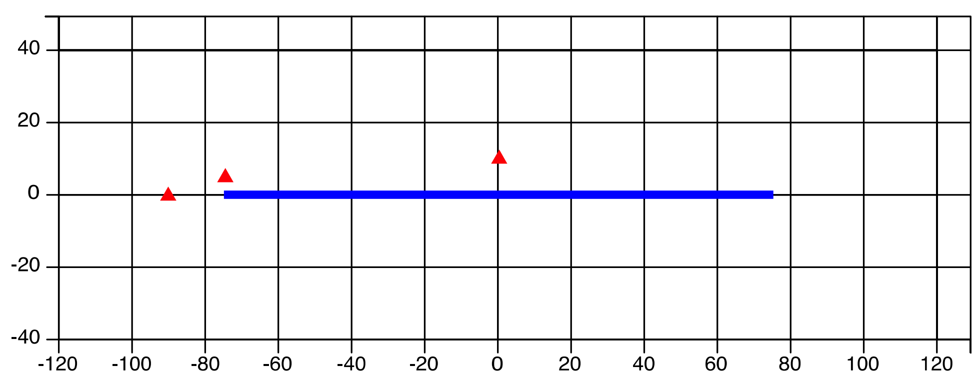

Figure 5.19 Location of three sites for example strike–slip fault.

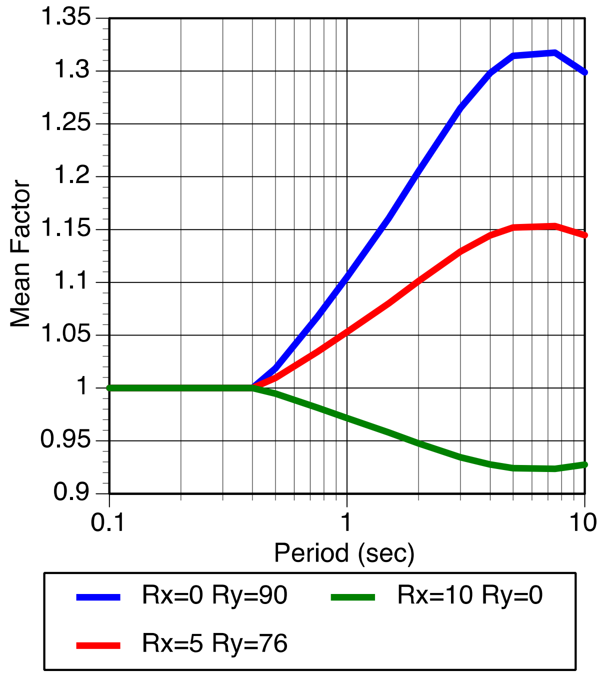

Figure 5.20 **Preferred strike–slip model of change in the mean of the natural log of the 5% damped pseudo-spectral acceleration for example magnitude 7.3 strike–slip rupture with sites located at *Rx* = 0, *Ry* = 90, *Rx* = 5, *Ry* = 76, *and Rx* = 10, *Ry* = 0.**

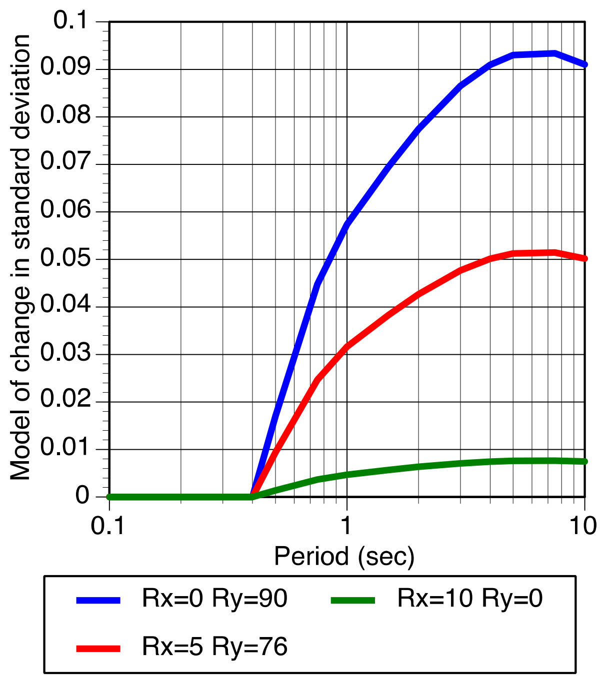

Figure 5.21 **Preferred strike–slip model of change in the standard deviation of the natural log of the 5% damped pseudo-spectral acceleration for example magnitude 7 strike–slip rupture with sites located at *Rx* = 0, *Ry* = 90, *Rx* = 5, *Ry* = 76, *and Rx* = 10, *Ry* = 0.**

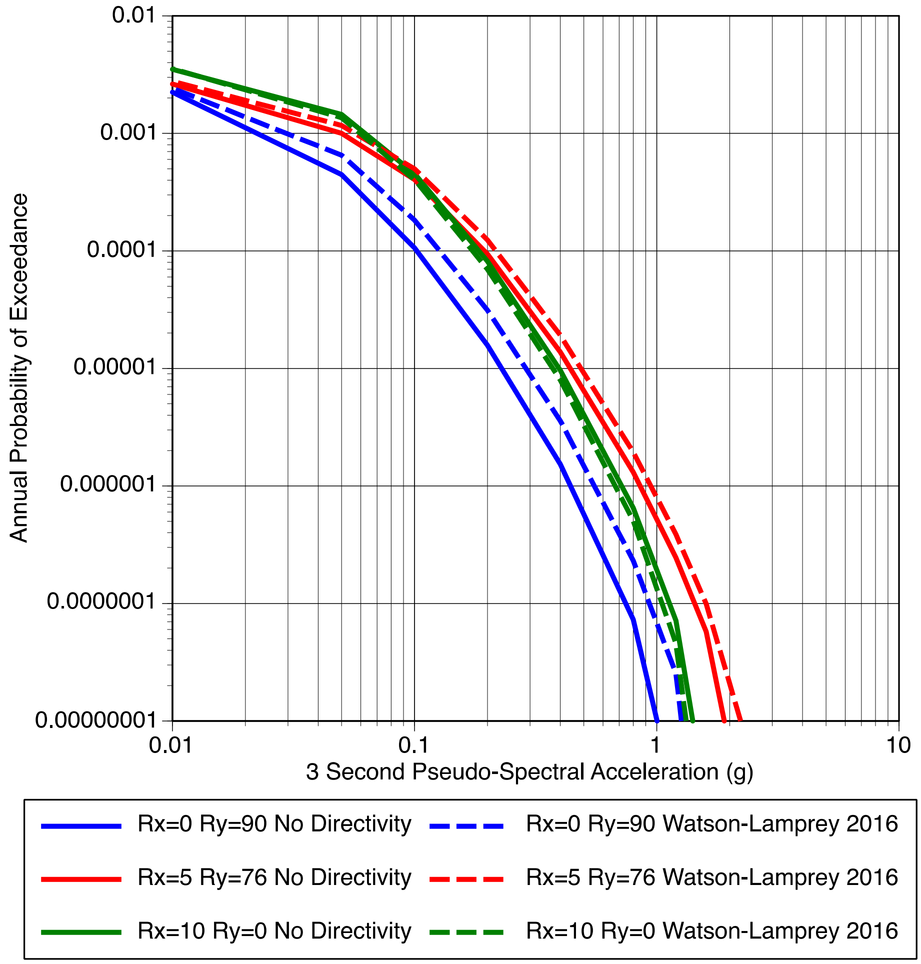

Figure 5.22 Hazard curves calculated with and without the preferred directivity model for 5% damped pseudo-spectral acceleration at 3 sec for example application with sites located at *Rx* = 0, *Ry* = 90, *Rx* = 5, *Ry* = 76, and *Rx* = 10, *Ry* = 0.

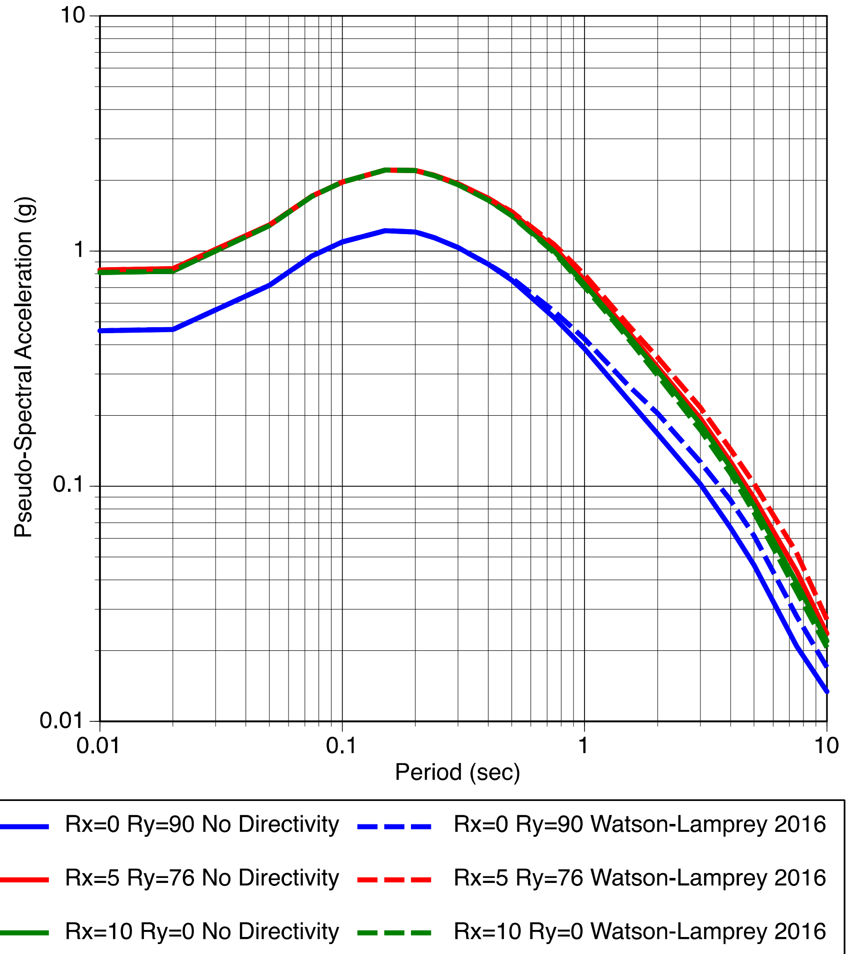

Figure 5.23 Uniform hazard spectra calculated with and without the preferred directivity model at an annual exceedance probability of 10^{-4} for the example application with sites located at *Rx* = 0, *Ry* = 90, *Rx* = 5, *Ry* = 76, *and Rx* = 10, *Ry* = 0.

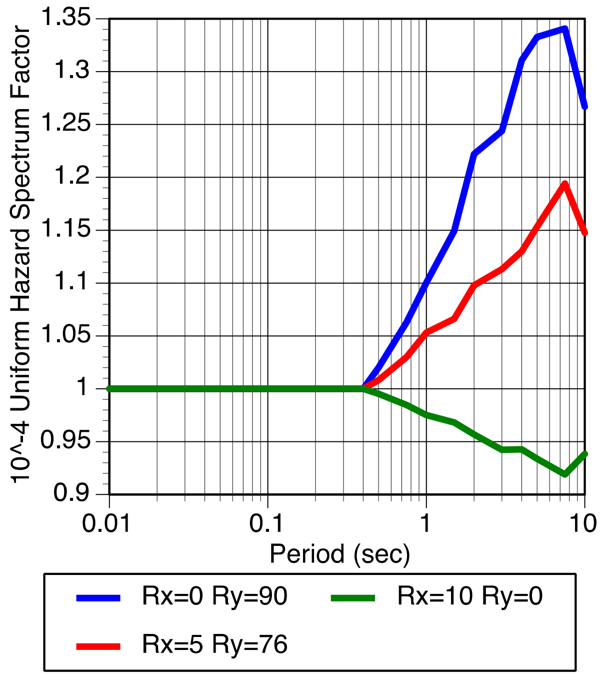

Figure 5.24 **The effect on the uniform hazard spectrum calculated with and without the preferred directivity model at an annual exceedance probability of 10^{-4} for the example application with sites located at *Rx* = 0*, Ry* = 90*, Rx* = 5*, Ry* = 76*, and Rx* = 10*, Ry* = 0.**

REFERENCES

Abrahamson N.A. (2000), Effects of rupture directivity on probabilistic seismic hazard analysis, *Proceedings of the 6th International Conference on Seismic Zonation*, Earthquake Engineering Research Institute Palm Springs, CA.

Chiou B.S.-J., Youngs R.R. (2008). An NGA model for the average horizontal component of peak ground motion and response spectra, *Earthq. Spectra*, 24: 173–215.

Chiou B.S.-J., Youngs R.R. (2014). Update of the Chiou and Youngs NGA model for the average horizontal component of peak ground motion and response spectra, *Earthq. Spectra*, 30: 1117–1153.

Rowshandel B. (2010), Directivity correction for the Next Generation Attenuation (NGA) relations, *Earthq. Spectra*: 26: 525–559.

Somerville P.G., Smith N.F., Graves R.W., Abrahamson N.A. (1997). Modification of empirical strong ground motion attenuation relations to include the amplitude and duration effects of rupture directivity, *Seismol. Res. Lett.,* 68(1): 199–222.

Spudich P., Chiou B.S.-J., Graves R.W., Collins N., Somerville P.G. (2004). A formulation of directivity for earthquake sources using isochrone theory, U.S. Geological Survey, *USGS Open-file Report 2004-1268*, Menlo Park, CA.

Spudich P., Chiou B.S.-J. [2008], Directivity in NGA earthquake ground motions: Analysis using isochrone theory. *Earthq. Spectra,* 24: 279–298.

Spudich P., Chiou B.S.-J. (2015), Strike-parallel and strike-normal coordinate system around geometrically complicated rupture traces – Used by NGA-West2 and further improvements, U.S. Geological Survey, *USGS Open-File Report 2015-1028*, Menlo Park, CA.

Spudich P., Rowshandel B., Shahi S. K., Baker J.W., Chiou, B.S.-J. (2013), Final report of the NGA-West2 directivity working group, *PEER Report No. 2013/09*, Pacific Earthquake Engineering Research Center, University of California, Berkeley, CA.

Watson-Lamprey J.A. (2007). The search for directivity, *Proceedings, Seismological Society of America Annual Meeting,* Kona, HI.

Youngs, R. R. (2015), Personal communication May 5, 2015.

Youngs R.R., Coppersmith K.J. (1985). Implications of fault slip rates and earthquake recurrence models to probabilistic seismic hazard estimates, *Bull. Seismol. Soc. Am*., 75(4): 939–964

LIST OF PEER REPORTS

PEER reports are available as a free PDF download from https://peer.berkeley.edu/peer-reports. In addition, printed hard copies of PEER reports can be ordered directly from our printer by following the instructions also at https://peer.berkeley.edu/peer-reports. For other related questions about the PEER Report Series, contact the Pacific Earthquake Engineering Research Center, 325 Davis Hall, Mail Code 1792, Berkeley, CA 94720. Tel.: (510) 642-3437; and Email: peer_center@berkeley.edu.

PEER 2018/03 *Probabilistic Seismic Hazard Analysis Code Verification*. Christie Hale, Norman Abrahamson, and Yousef Bozorgnia. July 2018.

PEER 2018/02 *Update of the BCHydro Subduction Ground-Motion Model using the NGA-Subduction Dataset.* Norman Abrahamson, Nicolas Kuehn, Zeynep Gulerce, Nicholas Gregor, Yousef Bozorgnia, Grace Parker, Jonathan Stewart, Brian Chiou, I. M. Idriss, Kenneth Campbell, and Robert Youngs. June 2018.

PEER 2018/01 *PEER Annual Report 2017–2018*. Khalid Mosalam, Amarnath Kasalanati, and Selim Günay. June 2018.

PEER 2017/12 *Experimental Investigation of the Behavior of Vintage and Retrofit Concentrically Braced Steel Frames under Cyclic Loading*. Barbara G. Simpson, Stephen A. Mahin, and Jiun-Wei Lai, December 2017.

PEER 2017/11 *Preliminary Studies on the Dynamic Response of a Seismically Isolated Prototype Gen-IV Sodium-Cooled Fast Reactor* (*PGSFR*). Benshun Shao, Andreas H. Schellenberg, Matthew J. Schoettler, and Stephen A. Mahin. December 2017.

PEER 2017/10 *Development of Time Histories for IEEE693 Testing and Analysis (including Seismically Isolated Equipment).* Shakhzod M. Takhirov, Eric Fujisaki, Leon Kempner, Michael Riley, and Brian Low. December 2017.

PEER 2017/09 *"R" Package for Computation of Earthquake Ground-Motion Response Spectra.* Pengfei Wang, Jonathan P. Stewart, Yousef Bozorgnia, David M. Boore, and Tadahiro Kishida. December 2017.

PEER 2017/08 *Influence of Kinematic SSI on Foundation Input Motions for Bridges on Deep Foundations*. Benjamin J. Turner, Scott J. Brandenberg, and Jonathan P. Stewart. November 2017.

PEER 2017/07 *A Nonlinear Kinetic Model for Multi-Stage Friction Pendulum Systems*. Paul L. Drazin and Sanjay Govindjee. September 2017.

PEER 2017/06 *Guidelines for Performance-Based Seismic Design of Tall Buildings, Version 2.02*. TBI Working Group led by co-chairs Ron Hamburger and Jack Moehle: Jack Baker, Jonathan Bray, C.B. Crouse, Greg Deierlein, John Hooper, Marshall Lew, Joe Maffei, Stephen Mahin, James Malley, Farzad Naeim, Jonathan Stewart, and John Wallace. May 2017.

PEER 2017/05 *Recommendations for Ergodic Nonlinear Site Amplification in Central and Eastern North America*. Youssef M.A. Hashash, Joseph A. Harmon, Okan Ilhan, Grace A. Parker, and Jonathan P. Stewart. March 2017.

PEER 2017/04 *Expert Panel Recommendations for Ergodic Site Amplification in Central and Eastern North America*. Jonathan P. Stewart, Grace A. Parker, Joseph P. Harmon, Gail M. Atkinson, David M. Boore, Robert B. Darragh, Walter J. Silva, and Youssef M.A. Hashash. March 2017.

PEER 2017/03 *NGA-East Ground-Motion Models for the U.S. Geological Survey National Seismic Hazard Maps*. Christine A. Goulet, Yousef Bozorgnia, Nicolas Kuehn, Linda Al Atik, Robert R. Youngs, Robert W. Graves, and Gail M. Atkinson. March 2017.

PEER 2017/02 *U.S.–New Zealand–Japan Workshop: Liquefaction-Induced Ground Movements Effects, University of California, Berkeley, California, 2–4 November 2016.* Jonathan D. Bray, Ross W. Boulanger, Misko Cubrinovski, Kohji Tokimatsu, Steven L. Kramer, Thomas O'Rourke, Ellen Rathje, Russell A. Green, Peter K. Robinson, and Christine Z. Beyzaei. March 2017.

PEER 2017/01 *2016 PEER Annual Report*. Khalid M. Mosalam, Amarnath Kasalanati, and Grace Kang. March 2017.

PEER 2016/10 *Performance-Based Robust Nonlinear Seismic Analysis with Application to Reinforced Concrete Bridge Systems*. Xiao Ling and Khalid M. Mosalam. December 2016.

PEER 2017/09 *Segmental Displacement Control Design for Seismically Isolated Bridges,* Kenneth A. Ogorzalek and Stephen A. Mahin. December 2016.

PEER 2016/08 *Resilience of Critical Structures, Infrastructure, and Communities*. Gian Paolo Cimellaro, Ali Zamani-Noori, Omar Kamouh, Vesna Terzic, and Stephen A. Mahin. December 2016.

PEER 2016/07 *Hybrid Simulation Theory for a Classical Nonlinear Dynamical System*. Paul L. Drazin and Sanjay Govindjee. September 2016.

PEER 2016/06 *California Earthquake Early Warning System Benefit Study*. Laurie A. Johnson, Sharyl Rabinovici, Grace S. Kang, and Stephen A. Mahin. July 2006.

PEER 2016/05 *Ground-Motion Prediction Equations for Arias Intensity Consistent with the NGA-West2 Ground-Motion Models.* Charlotte Abrahamson, Hao-Jun Michael Shi, and Brian Yang. July 2016.

PEER 2016/04 *The M_W 6.0 South Napa Earthquake of August 24, 2014: A Wake-Up Call for Renewed Investment in Seismic Resilience Across California.* Prepared for the California Seismic Safety Commission, Laurie A. Johnson and Stephen A. Mahin. May 2016.

PEER 2016/03 *Simulation Confidence in Tsunami-Driven Overland Flow.* Patrick Lynett. May 2016.

PEER 2016/02 *Semi-Automated Procedure for Windowing time Series and Computing Fourier Amplitude Spectra for the NGA-West2 Database.* Tadahiro Kishida, Olga-Joan Ktenidou, Robert B. Darragh, and Walter J. Silva. May 2016.

PEER 2016/01 *A Methodology for the Estimation of Kappa (κ) from Large Datasets: Example Application to Rock Sites in the NGA-East Database and Implications on Design Motions.* Olga-Joan Ktenidou, Norman A. Abrahamson, Robert B. Darragh, and Walter J. Silva. April 2016.

PEER 2015/13 *Self-Centering Precast Concrete Dual-Steel-Shell Columns for Accelerated Bridge Construction: Seismic Performance, Analysis, and Design*. Gabriele Guerrini, José I. Restrepo, Athanassios Vervelidis, and Milena Massari. December 2015.

PEER 2015/12 *Shear-Flexure Interaction Modeling for Reinforced Concrete Structural Walls and Columns under Reversed Cyclic Loading*. Kristijan Kolozvari, Kutay Orakcal, and John Wallace. December 2015.

PEER 2015/11 *Selection and Scaling of Ground Motions for Nonlinear Response History Analysis of Buildings in Performance-Based Earthquake Engineering*. N. Simon Kwong and Anil K. Chopra. December 2015.

PEER 2015/10 *Structural Behavior of Column-Bent Cap Beam-Box Girder Systems in Reinforced Concrete Bridges Subjected to Gravity and Seismic Loads. Part II: Hybrid Simulation and Post-Test Analysis*. Mohamed A. Moustafa and Khalid M. Mosalam. November 2015.

PEER 2015/09 *Structural Behavior of Column-Bent Cap Beam-Box Girder Systems in Reinforced Concrete Bridges Subjected to Gravity and Seismic Loads. Part I: Pre-Test Analysis and Quasi-Static Experiments*. Mohamed A. Moustafa and Khalid M. Mosalam. September 2015.

PEER 2015/08 *NGA-East: Adjustments to Median Ground-Motion Models for Center and Eastern North America*. August 2015.

PEER 2015/07 *NGA-East: Ground-Motion Standard-Deviation Models for Central and Eastern North America*. Linda Al Atik. June 2015.

PEER 2015/06 *Adjusting Ground-Motion Intensity Measures to a Reference Site for which V_{S30} = 3000 m/sec*. David M. Boore. May 2015.

PEER 2015/05 *Hybrid Simulation of Seismic Isolation Systems Applied to an APR-1400 Nuclear Power Plant.* Andreas H. Schellenberg, Alireza Sarebanha, Matthew J. Schoettler, Gilberto Mosqueda, Gianmario Benzoni, and Stephen A. Mahin. April 2015.

PEER 2015/04 *NGA-East: Median Ground-Motion Models for the Central and Eastern North America Region*. April 2015.

PEER 2015/03 *Single Series Solution for the Rectangular Fiber-Reinforced Elastomeric Isolator Compression Modulus*. James M. Kelly and Niel C. Van Engelen. March 2015.

PEER 2015/02 *A Full-Scale, Single-Column Bridge Bent Tested by Shake-Table Excitation.* Matthew J. Schoettler, José I. Restrepo, Gabriele Guerrini, David E. Duck, and Francesco Carrea. March 2015.

PEER 2015/01 *Concrete Column Blind Prediction Contest 2010: Outcomes and Observations.* Vesna Terzic, Matthew J. Schoettler, José I. Restrepo, and Stephen A Mahin. March 2015.

PEER 2014/20 *Stochastic Modeling and Simulation of Near-Fault Ground Motions for Performance-Based Earthquake Engineering*. Mayssa Dabaghi and Armen Der Kiureghian. December 2014.

PEER 2014/19 *Seismic Response of a Hybrid Fiber-Reinforced Concrete Bridge Column Detailed for Accelerated Bridge Construction*. Wilson Nguyen, William Trono, Marios Panagiotou, and Claudia P. Ostertag. December 2014.

PEER 2014/18 *Three-Dimensional Beam-Truss Model for Reinforced Concrete Walls and Slabs Subjected to Cyclic Static or Dynamic Loading*. Yuan Lu, Marios Panagiotou, and Ioannis Koutromanos. December 2014.

PEER 2014/17 *PEER NGA-East Database.* Christine A. Goulet, Tadahiro Kishida, Timothy D. Ancheta, Chris H. Cramer, Robert B. Darragh, Walter J. Silva, Youssef M.A. Hashash, Joseph Harmon, Jonathan P. Stewart, Katie E. Wooddell, and Robert R. Youngs. October 2014.

PEER 2014/16 *Guidelines for Performing Hazard-Consistent One-Dimensional Ground Response Analysis for Ground Motion Prediction*. Jonathan P. Stewart, Kioumars Afshari, and Youssef M.A. Hashash. October 2014.

PEER 2014/15 *NGA-East Regionalization Report: Comparison of Four Crustal Regions within Central and Eastern North America using Waveform Modeling and 5%-Damped Pseudo-Spectral Acceleration Response*. Jennifer Dreiling, Marius P. Isken, Walter D. Mooney, Martin C. Chapman, and Richard W. Godbee. October 2014.

PEER 2014/14 *Scaling Relations between Seismic Moment and Rupture Area of Earthquakes in Stable Continental Regions*. Paul Somerville. August 2014.

PEER 2014/13 *PEER Preliminary Notes and Observations on the August 24, 2014, South Napa Earthquake*. Grace S. Kang and Stephen A. Mahin, Editors. September 2014.

PEER 2014/12 *Reference-Rock Site Conditions for Central and Eastern North America: Part II – Attenuation (Kappa) Definition*. Kenneth W. Campbell, Youssef M.A. Hashash, Byungmin Kim, Albert R. Kottke, Ellen M. Rathje, Walter J. Silva, and Jonathan P. Stewart. August 2014.

PEER 2014/11 *Reference-Rock Site Conditions for Central and Eastern North America: Part I - Velocity Definition*. Youssef M.A. Hashash, Albert R. Kottke, Jonathan P. Stewart, Kenneth W. Campbell, Byungmin Kim, Ellen M. Rathje, Walter J. Silva, Sissy Nikolaou, and Cheryl Moss. August 2014.

PEER 2014/10 *Evaluation of Collapse and Non-Collapse of Parallel Bridges Affected by Liquefaction and Lateral Spreading*. Benjamin Turner, Scott J. Brandenberg, and Jonathan P. Stewart. August 2014.

PEER 2014/09 *PEER Arizona Strong-Motion Database and GMPEs Evaluation*. Tadahiro Kishida, Robert E. Kayen, Olga-Joan Ktenidou, Walter J. Silva, Robert B. Darragh, and Jennie Watson-Lamprey. June 2014.

PEER 2014/08 *Unbonded Pretensioned Bridge Columns with Rocking Detail*. Jeffrey A. Schaefer, Bryan Kennedy, Marc O. Eberhard, and John F. Stanton. June 2014.

PEER 2014/07 *Northridge 20 Symposium Summary Report: Impacts, Outcomes, and Next Steps*. May 2014.

PEER 2014/06 *Report of the Tenth Planning Meeting of NEES/E-Defense Collaborative Research on Earthquake Engineering*. December 2013.

PEER 2014/05 *Seismic Velocity Site Characterization of Thirty-One Chilean Seismometer Stations by Spectral Analysis of Surface Wave Dispersion*. Robert Kayen, Brad D. Carkin, Skye Corbet, Camilo Pinilla, Allan Ng, Edward Gorbis, and Christine Truong. April 2014.

PEER 2014/04 Effect of Vertical Acceleration on Shear Strength of Reinforced Concrete Columns. Hyerin Lee and Khalid M. Mosalam. April 2014.

PEER 2014/03 *Retest of Thirty-Year-Old Neoprene Isolation Bearings.* James M. Kelly and Niel C. Van Engelen. March 2014.

PEER 2014/02 *Theoretical Development of Hybrid Simulation Applied to Plate Structures.* Ahmed A. Bakhaty, Khalid M. Mosalam, and Sanjay Govindjee. January 2014.

PEER 2014/01 *Performance-Based Seismic Assessment of Skewed Bridges.* Peyman Kaviani, Farzin Zareian, and Ertugrul Taciroglu. January 2014.

PEER 2013/26 *Urban Earthquake Engineerin*g. Proceedings of the U.S.-Iran Seismic Workshop. December 2013.

PEER 2013/25 *Earthquake Engineering for Resilient Communities: 2013 PEER Internship Program Research Report Collection.* Heidi Tremayne (Editor), Stephen A. Mahin (Editor), Jorge Archbold Monterossa, Matt Brosman, Shelly Dean, Katherine deLaveaga, Curtis Fong, Donovan Holder, Rakeeb Khan, Elizabeth Jachens, David Lam, Daniela Martinez Lopez, Mara Minner, Geffen Oren, Julia Pavicic, Melissa Quinonez, Lorena Rodriguez, Sean Salazar, Kelli Slaven, Vivian Steyert, Jenny Taing, and Salvador Tena. December 2013.

PEER 2013/24 *NGA-West2 Ground Motion Prediction Equations for Vertical Ground Motions*. September 2013.

PEER 2013/23 *Coordinated Planning and Preparedness for Fire Following Major Earthquakes*. Charles Scawthorn. November 2013.

PEER 2013/22 *GEM-PEER Task 3 Project: Selection of a Global Set of Ground Motion Prediction Equations.* Jonathan P. Stewart, John Douglas, Mohammad B. Javanbarg, Carola Di Alessandro, Yousef Bozorgnia, Norman A. Abrahamson, David M. Boore, Kenneth W. Campbell, Elise Delavaud, Mustafa Erdik, and Peter J. Stafford. December 2013.

PEER 2013/21 *Seismic Design and Performance of Bridges with Columns on Rocking Foundations*. Grigorios Antonellis and Marios Panagiotou. September 2013.

PEER 2013/20 *Experimental and Analytical Studies on the Seismic Behavior of Conventional and Hybrid Braced Frames*. Jiun-Wei Lai and Stephen A. Mahin. September 2013.

PEER 2013/19 *Toward Resilient Communities: A Performance-Based Engineering Framework for Design and Evaluation of the Built Environment.* Michael William Mieler, Bozidar Stojadinovic, Robert J. Budnitz, Stephen A. Mahin, and Mary C. Comerio. September 2013.

PEER 2013/18 *Identification of Site Parameters that Improve Predictions of Site Amplification*. Ellen M. Rathje and Sara Navidi. July 2013.

PEER 2013/17 *Response Spectrum Analysis of Concrete Gravity Dams Including Dam-Water-Foundation Interaction*. Arnkjell Løkke and Anil K. Chopra. July 2013.

PEER 2013/16 *Effect of Hoop Reinforcement Spacing on the Cyclic Response of Large Reinforced Concrete Special Moment Frame Beams.* Marios Panagiotou, Tea Visnjic, Grigorios Antonellis, Panagiotis Galanis, and Jack P. Moehle. June 2013.

PEER 2013/15 *A Probabilistic Framework to Include the Effects of Near-Fault Directivity in Seismic Hazard Assessment*. Shrey Kumar Shahi, Jack W. Baker. October 2013.

PEER 2013/14 *Hanging-Wall Scaling using Finite-Fault Simulations.* Jennifer L. Donahue and Norman A. Abrahamson. September 2013.

PEER 2013/13 *Semi-Empirical Nonlinear Site Amplification and its Application in NEHRP Site Factors*. Jonathan P. Stewart and Emel Seyhan. November 2013.

PEER 2013/12 *Nonlinear Horizontal Site Response for the NGA-West2 Project.* Ronnie Kamai, Norman A. Abramson, Walter J. Silva. May 2013.

PEER 2013/11 *Epistemic Uncertainty for NGA-West2 Models.* Linda Al Atik and Robert R. Youngs. May 2013.

PEER 2013/10 *NGA-West 2 Models for Ground-Motion Directionality.* Shrey K. Shahi and Jack W. Baker. May 2013.

PEER 2013/09 *Final Report of the NGA-West2 Directivity Working Group.* Paul Spudich, Jeffrey R. Bayless, Jack W. Baker, Brian S.J. Chiou, Badie Rowshandel, Shrey Shahi, and Paul Somerville. May 2013.

PEER 2013/08 *NGA-West2 Model for Estimating Average Horizontal Values of Pseudo-Absolute Spectral Accelerations Generated by Crustal Earthquakes*. I. M. Idriss. May 2013.

PEER 2013/07 *Update of the Chiou and Youngs NGA Ground Motion Model for Average Horizontal Component of Peak Ground Motion and Response Spectra*. Brian Chiou and Robert Youngs. May 2013.

PEER 2013/06 *NGA-West2 Campbell-Bozorgnia Ground Motion Model for the Horizontal Components of PGA, PGV, and 5%-Damped Elastic Pseudo-Acceleration Response Spectra for Periods Ranging from 0.01 to 10 sec.* Kenneth W. Campbell and Yousef Bozorgnia. May 2013.

PEER 2013/05 *NGA-West 2 Equations for Predicting Response Spectral Accelerations for Shallow Crustal Earthquakes*. David M. Boore, Jonathan P. Stewart, Emel Seyhan, and Gail M. Atkinson. May 2013.

PEER 2013/04 *Update of the AS08 Ground-Motion Prediction Equations Based on the NGA-West2 Data Set*. Norman Abrahamson, Walter Silva, and Ronnie Kamai. May 2013.

PEER 2013/03 *PEER NGA-West2 Database.* Timothy D. Ancheta, Robert B. Darragh, Jonathan P. Stewart, Emel Seyhan, Walter J. Silva, Brian S.J. Chiou, Katie E. Wooddell, Robert W. Graves, Albert R. Kottke, David M. Boore, Tadahiro Kishida, and Jennifer L. Donahue. May 2013.

PEER 2013/02 *Hybrid Simulation of the Seismic Response of Squat Reinforced Concrete Shear Walls*. Catherine A. Whyte and Bozidar Stojadinovic. May 2013.

PEER 2013/01 *Housing Recovery in Chile: A Qualitative Mid-program Review*. Mary C. Comerio. February 2013.

PEER 2012/08 *Guidelines for Estimation of Shear Wave Velocity.* Bernard R. Wair, Jason T. DeJong, and Thomas Shantz. December 2012.

PEER 2012/07 *Earthquake Engineering for Resilient Communities: 2012 PEER Internship Program Research Report Collection.* Heidi Tremayne (Editor), Stephen A. Mahin (Editor), Collin Anderson, Dustin Cook, Michael Erceg, Carlos Esparza, Jose Jimenez, Dorian Krausz, Andrew Lo, Stephanie Lopez, Nicole McCurdy, Paul Shipman, Alexander Strum, Eduardo Vega. December 2012.

PEER 2012/06 *Fragilities for Precarious Rocks at Yucca Mountain.* Matthew D. Purvance, Rasool Anooshehpoor, and James N. Brune. December 2012.

PEER 2012/05 *Development of Simplified Analysis Procedure for Piles in Laterally Spreading Layered Soils.* Christopher R. McGann, Pedro Arduino, and Peter Mackenzie–Helnwein. December 2012.

PEER 2012/04 *Unbonded Pre-Tensioned Columns for Bridges in Seismic Regions.* Phillip M. Davis, Todd M. Janes, Marc O. Eberhard, and John F. Stanton. December 2012.

PEER 2012/03 *Experimental and Analytical Studies on Reinforced Concrete Buildings with Seismically Vulnerable Beam-Column Joints*. Sangjoon Park and Khalid M. Mosalam. October 2012.

PEER 2012/02 *Seismic Performance of Reinforced Concrete Bridges Allowed to Uplift during Multi-Directional Excitation*. Andres Oscar Espinoza and Stephen A. Mahin. July 2012.

PEER 2012/01 *Spectral Damping Scaling Factors for Shallow Crustal Earthquakes in Active Tectonic Regions.* Sanaz Rezaeian, Yousef Bozorgnia, I. M. Idriss, Kenneth Campbell, Norman Abrahamson, and Walter Silva. July 2012.

PEER 2011/10 *Earthquake Engineering for Resilient Communities: 2011 PEER Internship Program Research Report Collection*. Heidi Faison and Stephen A. Mahin, Editors. December 2011.

PEER 2011/09 *Calibration of Semi-Stochastic Procedure for Simulating High-Frequency Ground Motions*. Jonathan P. Stewart, Emel Seyhan, and Robert W. Graves. December 2011.

PEER 2011/08 *Water Supply in regard to Fire Following Earthquake*. Charles Scawthorn. November 2011.

PEER 2011/07 *Seismic Risk Management in Urban Areas*. Proceedings of a U.S.-Iran-Turkey Seismic Workshop. September 2011.

PEER 2011/06 *The Use of Base Isolation Systems to Achieve Complex Seismic Performance Objectives*. Troy A. Morgan and Stephen A. Mahin. July 2011.

PEER 2011/05 *Case Studies of the Seismic Performance of Tall Buildings Designed by Alternative Means.* Task 12 Report for the Tall Buildings Initiative. Jack Moehle, Yousef Bozorgnia, Nirmal Jayaram, Pierson Jones, Mohsen Rahnama, Nilesh Shome, Zeynep Tuna, John Wallace, Tony Yang, and Farzin Zareian. July 2011.

PEER 2011/04 *Recommended Design Practice for Pile Foundations in Laterally Spreading Ground.* Scott A. Ashford, Ross W. Boulanger, and Scott J. Brandenberg. June 2011.

PEER 2011/03 *New Ground Motion Selection Procedures and Selected Motions for the PEER Transportation Research Program*. Jack W. Baker, Ting Lin, Shrey K. Shahi, and Nirmal Jayaram. March 2011.

PEER 2011/02 *A Bayesian Network Methodology for Infrastructure Seismic Risk Assessment and Decision Support*. Michelle T. Bensi, Armen Der Kiureghian, and Daniel Straub. March 2011.

PEER 2011/01 *Demand Fragility Surfaces for Bridges in Liquefied and Laterally Spreading Ground.* Scott J. Brandenberg, Jian Zhang, Pirooz Kashighandi, Yili Huo, and Minxing Zhao. March 2011.

PEER 2010/05 *Guidelines for Performance-Based Seismic Design of Tall Buildings.* Developed by the Tall Buildings Initiative. November 2010.

PEER 2010/04 *Application Guide for the Design of Flexible and Rigid Bus Connections between Substation Equipment Subjected to Earthquakes.* Jean-Bernard Dastous and Armen Der Kiureghian. September 2010.

PEER 2010/03 *Shear Wave Velocity as a Statistical Function of Standard Penetration Test Resistance and Vertical Effective Stress at Caltrans Bridge Sites.* Scott J. Brandenberg, Naresh Bellana, and Thomas Shantz. June 2010.

PEER 2010/02 *Stochastic Modeling and Simulation of Ground Motions for Performance-Based Earthquake Engineering.* Sanaz Rezaeian and Armen Der Kiureghian. June 2010.

PEER 2010/01 *Structural Response and Cost Characterization of Bridge Construction Using Seismic Performance Enhancement Strategies.* Ady Aviram, Božidar Stojadinović, Gustavo J. Parra-Montesinos, and Kevin R. Mackie. March 2010.

PEER 2009/03 *The Integration of Experimental and Simulation Data in the Study of Reinforced Concrete Bridge Systems Including Soil-Foundation-Structure Interaction.* Matthew Dryden and Gregory L. Fenves. November 2009.

PEER 2009/02 *Improving Earthquake Mitigation through Innovations and Applications in Seismic Science, Engineering, Communication, and Response*. Proceedings of a U.S.-Iran Seismic Workshop. October 2009.

PEER 2009/01 *Evaluation of Ground Motion Selection and Modification Methods: Predicting Median Interstory Drift Response of Buildings*. Curt B. Haselton, Editor. June 2009.

PEER 2008/10 *Technical Manual for Strata.* Albert R. Kottke and Ellen M. Rathje. February 2009.

PEER 2008/09 *NGA Model for Average Horizontal Component of Peak Ground Motion and Response Spectra.* Brian S.-J. Chiou and Robert R. Youngs. November 2008.

PEER 2008/08 *Toward Earthquake-Resistant Design of Concentrically Braced Steel Structures*. Patxi Uriz and Stephen A. Mahin. November 2008.

PEER 2008/07 *Using OpenSees for Performance-Based Evaluation of Bridges on Liquefiable Soils*. Stephen L. Kramer, Pedro Arduino, and HyungSuk Shin. November 2008.

PEER 2008/06 *Shaking Table Tests and Numerical Investigation of Self-Centering Reinforced Concrete Bridge Columns*. Hyung IL Jeong, Junichi Sakai, and Stephen A. Mahin. September 2008.

PEER 2008/05 *Performance-Based Earthquake Engineering Design Evaluation Procedure for Bridge Foundations Undergoing Liquefaction-Induced Lateral Ground Displacement*. Christian A. Ledezma and Jonathan D. Bray. August 2008.

PEER 2008/04 *Benchmarking of Nonlinear Geotechnical Ground Response Analysis Procedures.* Jonathan P. Stewart, Annie On-Lei Kwok, Youssef M. A. Hashash, Neven Matasovic, Robert Pyke, Zhiliang Wang, and Zhaohui Yang. August 2008.

PEER 2008/03 *Guidelines for Nonlinear Analysis of Bridge Structures in California.* Ady Aviram, Kevin R. Mackie, and Božidar Stojadinović. August 2008.

PEER 2008/02 *Treatment of Uncertainties in Seismic-Risk Analysis of Transportation Systems*. Evangelos Stergiou and Anne S. Kiremidjian. July 2008.

PEER 2008/01 *Seismic Performance Objectives for Tall Buildings.* William T. Holmes, Charles Kircher, William Petak, and Nabih Youssef. August 2008.

PEER 2007/12 *An Assessment to Benchmark the Seismic Performance of a Code-Conforming Reinforced Concrete Moment-Frame Building.* Curt Haselton, Christine A. Goulet, Judith Mitrani-Reiser, James L. Beck, Gregory G. Deierlein, Keith A. Porter, Jonathan P. Stewart, and Ertugrul Taciroglu. August 2008.

PEER 2007/11 *Bar Buckling in Reinforced Concrete Bridge Columns.* Wayne A. Brown, Dawn E. Lehman, and John F. Stanton. February 2008.

PEER 2007/10 *Computational Modeling of Progressive Collapse in Reinforced Concrete Frame Structures*. Mohamed M. Talaat and Khalid M. Mosalam. May 2008.

PEER 2007/09 *Integrated Probabilistic Performance-Based Evaluation of Benchmark Reinforced Concrete Bridges*. Kevin R. Mackie, John-Michael Wong, and Božidar Stojadinović. January 2008.

PEER 2007/08 *Assessing Seismic Collapse Safety of Modern Reinforced Concrete Moment-Frame Buildings*. Curt B. Haselton and Gregory G. Deierlein. February 2008.

PEER 2007/07 *Performance Modeling Strategies for Modern Reinforced Concrete Bridge Columns*. Michael P. Berry and Marc O. Eberhard. April 2008.

PEER 2007/06 *Development of Improved Procedures for Seismic Design of Buried and Partially Buried Structures*. Linda Al Atik and Nicholas Sitar. June 2007.

PEER 2007/05 *Uncertainty and Correlation in Seismic Risk Assessment of Transportation Systems*. Renee G. Lee and Anne S. Kiremidjian. July 2007.

PEER 2007/04 *Numerical Models for Analysis and Performance-Based Design of Shallow Foundations Subjected to Seismic Loading.* Sivapalan Gajan, Tara C. Hutchinson, Bruce L. Kutter, Prishati Raychowdhury, José A. Ugalde, and Jonathan P. Stewart. May 2008.

PEER 2007/03 *Beam-Column Element Model Calibrated for Predicting Flexural Response Leading to Global Collapse of RC Frame Buildings*. Curt B. Haselton, Abbie B. Liel, Sarah Taylor Lange, and Gregory G. Deierlein. May 2008.

PEER 2007/02 *Campbell-Bozorgnia NGA Ground Motion Relations for the Geometric Mean Horizontal Component of Peak and Spectral Ground Motion Parameters*. Kenneth W. Campbell and Yousef Bozorgnia. May 2007.

PEER 2007/01 *Boore-Atkinson NGA Ground Motion Relations for the Geometric Mean Horizontal Component of Peak and Spectral Ground Motion Parameters*. David M. Boore and Gail M. Atkinson. May 2007.

PEER 2006/12 Societal Implications of Performance-Based Earthquake Engineering. Peter J. May. May 2007.

PEER 2006/11 *Probabilistic Seismic Demand Analysis Using Advanced Ground Motion Intensity Measures, Attenuation Relationships, and Near-Fault Effects*. Polsak Tothong and C. Allin Cornell. March 2007.

PEER 2006/10 *Application of the PEER PBEE Methodology to the I-880 Viaduct.* Sashi Kunnath. February 2007.

PEER 2006/09 *Quantifying Economic Losses from Travel Forgone Following a Large Metropolitan Earthquake*. James Moore, Sungbin Cho, Yue Yue Fan, and Stuart Werner. November 2006.

PEER 2006/08 *Vector-Valued Ground Motion Intensity Measures for Probabilistic Seismic Demand Analysis*. Jack W. Baker and C. Allin Cornell. October 2006.

PEER 2006/07 *Analytical Modeling of Reinforced Concrete Walls for Predicting Flexural and Coupled–Shear-Flexural Responses*. Kutay Orakcal, Leonardo M. Massone, and John W. Wallace. October 2006.

PEER 2006/06 *Nonlinear Analysis of a Soil-Drilled Pier System under Static and Dynamic Axial Loading*. Gang Wang and Nicholas Sitar. November 2006.

PEER 2006/05 *Advanced Seismic Assessment Guidelines.* Paolo Bazzurro, C. Allin Cornell, Charles Menun, Maziar Motahari, and Nicolas Luco. September 2006.

PEER 2006/04 *Probabilistic Seismic Evaluation of Reinforced Concrete Structural Components and Systems*. Tae Hyung Lee and Khalid M. Mosalam. August 2006.

PEER 2006/03 *Performance of Lifelines Subjected to Lateral Spreading.* Scott A. Ashford and Teerawut Juirnarongrit. July 2006.

PEER 2006/02 *Pacific Earthquake Engineering Research Center Highway Demonstration Project.* Anne Kiremidjian, James Moore, Yue Yue Fan, Nesrin Basoz, Ozgur Yazali, and Meredith Williams. April 2006.

PEER 2006/01 *Bracing Berkeley. A Guide to Seismic Safety on the UC Berkeley Campus.* Mary C. Comerio, Stephen Tobriner, and Ariane Fehrenkamp. January 2006.

PEER 2005/17 *Earthquake Simulation Tests on Reducing Residual Displacements of Reinforced Concrete Bridges.* Junichi Sakai, Stephen A Mahin, and Andres Espinoza. December 2005.

PEER 2005/16 *Seismic Response and Reliability of Electrical Substation Equipment and Systems.* Junho Song, Armen Der Kiureghian, and Jerome L. Sackman. April 2006.

PEER 2005/15 *CPT-Based Probabilistic Assessment of Seismic Soil Liquefaction Initiation.* R. E. S. Moss, R. B. Seed, R. E. Kayen, J. P. Stewart, and A. Der Kiureghian. April 2006.

PEER 2005/14 *Workshop on Modeling of Nonlinear Cyclic Load-Deformation Behavior of Shallow Foundations.* Bruce L. Kutter, Geoffrey Martin, Tara Hutchinson, Chad Harden, Sivapalan Gajan, and Justin Phalen. March 2006.

PEER 2005/13 *Stochastic Characterization and Decision Bases under Time-Dependent Aftershock Risk in Performance-Based Earthquake Engineering*. Gee Liek Yeo and C. Allin Cornell. July 2005.

PEER 2005/12 *PEER Testbed Study on a Laboratory Building: Exercising Seismic Performance Assessment.* Mary C. Comerio, Editor. November 2005.

PEER 2005/11 *Van Nuys Hotel Building Testbed Report: Exercising Seismic Performance Assessment.* Helmut Krawinkler, Editor. October 2005.

PEER 2005/10 *First NEES/E-Defense Workshop on Collapse Simulation of Reinforced Concrete Building Structures.* September 2005.

PEER 2005/09 *Test Applications of Advanced Seismic Assessment Guidelines.* Joe Maffei, Karl Telleen, Danya Mohr, William Holmes, and Yuki Nakayama. August 2006.

PEER 2005/08 *Damage Accumulation in Lightly Confined Reinforced Concrete Bridge Columns.* R. Tyler Ranf, Jared M. Nelson, Zach Price, Marc O. Eberhard, and John F. Stanton. April 2006.

PEER 2005/07 *Experimental and Analytical Studies on the Seismic Response of Freestanding and Anchored Laboratory Equipment.* Dimitrios Konstantinidis and Nicos Makris. January 2005.

PEER 2005/06 *Global Collapse of Frame Structures under Seismic Excitations*. Luis F. Ibarra and Helmut Krawinkler. September 2005.

PEER 2005//05 *Performance Characterization of Bench- and Shelf-Mounted Equipment.* Samit Ray Chaudhuri and Tara C. Hutchinson. May 2006.

PEER 2005/04 *Numerical Modeling of the Nonlinear Cyclic Response of Shallow Foundations.* Chad Harden, Tara Hutchinson, Geoffrey R. Martin, and Bruce L. Kutter. August 2005.

PEER 2005/03 *A Taxonomy of Building Components for Performance-Based Earthquake Engineering.* Keith A. Porter. September 2005.

PEER 2005/02 *Fragility Basis for California Highway Overpass Bridge Seismic Decision Making*. Kevin R. Mackie and Božidar Stojadinović. June 2005.

PEER 2005/01 *Empirical Characterization of Site Conditions on Strong Ground Motion.* Jonathan P. Stewart, Yoojoong Choi, and Robert W. Graves. June 2005.

PEER 2004/09 *Electrical Substation Equipment Interaction: Experimental Rigid Conductor Studies.* Christopher Stearns and André Filiatrault. February 2005.

PEER 2004/08 *Seismic Qualification and Fragility Testing of Line Break 550-kV Disconnect Switches.* Shakhzod M. Takhirov, Gregory L. Fenves, and Eric Fujisaki. January 2005.

PEER 2004/07 *Ground Motions for Earthquake Simulator Qualification of Electrical Substation Equipment.* Shakhzod M. Takhirov, Gregory L. Fenves, Eric Fujisaki, and Don Clyde. January 2005.

PEER 2004/06 *Performance-Based Regulation and Regulatory Regimes.* Peter J. May and Chris Koski. September 2004.

PEER 2004/05 *Performance-Based Seismic Design Concepts and Implementation: Proceedings of an International Workshop.* Peter Fajfar and Helmut Krawinkler, Editors. September 2004.

PEER 2004/04 *Seismic Performance of an Instrumented Tilt-up Wall Building.* James C. Anderson and Vitelmo V. Bertero. July 2004.

PEER 2004/03 *Evaluation and Application of Concrete Tilt-up Assessment Methodologies.* Timothy Graf and James O. Malley. October 2004.

PEER 2004/02 *Analytical Investigations of New Methods for Reducing Residual Displacements of Reinforced Concrete Bridge Columns.* Junichi Sakai and Stephen A. Mahin. August 2004.

PEER 2004/01 *Seismic Performance of Masonry Buildings and Design Implications.* Kerri Anne Taeko Tokoro, James C. Anderson, and Vitelmo V. Bertero. February 2004.

PEER 2003/18 *Performance Models for Flexural Damage in Reinforced Concrete Columns.* Michael Berry and Marc Eberhard. August 2003.

PEER 2003/17 *Predicting Earthquake Damage in Older Reinforced Concrete Beam-Column Joints.* Catherine Pagni and Laura Lowes. October 2004.

PEER 2003/16 *Seismic Demands for Performance-Based Design of Bridges.* Kevin Mackie and Božidar Stojadinović. August 2003.

PEER 2003/15 *Seismic Demands for Nondeteriorating Frame Structures and Their Dependence on Ground Motions.* Ricardo Antonio Medina and Helmut Krawinkler. May 2004.

PEER 2003/14 *Finite Element Reliability and Sensitivity Methods for Performance-Based Earthquake Engineering*. Terje Haukaas and Armen Der Kiureghian. April 2004.

PEER 2003/13 *Effects of Connection Hysteretic Degradation on the Seismic Behavior of Steel Moment-Resisting Frames.* Janise E. Rodgers and Stephen A. Mahin. March 2004.

PEER 2003/12 *Implementation Manual for the Seismic Protection of Laboratory Contents: Format and Case Studies*. William T. Holmes and Mary C. Comerio. October 2003.

PEER 2003/11 *Fifth U.S.-Japan Workshop on Performance-Based Earthquake Engineering Methodology for Reinforced Concrete Building Structures*. February 2004.

PEER 2003/10 *A Beam-Column Joint Model for Simulating the Earthquake Response of Reinforced Concrete Frames.* Laura N. Lowes, Nilanjan Mitra, and Arash Altoontash. February 2004.

PEER 2003/09 *Sequencing Repairs after an Earthquake: An Economic Approach.* Marco Casari and Simon J. Wilkie. April 2004.

PEER 2003/08 *A Technical Framework for Probability-Based Demand and Capacity Factor Design (DCFD) Seismic Formats*. Fatemeh Jalayer and C. Allin Cornell. November 2003.

PEER 2003/07 *Uncertainty Specification and Propagation for Loss Estimation Using FOSM Methods.* Jack W. Baker and C. Allin Cornell. September 2003.

PEER 2003/06 *Performance of Circular Reinforced Concrete Bridge Columns under Bidirectional Earthquake Loading*. Mahmoud M. Hachem, Stephen A. Mahin, and Jack P. Moehle. February 2003.

PEER 2003/05 *Response Assessment for Building-Specific Loss Estimation.* Eduardo Miranda and Shahram Taghavi. September 2003.

PEER 2003/04 *Experimental Assessment of Columns with Short Lap Splices Subjected to Cyclic Loads*. Murat Melek, John W. Wallace, and Joel Conte. April 2003.

PEER 2003/03 *Probabilistic Response Assessment for Building-Specific Loss Estimation*. Eduardo Miranda and Hesameddin Aslani. September 2003.

PEER 2003/02 *Software Framework for Collaborative Development of Nonlinear Dynamic Analysis Program*. Jun Peng and Kincho H. Law. September 2003.

PEER 2003/01 *Shake Table Tests and Analytical Studies on the Gravity Load Collapse of Reinforced Concrete Frames.* Kenneth John Elwood and Jack P. Moehle. November 2003.

PEER 2002/24 *Performance of Beam to Column Bridge Joints Subjected to a Large Velocity Pulse.* Natalie Gibson, André Filiatrault, and Scott A. Ashford. April 2002.

PEER 2002/23 *Effects of Large Velocity Pulses on Reinforced Concrete Bridge Columns.* Greg L. Orozco and Scott A. Ashford. April 2002.

PEER 2002/22 *Characterization of Large Velocity Pulses for Laboratory Testing.* Kenneth E. Cox and Scott A. Ashford. April 2002.

PEER 2002/21 *Fourth U.S.-Japan Workshop on Performance-Based Earthquake Engineering Methodology for Reinforced Concrete Building Structures*. December 2002.

PEER 2002/20 *Barriers to Adoption and Implementation of PBEE Innovations.* Peter J. May. August 2002.

PEER 2002/19 *Economic-Engineered Integrated Models for Earthquakes: Socioeconomic Impacts.* Peter Gordon, James E. Moore II, and Harry W. Richardson. July 2002.

PEER 2002/18 *Assessment of Reinforced Concrete Building Exterior Joints with Substandard Details.* Chris P. Pantelides, Jon Hansen, Justin Nadauld, and Lawrence D. Reaveley. May 2002.

PEER 2002/17 *Structural Characterization and Seismic Response Analysis of a Highway Overcrossing Equipped with Elastomeric Bearings and Fluid Dampers: A Case Study*. Nicos Makris and Jian Zhang. November 2002.

PEER 2002/16 *Estimation of Uncertainty in Geotechnical Properties for Performance-Based Earthquake Engineering*. Allen L. Jones, Steven L. Kramer, and Pedro Arduino. December 2002.

PEER 2002/15 *Seismic Behavior of Bridge Columns Subjected to Various Loading Patterns*. Asadollah Esmaeily-Gh. and Yan Xiao. December 2002.

PEER 2002/14 *Inelastic Seismic Response of Extended Pile Shaft Supported Bridge Structures.* T.C. Hutchinson, R.W. Boulanger, Y.H. Chai, and I.M. Idriss. December 2002.

PEER 2002/13 *Probabilistic Models and Fragility Estimates for Bridge Components and Systems.* Paolo Gardoni, Armen Der Kiureghian, and Khalid M. Mosalam. June 2002.

PEER 2002/12 *Effects of Fault Dip and Slip Rake on Near-Source Ground Motions: Why Chi-Chi Was a Relatively Mild M7.6 Earthquake*. Brad T. Aagaard, John F. Hall, and Thomas H. Heaton. December 2002.

PEER 2002/11 *Analytical and Experimental Study of Fiber-Reinforced Strip Isolators*. James M. Kelly and Shakhzod M. Takhirov. September 2002.

PEER 2002/10 *Centrifuge Modeling of Settlement and Lateral Spreading with Comparisons to Numerical Analyses***.** Sivapalan Gajan and Bruce L. Kutter. January 2003.

PEER 2002/09 *Documentation and Analysis of Field Case Histories of Seismic Compression during the 1994 Northridge, California, Earthquake*. Jonathan P. Stewart, Patrick M. Smith, Daniel H. Whang, and Jonathan D. Bray. October 2002.

PEER 2002/08 *Component Testing, Stability Analysis and Characterization of Buckling-Restrained Unbonded Braces^{TM}*. Cameron Black, Nicos Makris, and Ian Aiken. September 2002.

PEER 2002/07 *Seismic Performance of Pile-Wharf Connections.* Charles W. Roeder, Robert Graff, Jennifer Soderstrom, and Jun Han Yoo. December 2001.

PEER 2002/06 *The Use of Benefit-Cost Analysis for Evaluation of Performance-Based Earthquake Engineering Decisions*. Richard O. Zerbe and Anthony Falit-Baiamonte. September 2001.

PEER 2002/05 *Guidelines, Specifications, and Seismic Performance Characterization of Nonstructural Building Components and Equipment*. André Filiatrault, Constantin Christopoulos, and Christopher Stearns. September 2001.

PEER 2002/04 *Consortium of Organizations for Strong-Motion Observation Systems and the Pacific Earthquake Engineering Research Center Lifelines Program: Invited Workshop on Archiving and Web Dissemination of Geotechnical Data, 4–5 October 2001*. September 2002.

PEER 2002/03 *Investigation of Sensitivity of Building Loss Estimates to Major Uncertain Variables for the Van Nuys Testbed*. Keith A. Porter, James L. Beck, and Rustem V. Shaikhutdinov. August 2002.

PEER 2002/02 *The Third U.S.-Japan Workshop on Performance-Based Earthquake Engineering Methodology for Reinforced Concrete Building Structures*. July 2002.

PEER 2002/01 *Nonstructural Loss Estimation: The UC Berkeley Case Study.* Mary C. Comerio and John C. Stallmeyer. December 2001.

PEER 2001/16 *Statistics of SDF-System Estimate of Roof Displacement for Pushover Analysis of Buildings.* Anil K. Chopra, Rakesh K. Goel, and Chatpan Chintanapakdee. December 2001.

PEER 2001/15 *Damage to Bridges during the 2001 Nisqually Earthquake.* R. Tyler Ranf, Marc O. Eberhard, and Michael P. Berry. November 2001.

PEER 2001/14 *Rocking Response of Equipment Anchored to a Base Foundation.* Nicos Makris and Cameron J. Black. September 2001.

PEER 2001/13 *Modeling Soil Liquefaction Hazards for Performance-Based Earthquake Engineering*. Steven L. Kramer and Ahmed-W. Elgamal. February 2001.

PEER 2001/12 *Development of Geotechnical Capabilities in OpenSees*. Boris Jeremić. September 2001.

PEER 2001/11 *Analytical and Experimental Study of Fiber-Reinforced Elastomeric Isolators*. James M. Kelly and Shakhzod M. Takhirov. September 2001.

PEER 2001/10 *Amplification Factors for Spectral Acceleration in Active Regions.* Jonathan P. Stewart, Andrew H. Liu, Yoojoong Choi, and Mehmet B. Baturay. December 2001.

PEER 2001/09 *Ground Motion Evaluation Procedures for Performance-Based Design.* Jonathan P. Stewart, Shyh-Jeng Chiou, Jonathan D. Bray, Robert W. Graves, Paul G. Somerville, and Norman A. Abrahamson. September 2001.

PEER 2001/08 *Experimental and Computational Evaluation of Reinforced Concrete Bridge Beam-Column Connections for Seismic Performance*. Clay J. Naito, Jack P. Moehle, and Khalid M. Mosalam. November 2001.

PEER 2001/07 *The Rocking Spectrum and the Shortcomings of Design Guidelines.* Nicos Makris and Dimitrios Konstantinidis. August 2001.

PEER 2001/06 *Development of an Electrical Substation Equipment Performance Database for Evaluation of Equipment Fragilities*. Thalia Agnanos. April 1999.

PEER 2001/05 *Stiffness Analysis of Fiber-Reinforced Elastomeric Isolators.* Hsiang-Chuan Tsai and James M. Kelly. May 2001.

PEER 2001/04 *Organizational and Societal Considerations for Performance-Based Earthquake Engineering*. Peter J. May. April 2001.

PEER 2001/03 *A Modal Pushover Analysis Procedure to Estimate Seismic Demands for Buildings: Theory and Preliminary Evaluation*. Anil K. Chopra and Rakesh K. Goel. January 2001.

PEER 2001/02 *Seismic Response Analysis of Highway Overcrossings Including Soil-Structure Interaction*. Jian Zhang and Nicos Makris. March 2001.

PEER 2001/01 *Experimental Study of Large Seismic Steel Beam-to-Column Connections.* Egor P. Popov and Shakhzod M. Takhirov. November 2000.

PEER 2000/10 *The Second U.S.-Japan Workshop on Performance-Based Earthquake Engineering Methodology for Reinforced Concrete Building Structures*. March 2000.

PEER 2000/09 *Structural Engineering Reconnaissance of the August 17, 1999 Earthquake: Kocaeli (Izmit), Turkey.* Halil Sezen, Kenneth J. Elwood, Andrew S. Whittaker, Khalid Mosalam, John J. Wallace, and John F. Stanton. December 2000.

PEER 2000/08 *Behavior of Reinforced Concrete Bridge Columns Having Varying Aspect Ratios and Varying Lengths of Confinement*. Anthony J. Calderone, Dawn E. Lehman, and Jack P. Moehle. January 2001.

PEER 2000/07 *Cover-Plate and Flange-Plate Reinforced Steel Moment-Resisting Connections.* Taejin Kim, Andrew S. Whittaker, Amir S. Gilani, Vitelmo V. Bertero, and Shakhzod M. Takhirov. September 2000.

PEER 2000/06 *Seismic Evaluation and Analysis of 230-kV Disconnect Switches.* Amir S. J. Gilani, Andrew S. Whittaker, Gregory L. Fenves, Chun-Hao Chen, Henry Ho, and Eric Fujisaki. July 2000.

PEER 2000/05 *Performance-Based Evaluation of Exterior Reinforced Concrete Building Joints for Seismic Excitation*. Chandra Clyde, Chris P. Pantelides, and Lawrence D. Reaveley. July 2000.

PEER 2000/04 *An Evaluation of Seismic Energy Demand: An Attenuation Approach*. Chung-Che Chou and Chia-Ming Uang. July 1999.

PEER 2000/03 *Framing Earthquake Retrofitting Decisions: The Case of Hillside Homes in Los Angeles.* Detlof von Winterfeldt, Nels Roselund, and Alicia Kitsuse. March 2000.

PEER 2000/02 *U.S.-Japan Workshop on the Effects of Near-Field Earthquake Shaking*. Andrew Whittaker, Editor. July 2000.

PEER 2000/01 *Further Studies on Seismic Interaction in Interconnected Electrical Substation Equipment.* Armen Der Kiureghian, Kee-Jeung Hong, and Jerome L. Sackman. November 1999.

PEER 1999/14 *Seismic Evaluation and Retrofit of 230-kV Porcelain Transformer Bushings*. Amir S. Gilani, Andrew S. Whittaker, Gregory L. Fenves, and Eric Fujisaki. December 1999.

PEER 1999/13 *Building Vulnerability Studies: Modeling and Evaluation of Tilt-up and Steel Reinforced Concrete Buildings*. John W. Wallace, Jonathan P. Stewart, and Andrew S. Whittaker, Editors. December 1999.

PEER 1999/12 *Rehabilitation of Nonductile RC Frame Building Using Encasement Plates and Energy-Dissipating Devices*. Mehrdad Sasani, Vitelmo V. Bertero, James C. Anderson. December 1999.

PEER 1999/11 *Performance Evaluation Database for Concrete Bridge Components and Systems under Simulated Seismic Loads*. Yael D. Hose and Frieder Seible. November 1999.

PEER 1999/10 *U.S.-Japan Workshop on Performance-Based Earthquake Engineering Methodology for Reinforced Concrete Building Structures*. December 1999.

PEER 1999/09 *Performance Improvement of Long Period Building Structures Subjected to Severe Pulse-Type Ground Motions*. James C. Anderson, Vitelmo V. Bertero, and Raul Bertero. October 1999.

PEER 1999/08 *Envelopes for Seismic Response Vectors.* Charles Menun and Armen Der Kiureghian. July 1999.

PEER 1999/07 *Documentation of Strengths and Weaknesses of Current Computer Analysis Methods for Seismic Performance of Reinforced Concrete Members*. William F. Cofer. November 1999.

PEER 1999/06 *Rocking Response and Overturning of Anchored Equipment under Seismic Excitations*. Nicos Makris and Jian Zhang. November 1999.

PEER 1999/05 *Seismic Evaluation of 550 kV Porcelain Transformer Bushings.* Amir S. Gilani, Andrew S. Whittaker, Gregory L. Fenves, and Eric Fujisaki. October 1999.

PEER 1999/04 *Adoption and Enforcement of Earthquake Risk-Reduction Measures.* Peter J. May, Raymond J. Burby, T. Jens Feeley, and Robert Wood. August 1999.

PEER 1999/03 *Task 3 Characterization of Site Response General Site Categories*. Adrian Rodriguez-Marek, Jonathan D. Bray and Norman Abrahamson. February 1999.

PEER 1999/02 *Capacity-Demand-Diagram Methods for Estimating Seismic Deformation of Inelastic Structures: SDF Systems*. Anil K. Chopra and Rakesh Goel. April 1999.

PEER 1999/01 *Interaction in Interconnected Electrical Substation Equipment Subjected to Earthquake Ground Motions*. Armen Der Kiureghian, Jerome L. Sackman, and Kee-Jeung Hong. February 1999.

PEER 1998/08 *Behavior and Failure Analysis of a Multiple-Frame Highway Bridge in the 1994 Northridge Earthquake*. Gregory L. Fenves and Michael Ellery. December 1998.

PEER 1998/07 *Empirical Evaluation of Inertial Soil-Structure Interaction Effects.* Jonathan P. Stewart, Raymond B. Seed, and Gregory L. Fenves. November 1998.

PEER 1998/06 *Effect of Damping Mechanisms on the Response of Seismic Isolated Structures*. Nicos Makris and Shih-Po Chang. November 1998.

PEER 1998/05 *Rocking Response and Overturning of Equipment under Horizontal Pulse-Type Motions*. Nicos Makris and Yiannis Roussos. October 1998.

PEER 1998/04 *Pacific Earthquake Engineering Research Invitational Workshop Proceedings, May 14–15, 1998: Defining the Links between Planning, Policy Analysis, Economics and Earthquake Engineering*. Mary Comerio and Peter Gordon. September 1998.

PEER 1998/03 *Repair/Upgrade Procedures for Welded Beam to Column Connections*. James C. Anderson and Xiaojing Duan. May 1998.

PEER 1998/02 *Seismic Evaluation of 196 kV Porcelain Transformer Bushings.* Amir S. Gilani, Juan W. Chavez, Gregory L. Fenves, and Andrew S. Whittaker. May 1998.

PEER 1998/01 *Seismic Performance of Well-Confined Concrete Bridge Columns.* Dawn E. Lehman and Jack P. Moehle. December 2000.

PEER REPORTS: ONE HUNDRED SERIES

PEER 2012/103 *Performance-Based Seismic Demand Assessment of Concentrically Braced Steel Frame Buildings.* Chui-Hsin Chen and Stephen A. Mahin. December 2012.

PEER 2012/102 *Procedure to Restart an Inteuted Hybrid Simulation: Addendum to PEER Report 2010/103.* Vesna Terzic and Bozidar Stojadinovic. October 2012.

PEER 2012/101 *Mechanics of Fiber Reinforced Bearings.* James M. Kelly and Andrea Calabrese. February 2012.

PEER 2011/107 *Nonlinear Site Response and Seismic Compression at Vertical Array Strongly Shaken by 2007 Niigata-ken Chuetsu-oki Earthquake.* Eric Yee, Jonathan P. Stewart, and Kohji Tokimatsu. December 2011.

PEER 2011/106 *Self Compacting Hybrid Fiber Reinforced Concrete Composites for Bridge Columns.* Pardeep Kumar, Gabriel Jen, William Trono, Marios Panagiotou, and Claudia Ostertag. September 2011.

PEER 2011/105 *Stochastic Dynamic Analysis of Bridges Subjected to Spacially Varying Ground Motions.* Katerina Konakli and Armen Der Kiureghian. August 2011.

PEER 2011/104 *Design and Instrumentation of the 2010 E-Defense Four-Story Reinforced Concrete and Post-Tensioned Concrete Buildings.* Takuya Nagae, Kenichi Tahara, Taizo Matsumori, Hitoshi Shiohara, Toshimi Kabeyasawa, Susumu Kono, Minehiro Nishiyama (Japanese Research Team) and John Wallace, Wassim Ghannoum, Jack Moehle, Richard Sause, Wesley Keller, Zeynep Tuna (U.S. Research Team). June 2011.

PEER 2011/103 *In-Situ Monitoring of the Force Output of Fluid Dampers: Experimental Investigation.* Dimitrios Konstantinidis, James M. Kelly, and Nicos Makris. April 2011.

PEER 2011/102 *Ground-Motion Prediction Equations 1964–2010.* John Douglas. April 2011.

PEER 2011/101 *Report of the Eighth Planning Meeting of NEES/E-Defense Collaborative Research on Earthquake Engineering.* Convened by the Hyogo Earthquake Engineering Research Center (NIED), NEES Consortium, Inc. February 2011.

PEER 2010/111 *Modeling and Acceptance Criteria for Seismic Design and Analysis of Tall Buildings.* Task 7 Report for the Tall Buildings Initiative - Published jointly by the Applied Technology Council. October 2010.

PEER 2010/110 *Seismic Performance Assessment and Probabilistic Repair Cost Analysis of Precast Concrete Cladding Systems for Multistory Buildlings.* Jeffrey P. Hunt and Božidar Stojadinovic. November 2010.

PEER 2010/109 *Report of the Seventh Joint Planning Meeting of NEES/E-Defense Collaboration on Earthquake Engineering. Held at the E-Defense, Miki, and Shin-Kobe, Japan, September 18–19, 2009.* August 2010.

PEER 2010/108 *Probabilistic Tsunami Hazard in California.* Hong Kie Thio, Paul Somerville, and Jascha Polet, preparers. October 2010.

PEER 2010/107 *Performance and Reliability of Exposed Column Base Plate Connections for Steel Moment-Resisting Frames.* Ady Aviram, Božidar Stojadinovic, and Armen Der Kiureghian. August 2010.

PEER 2010/106 *Verification of Probabilistic Seismic Hazard Analysis Computer Programs.* Patricia Thomas, Ivan Wong, and Norman Abrahamson. May 2010.

PEER 2010/105 *Structural Engineering Reconnaissance of the April 6, 2009, Abruzzo, Italy, Earthquake, and Lessons Learned.* M. Selim Günay and Khalid M. Mosalam. April 2010.

PEER 2010/104 *Simulating the Inelastic Seismic Behavior of Steel Braced Frames, Including the Effects of Low-Cycle Fatigue.* Yuli Huang and Stephen A. Mahin. April 2010.

PEER 2010/103 *Post-Earthquake Traffic Capacity of Modern Bridges in California.* Vesna Terzic and Božidar Stojadinović. March 2010.

PEER 2010/102 *Analysis of Cumulative Absolute Velocity (CAV) and JMA Instrumental Seismic Intensity (I_{JMA}) Using the PEER–NGA Strong Motion Database.* Kenneth W. Campbell and Yousef Bozorgnia. February 2010.

PEER 2010/101 *Rocking Response of Bridges on Shallow Foundations.* Jose A. Ugalde, Bruce L. Kutter, and Boris Jeremic. April 2010.

PEER 2009/109 *Simulation and Performance-Based Earthquake Engineering Assessment of Self-Centering Post-Tensioned Concrete Bridge Systems.* Won K. Lee and Sarah L. Billington. December 2009.

PEER 2009/108 *PEER Lifelines Geotechnical Virtual Data Center.* J. Carl Stepp, Daniel J. Ponti, Loren L. Turner, Jennifer N. Swift, Sean Devlin, Yang Zhu, Jean Benoit, and John Bobbitt. September 2009.

PEER 2009/107 *Experimental and Computational Evaluation of Current and Innovative In-Span Hinge Details in Reinforced Concrete Box-Girder Bridges: Part 2: Post-Test Analysis and Design Recommendations.* Matias A. Hube and Khalid M. Mosalam. December 2009.

PEER 2009/106 *Shear Strength Models of Exterior Beam-Column Joints without Transverse Reinforcement.* Sangjoon Park and Khalid M. Mosalam. November 2009.

PEER 2009/105 *Reduced Uncertainty of Ground Motion Prediction Equations through Bayesian Variance Analysis.* Robb Eric S. Moss. November 2009.

PEER 2009/104 *Advanced Implementation of Hybrid Simulation.* Andreas H. Schellenberg, Stephen A. Mahin, Gregory L. Fenves. November 2009.

PEER 2009/103 *Performance Evaluation of Innovative Steel Braced Frames.* T. Y. Yang, Jack P. Moehle, and Božidar Stojadinovic. August 2009.

PEER 2009/102 *Reinvestigation of Liquefaction and Nonliquefaction Case Histories from the 1976 Tangshan Earthquake.* Robb Eric Moss, Robert E. Kayen, Liyuan Tong, Songyu Liu, Guojun Cai, and Jiaer Wu. August 2009.

PEER 2009/101 *Report of the First Joint Planning Meeting for the Second Phase of NEES/E-Defense Collaborative Research on Earthquake Engineering.* Stephen A. Mahin et al. July 2009.

PEER 2008/104 *Experimental and Analytical Study of the Seismic Performance of Retaining Structures.* Linda Al Atik and Nicholas Sitar. January 2009.

PEER 2008/103 *Experimental and Computational Evaluation of Current and Innovative In-Span Hinge Details in Reinforced Concrete Box-Girder Bridges. Part 1: Experimental Findings and Pre-Test Analysis.* Matias A. Hube and Khalid M. Mosalam. January 2009.

PEER 2008/102 *Modeling of Unreinforced Masonry Infill Walls Considering In-Plane and Out-of-Plane Interaction.* Stephen Kadysiewski and Khalid M. Mosalam. January 2009.

PEER 2008/101 *Seismic Performance Objectives for Tall Buildings.* William T. Holmes, Charles Kircher, William Petak, and Nabih Youssef. August 2008.

PEER 2007/101 *Generalized Hybrid Simulation Framework for Structural Systems Subjected to Seismic Loading*. Tarek Elkhoraibi and Khalid M. Mosalam. July 2007.

PEER 2007/100 *Seismic Evaluation of Reinforced Concrete Buildings Including Effects of Masonry Infill Walls.* Alidad Hashemi and Khalid M. Mosalam. July 2007.

The Pacifi c Earthquake Engineering Research Center (PEER) is a multi-institutional research and education center with headquarters at the University of California, Berkeley. Investigators from over 20 universities, several consulting companies, and researchers at various state and federal government agencies contribute to research programs focused on performance-based earthquake engineering.

These research programs aim to identify and reduce the risks from major earthquakes to life safety and to the economy by including research in a wide variety of disciplines including structural and geotechnical engineering, geology/ seismology, lifelines, transportation, architecture, economics, risk management, and public policy.

PEER is supported by federal, state, local, and regional agencies, together with industry partners.

PEER Core Institutions

University of California, Berkeley (Lead Institution)
California Institute of Technology
Oregon State University
Stanford University
University of California, Davis
University of California, Irvine
University of California, Los Angeles
University of California, San Diego
University of Nevada, Reno
University of Southern California
University of Washington

PEER reports can be ordered at https://peer.berkeley.edu/peer-reports or by contacting

Pacific Earthquake Engineering Research Center
University of California, Berkeley
325 Davis Hall, Mail Code 1792
Berkeley, CA 94720-1792
Tel: 510-642-3437
Email: peer_center@berkeley.edu

ISSN 2770-8314
https://doi.org/10.55461/USOP6050